MEASUREMENT OF THE ELECTRON DRIFT VELOCITY IN SILICON

Thesis by

Valentin Rodriguez

In Partial Fulfillment of the Requirements

For the Degree of

Doctor of Philosophy

California Institute of Technology

Pasadena, California

1969

(Submitted June 27, 1968)

ABSTRACT

The drift velocity of electrons in silicon at high electric fields is measured in the ⟨111⟩ direction over the range of lattice temperatures from 4.2°K to 300°K. This information is obtained from measurements of pure unipolar (sclc) space-charge-limited current. Structures of the type n^+ n n^+ and n^+ p n^+ have been manufactured to study this current. The experimental V-I characteristics obtained from these structures offer a consistent picture. The theoretical models adopted are simple and adequate.

The drift velocity is found to increase monotonically with electric field strength in the range of lattice temperatures covered. It is established that a limiting drift velocity exists at high electric fields. Its temperature dependence is measured from 4.2°K to 300°K. No indication of a negative differential mobility - as observed in GaAs and Ge below 77°K - is present. At 300°K and 77°K the velocity-field relationship is determined from the linear (low field) range up to a field strength of the order of 10^5 volt/cm. A comparison with results obtained by other authors at those two temperatures yields good agreement, in particular at 300°K.

A fairly complete treatment of the influence on unipolar sclc of: (1) trapping, (2) geometry, (3) ionized impurities, (4) illumination, and (5) thermal carriers, is presented. In particular, the effect of giant trapping and normal trapping is studied in detail.

The threshold voltage is measured as a function of lattice temperature from 4.2°K to 300°K. In the range from 4.2°K to 50°K, its temperature dependence is correlated to that of the trapping cross-section for the compensated donor atoms. Above 77°K, the temperature dependence of the threshold voltage is linked to that of the Debye length. From this analysis, the degree of compensation of the material is derived in a simple way.

ACKNOWLEDGMENTS

The author is greatly indebted to Dr. M-A. Nicolet for his patience, encouragement, and guidance during the course of this work. The financial support of Fairchild Camera and Instrument through a Fairchild Fellowship is gratefully acknowledged. This work was also supported in part by the Naval Ordnance Test Station in Pasadena, California.

I am also indebted to C. A. Bittmann for arranging a program with Fairchild Semiconductor through which I was able to manufacture most of the samples used for this work.

TABLE OF CONTENTS

CHAPTER IV

THEORETICAL ANALYSIS AND EXPERIMENTAL RESULTS FOR THE LIMITING DRIFT VELOCITY

INTRODUCTION

The flow of unipolar sclc (space-charge-limited current) through solids has received considerable attention in recent years. Attempts have been made to find practical applications for its properties. This has met with little success. However, in the process, a vast amount of information has been gathered regarding its behavior under the influence of distinct phenomena. In this work, a different view point is taken. Rather than considering unipolar sclc as an end by itself, it is used as a tool to achieve a better understanding about the complex nature of solids. This approach has been taken by several authors before, mainly, to determine: (1) the presence of traps, (2) the trapping parameters, and (3) the influence of trapping in preventing and reducing the flow of current. Here, the emphasis is placed in understanding from measurements of "pure" unipolar sclc the behavior of the drift velocity as a function of the electric field strength and lattice temperature. Before this can be accomplished, however, the influence of a field dependent mobility on sclc must be well understood. Various structures of the type n^+ p n^+ and n^+ n n^+, with different thicknesses and resistivities, have been manufactured to study segments or the entire field-velocity relationship.

Chapter I encompasses all the pertinent models which describe the flow of pure unipolar sclc under the influence of various initial

conditions; some previously obtained by several authors, some extended to meet the conditions present in this work, and some derived here to apply to very specific situations encountered in the experimental analysis of the field-velocity relationship. The presentation of a simple analytical treatment to provide a comparison with the experimental findings takes priority and overrules a detailed analysis. For a better and more complete treatment, the reader is referred in the text to the work of several authors who have considered the various models in great detail.

Chapter II gives a short description of the manufacturing procedure employed to fabricate the structures. It also describes the techniques used to obtain the various structure parameters, and the apparatus employed to measure the V-I characteristics and to vary the environmental temperature from 300°K to 4.2°K.

The experimental results, apart from those on the temperature dependence of the limiting drift velocity, are presented in chapter III. The threshold voltage is analyzed independently from the V-I characteristics because of its remarkable content of information about the structures and on the properties of the material. The characteristics of the structures are divided into two regimes for voltages below and above threshold. The former yields information, primarily, on trapping phenomena, and the latter on the field dependence of the carrier mobility. The field-velocity relationship as obtained from sclc measurements for electrons in silicon is compared with

determinations by several authors. An effort is made to explain qualitatively the discrepancies encountered. Finally, the influence of geometry and heating of the structures on the V-I characteristics is considered in detail.

The experimental results on the temperature dependence of the limiting drift velocity are illustrated and compared with theory in chapter IV. An effort is made to present that information about the band structure, the low field mobility, and the energy distribution of the electrons which is pertinent to the analysis of the high field mobility. The currently available theories for the limiting drift velocity are included and expanded to apply for silicon oriented in the $\langle 111 \rangle$ direction and for the field strengths and lattice temperatures considered experimentally.

CHAPTER I

ANALYSIS OF UNIPOLAR S.C.L.C.

1.1 Introduction. With the advent of Quantum Mechanics, the classical picture of an insulator as a material suited only to provide electrical insulation was drastically changed. In principle, it appeared feasible - by analogy with a vacuum tube diode - to carry high current densities through an insulator provided with suitable contacts. More specifically, Mott and Gurney[1.1] predicted in 1940 what the dc characteristics of such currents in an insulator or semiconductor should be. Because this current flow is dominated by the space charge in front of the emitter, it has come to be known as unipolar "space-charge-limited current" (sclc). According to their model, which assumes: (1) planar geometry, (2) no traps or impurities, (3) a field-velocity relation $v = \mu E$ valid at any field strength, (4) no thermally generated charge carriers, (5) a finite concentration of carriers at the emitter boundary, (6) negligible diffusion, unipolar sclc is described by the expression

$$J = (9/8)\, \varepsilon\varepsilon_o \mu\, V^2/W^3 \quad , \qquad (1.1)$$

where $\varepsilon\varepsilon_o$ is the dielectric constant of the solid, μ the mobility of the charge carriers, W the thickness of the insulator, and V the

applied voltage. In general, this expression represents the flow of pure unipolar sclc in a solid after the effect of impurities and trapping is overcome, as long as the field velocity relation $v = \mu E$ holds. Since the original description of unipolar sclc, a number of other models with different sets of conditions have been proposed. For instance, the problem has been tackled by Rose[1.2] in the presence of traps, by Shockley and Prim[1.3] for a finite impurity concentration and by Dacey[1.4] for a field dependent mobility. This situation essentially reflects the complexity of solids. A unified theory of unipolar sclc is difficult because of its dependence upon the characteristics of the particular solid through which it is to flow. However, it is possible to distinguish two regimes of interest: (1) the trap and impurity dominated range, where the quality and purity of the material play a dominant role; and (2) the range of pure unipolar sclc, where the current is affected only by the field-velocity relationship and the dielectric constant of the material. Because of the existence of the first regime, unipolar sclc has emerged as a powerful tool in the study of electronic properties of solids.

An analysis of the trap dominated range yields information about their location in energy, density, and trapping cross-sections for both types of carriers. An analysis of pure unipolar sclc yields information, primarily, about the field velocity relationship. In this chapter, the tools with which this information is extracted from

unipolar sclc are presented and analyzed.

1.2 Approximations to the current flow equation. In the forthcoming analysis, we shall consider one dimensional and one carrier (electrons) currents through n and p- type crystals. However, the results apply equally well to holes, and can easily be extended to other geometries by introducing a different geometrical factor. The energy band scheme for an n-type crystal with electron injecting contacts is illustrated in figure (1.1a). At steady state, the current density is free of divergence and given by

$$J = e\, v\,(E)\,(n + n_o) + \mu k\, T \frac{dn}{dx} \quad , \qquad (1.2)$$

where n and n_o are, respectively, the densities of injected and thermal electrons, v(E) their drift velocity, k the Boltzmann constant, T the lattice temperature and E the electric field strength at any position x measured from the emitter electrode. Since the bulk is no longer neutral because of the injected electrons, whose density varies from a high value at the emitter to a low value at the collector, the electric field has a divergence which is given by Poisson's equation:

$$\varepsilon\varepsilon_o \frac{dE}{dx} = - e\, n \quad , \qquad (1.3)$$

where e is the electronic charge. Substituting for the electron density

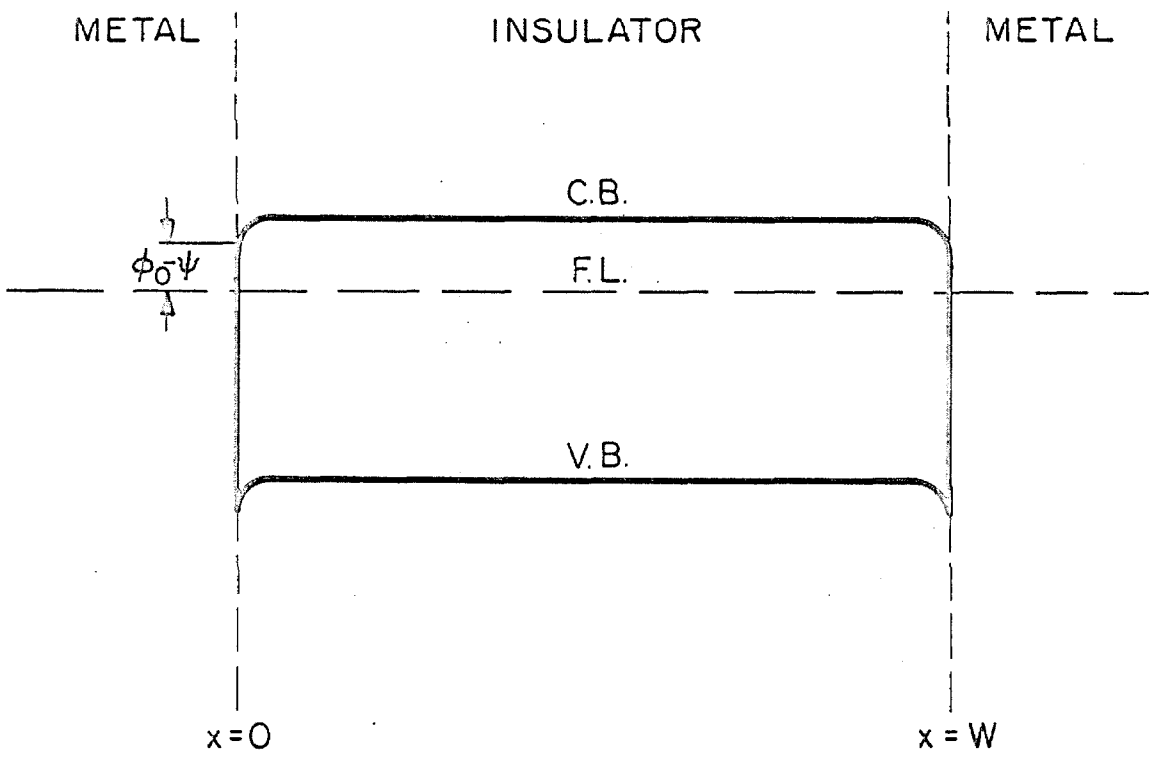

Figure 1.1a

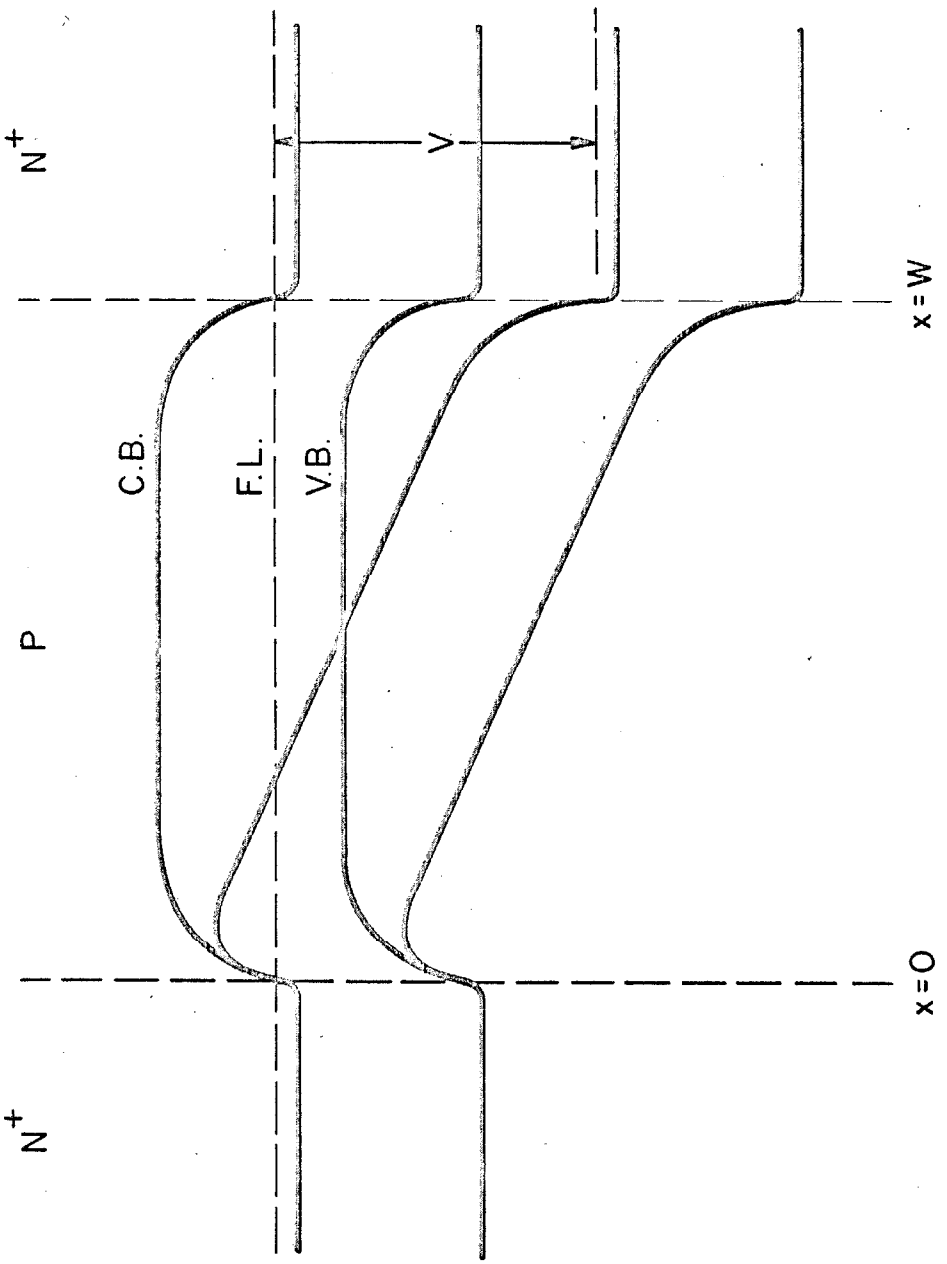

Figure 1.1b

in (1.2), the following second order differential equation results:

$$- J = \varepsilon\varepsilon_o \, v(E) \frac{dE}{dx} + e \, n_o \, v(E) + \mu \frac{kT}{e} \varepsilon\varepsilon_o \frac{d^2E}{dx^2} \quad . \tag{1.4}$$

In order to find a unique solution to this equation, it is necessary to stipulate two boundary conditions. It is customary to consider a semi-infinite bulk. Consequently, at the collector, $n \to n_o$ as $x \to \infty$. At the emitter it is assumed that $E(0) = 0$ which neglects the potential minimum created in the bulk by the injected electrons. Essentially, these boundary conditions imply a complete disregard for the physical nature of the contacts. It is, thus, consistent to obtain the applied voltage as the integral of the electric field. We shall inquire briefly into the nature of these assumptions with regard to the temperature dependence of punch-through covered in section 3.1.1. For a more general treatment of boundary conditions, the reader is referred to Lampert's technical report PT-1445,[1.5] where he has scouted the field and commented in general terms for and about other possible conditions at the contacts.

To seek the general solution of equation (1.4) is not practical. A more realistic approach is to formulate models in which one or more of the contributions to the current density are dominant. In the following discussion, the models pertinent to our investigation are described. The emphasis is placed in enumerating the solutions for the various approximations, rather than in describing the procedure followed in obtaining the results.

Unless otherwise stated, the relation $v = \mu E$ is assumed to hold at any field strength. The contribution of diffusion to the current density is considered to be negligible in all instances. Diffusion dominates the drift contribution to the current density in the vicinity of the emitter, however, it has been shown by Shockley and Prim[1.3] that for applied voltages greater than approximately 25 millivolts, the current is carried chiefly by drift. In general, it will only have an appreciable effect for low applied voltages and thin samples.

Assuming the crystal to be an ideal insulator ($n_o = 0$), equation (1.4) reduces to

$$- J = \mu \varepsilon\varepsilon_o E \frac{dE}{dx} \quad . \tag{1.5}$$

With the set of conditions, $E(0) = 0$ and $V(0) = 0$, the solution of this differential equation is

$$J = (9/8)\, \varepsilon\varepsilon_o \mu \; V^2/W^3 \quad . \tag{1.6}$$

The assumption of an infinite supply of carriers at the emitter is implicit in this result. If a finite concentration, equal to the thermal density of electrons at the emitter interface, is assumed instead of $E(x = 0) = 0$, the solution of (1.5) is

$$V = \frac{2}{3} \sqrt{\left(\frac{2J}{\varepsilon\varepsilon_o \mu}\right)} \left[(W + x_o)^{3/2} - x_o^{3/2} \right] \quad , \tag{1.7}$$

where

$$x_o = \frac{J \varepsilon \varepsilon_o}{2\mu N_o^2 e^2} \quad , \tag{1.8}$$

and

$$N_o = N_c \; e^{-(\psi - \Phi)/kT} \quad . \tag{1.9}$$

$\psi - \Phi$ is the energy barrier at the contact. This is Mott and Gurney's original result. For low applied voltages, the expression reduces to (1.6). For large applied voltages, the effect of space charge is overcome and the current density is ohmic, given by

$$J = e\mu N_o V/W \quad . \tag{1.10}$$

Eventually, for very high voltages, the current density saturates at

$$J_{th} = e N_o v_{th}/\sqrt{2\pi} \quad , \tag{1.11}$$

where v_{th} is given by $(kT/m^*)^{1/2}$ and m^* is the effective mass of the carriers. J_{th} is the unilateral thermal current density at thermal equilibrium flowing from the emitter into the insulator.

The next degree of difficulty is introduced by considering a non-negligible density of thermal electrons. Equation (1.4) reduces to

$$- J = \varepsilon\varepsilon_o \mu E \frac{dE}{dx} + e n_o \mu E \tag{1.12}$$

A solution has been worked out by Lampert[1.5]. For convenience, he performed the following change to dimensionless variables

$$u = \frac{n_o}{n} = \frac{e n_o \mu E(x)}{J}$$

$$\omega = \frac{e^2 n_o^2 \mu x}{\varepsilon\varepsilon_o J}$$

$$v = \frac{e^3 n_o^3 \mu^2 V(x)}{\varepsilon \varepsilon_o J^2} \quad ,$$

and from the solution to the reduced differential equation

$$\omega = - u - \ln (1 - u) \quad ,$$

found the current density and applied voltage to be given by

$$J = \frac{e^2 n_o^2 \mu W}{\varepsilon\varepsilon_o} \frac{1}{\omega_c} \quad , \tag{1.13}$$

and

$$V = \frac{e\, n_o\, W^2}{\varepsilon \varepsilon_o} \frac{v_c}{\omega_c} \quad , \tag{1.14}$$

where the subscript c refers to the collector interface. A closed form expression for J in terms of V is impossible, however, the solution can be divided into two regimes where explicit relations exist for the dc characteristic. For low applied voltages, the current flow is ohmic, due to the thermal charge carriers, and given by

$$J = e\, n_o\, \mu\, V/W \quad . \tag{1.15}$$

At sufficiently high applied voltages, the contribution to the current density due to the injected electrons dominates and it is given by (1.6). The cross-over voltage V_Ω at which the average density of injected electrons equals the thermal density is found by equating the two contributions. This yields

$$V_\Omega = (8/9)\, e\, n_o\, W^2/\varepsilon\varepsilon_o \quad . \tag{1.16}$$

One of the requirements for observing unipolar sclc in a solid is implicit in this relation, namely, that the dielectric relaxation

time of the crystal, $\varepsilon\varepsilon_o/\mu n_o e$, must be large as compared to the transit time of the charge carriers.

In the transition region, the solution must be found numerically by tabulating values for $1/\omega_c$ and v_c/ω_c^2 vs u. The solution for the entire dc characteristic is given as a normalized log-log plot in figure (1.2).

Up to now, we have considered injection of electrons into an n-type crystal. Another possibility is to study injection of electrons into a p-type crystal. The energy band scheme is illustrated in figure (1.1b). The dc characteristics are greatly affected by the density of p-type impurities in the crystal, in particular, at low applied voltages. One of the junctions is always reverse biased and, consequently, appreciable current will not flow until the base region is depleted of mobile holes and the electric field reaches the electron emitting contact. Since the crystal is p-type, the density of thermal electrons can be neglected. Under the previous set of conditions, the differential equation which governs the current flow is

$$- J = \mu\varepsilon\varepsilon_o E \frac{dE}{dx} - \mu\varepsilon\varepsilon_o e N_I E \quad , \tag{1.17}$$

where N_I is the density of impurities in the crystal, assumed to be independent of x and totally ionized. Thus, (1.17) describes the

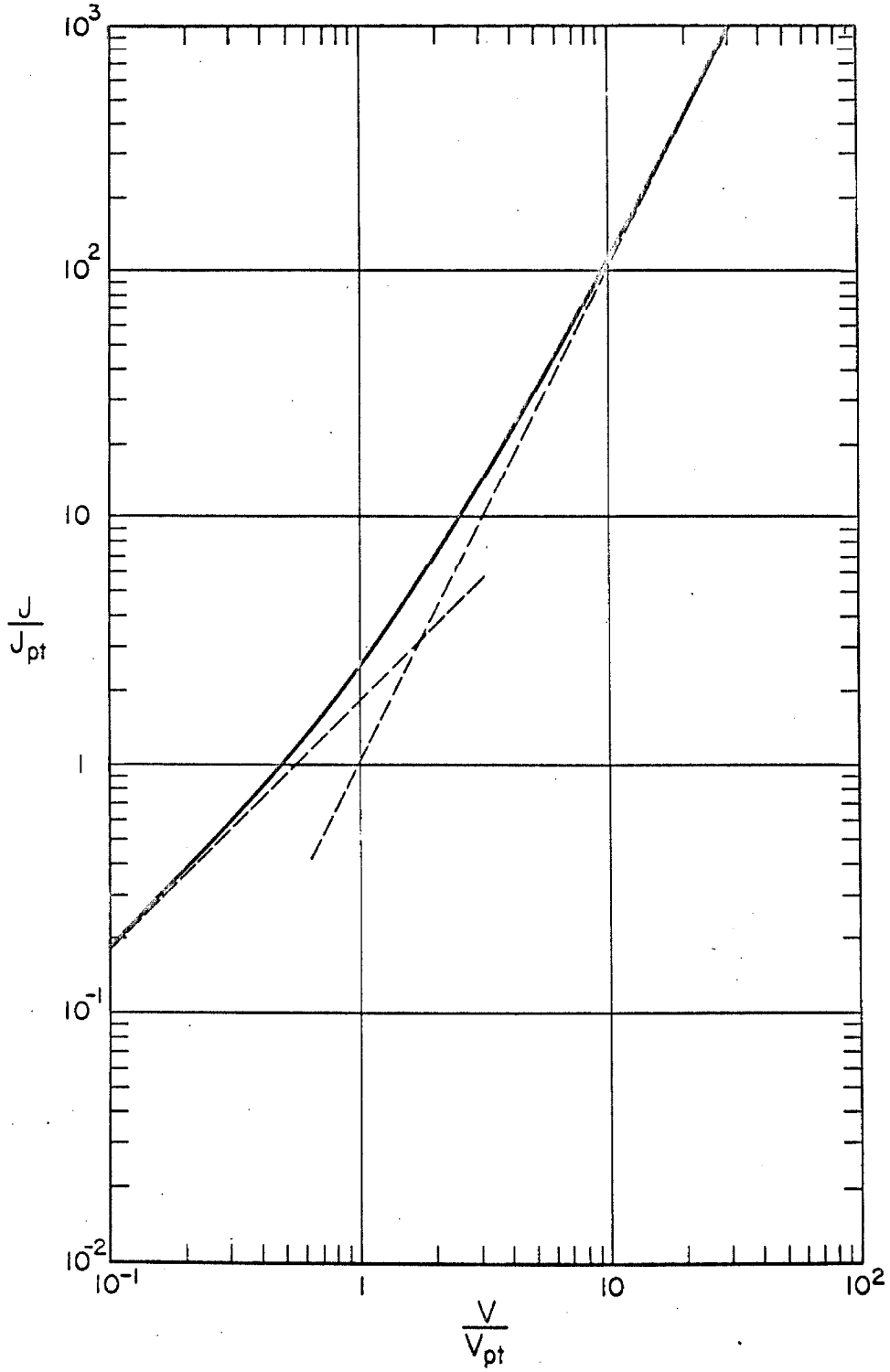

Figure 1.2

current flow after the mobile holes have been removed from the bulk. The voltage required to deplete the crystal is referred to as punch-through (V_{pt}) since, at this threshold, the depletion regions of the forward and reverse biased contacts meet and electrons can be readily injected into the base. Its value is found by integrating (1.17) with $J = 0$, which yields

$$V_{pt} = \frac{e\, N_I\, W^2}{2\varepsilon\varepsilon_o} \quad . \tag{1.18}$$

Below V_{pt}, the behavior is that of a floating base transistor. This range will not be explored any further analytically because of the complications involved. A qualitative description is given in section (3.2.1).

The solution of equation (1.17) has been obtained by Shockley and Prim[1.3]. A closed form expression for J as a function of V is not possible, except at high applied voltages where the behavior is described by (1.6). It is convenient to introduce J_{pt} and V_{pt} related by the expression

$$J_{pt} = 9/8\ \varepsilon\varepsilon_o \mu\ V_{pt}^2/W^3 \quad . \tag{1.19}$$

This is the current density that would flow through the structure if the resistivity of the crystal was infinite. J and V are then given by

$$J = J_{pt}\ (32/9)\ [e^{\beta} - \beta - 1]^{-1} \qquad (1.20)$$

and

$$V = V_{pt}\ (e^{2\beta} - 4\ e^{\beta} + 2\ \beta + 3)\ (e^{\beta} - \beta - 1)^{2}\ , \qquad (1.21)$$

where

$$\beta = t\mu\ e\ N_I/\epsilon\epsilon_o$$

and t is the transit time for the electrons in a crystal of thickness W. In the limit, for $\beta \to 0$,

$$J/J_{pt} \to\ (V/V_{pt})^{2}\ , \qquad (1.22)$$

as expected when the density of injected electrons more than compensates the effect of ionized impurities in the crystal. The solution for the entire dc characteristic is given as a normalized log-log plot in figure (1.3).

The previous model can be easily extended to account for the presence of trapping centers distributed uniformly throughout the crystal. The threshold voltage at which the current density increases sharply to the pure unipolar sclc value is now given by the density of ionized impurities and empty trapping centers at thermal equilibrium. Physically, threshold is the voltage required to deplete the base region of mobile holes and to fill the empty trapping states N_T. It is given by the expression

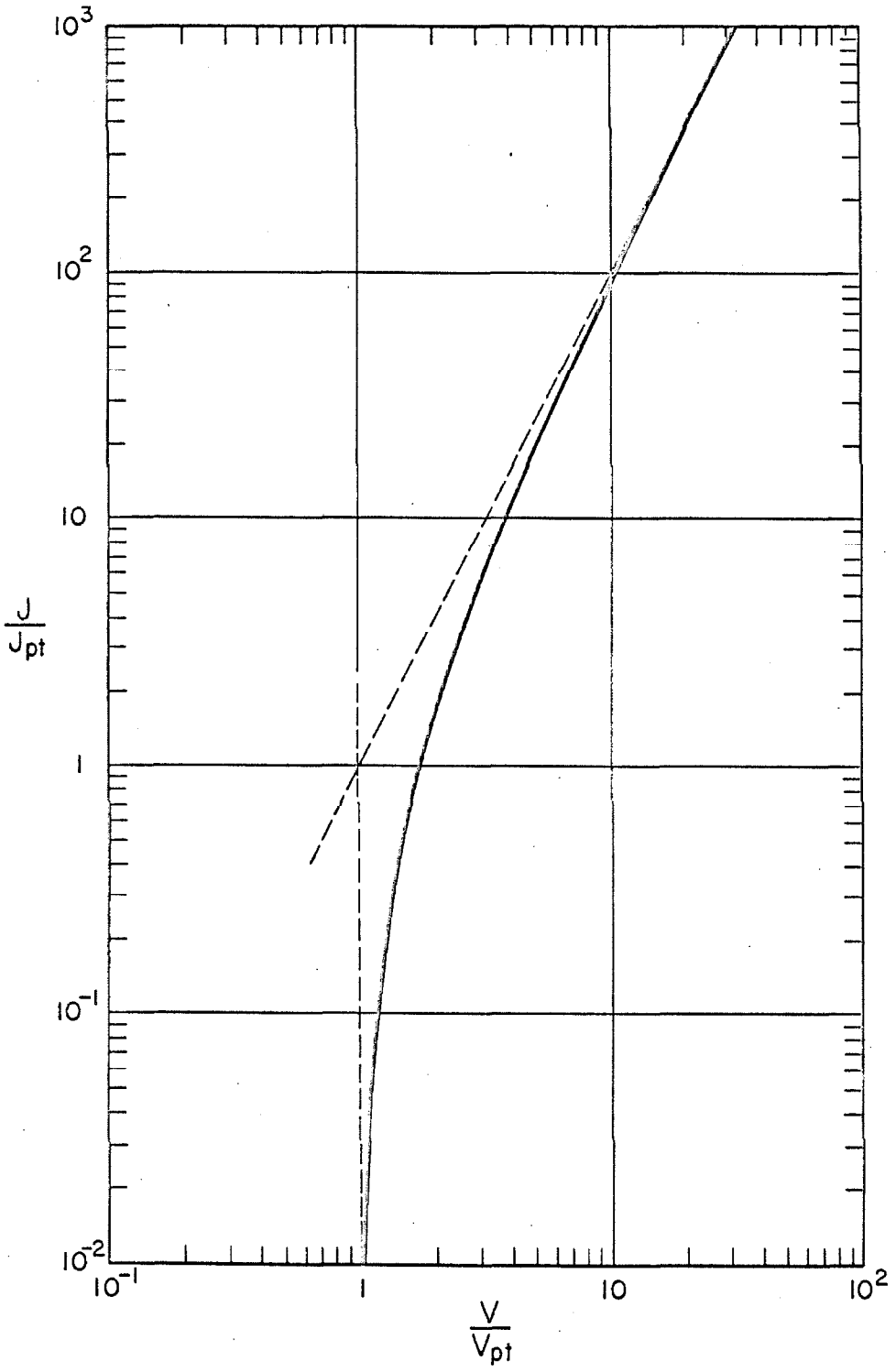

Figure 1.3

$$V_{Th} = \frac{eW^2}{2\varepsilon\varepsilon_o}(N_T + N_I). \qquad (1.23)$$

The solution of (1.17), again, holds for applied voltages above V_{Th}. Below V_{Th}, the current density can have literally any dependence on applied voltage depending on the distribution in energy and the density of trapping centers. Thus, it is more realistic to look at this range, for the specific cases at hand, in the context of the experimental results as is done in section 3.2.1. In general, trapping is disregarded entirely in this chapter and dealt with in the above mentioned section only to the extent of describing its effect on the V-I characteristics obtained experimentally for the various structures.

The restriction of a field independent mobility is now lifted and the complete field-velocity relationship is taken into consideration. The mobility dependence on the electric field is assumed to be of the form shown in figure (1.4). At low electric fields, the mobility is a constant and, at high electric fields, the drift velocity is a constant. The transition region for intermediate field strengths is approximated by various empirical relations.

If, in deriving expressions (1.20) and (1.21), the assumption of a constant drift velocity is made, a two-fold integration of Poisson's equation yields

$$J = 2\varepsilon\varepsilon_o v_s \frac{V - V_{Th}}{W^2} \qquad (1.24)$$

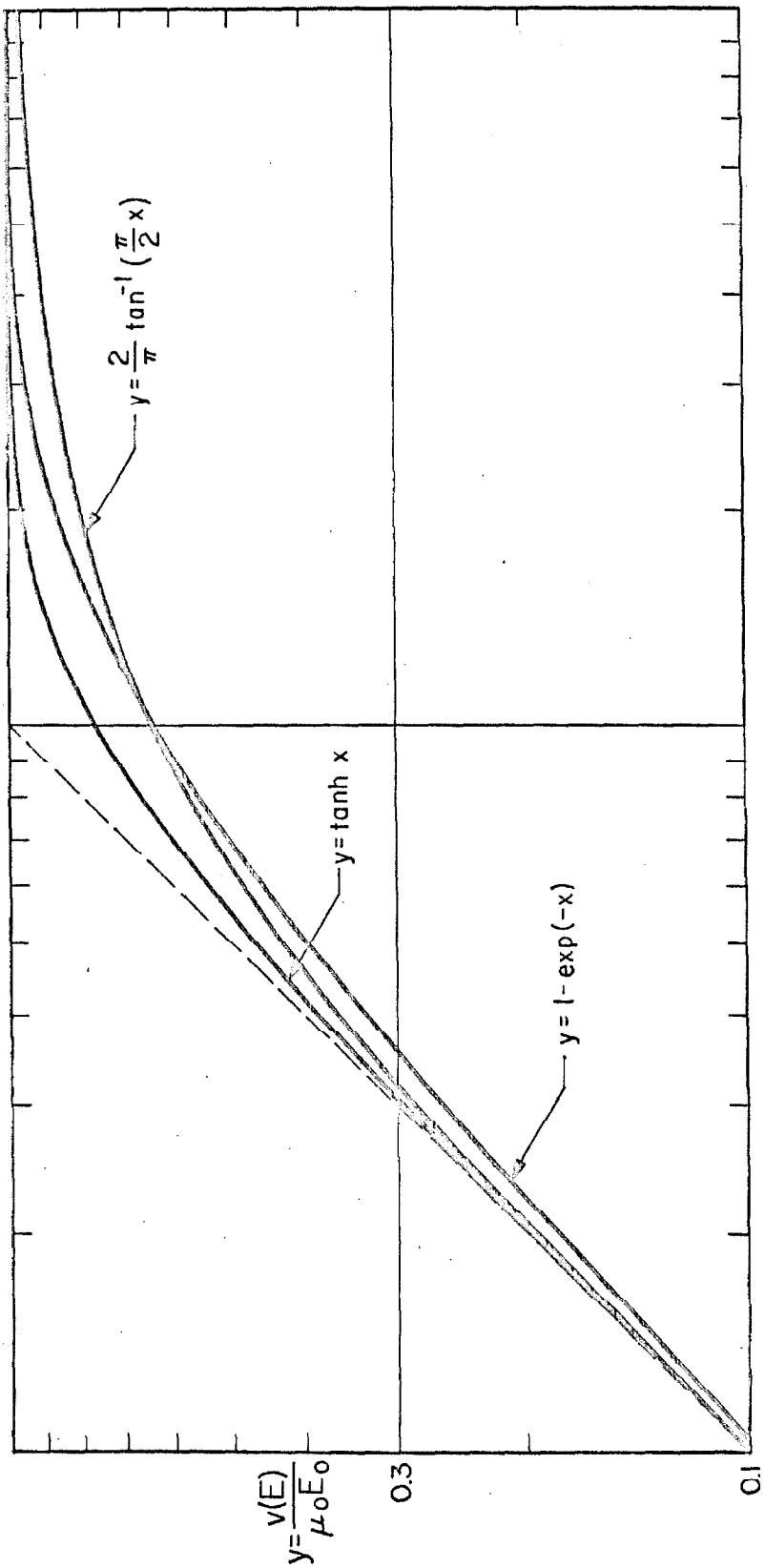
$y = \frac{2}{\pi} \tan^{-1}\left(\frac{\pi}{2} x\right)$
y = tanh x
y = 1 - exp(-x)
$y = \frac{v(E)}{\mu_o E_o}$
0.3
0.1
$x = \frac{E}{E_o}$

Figure 1.4

where V_s is the limiting value of the drift velocity. The current density increases linearly with applied voltage above threshold. This relation assumes that the built-in electric field is of enough strength at threshold to bias the entire crystal in the limiting velocity range of the field-velocity relationship. This model is of particular significance in evaluating the limiting velocity from pure unipolar sclc measurements. Equation (1.24) is illustrated as a normalized log-log plot in figure (1.5).

The two limits of the field-velocity relationship have now been considered in the context of the various approximations to the equations governing the current flow. There remains to study the effect of the transition region in the dc characteristics. This is done for the simplest possible case which assumes an ideal insulator-no impurities, traps, or thermally generated carriers. The contribution of diffusion to the current flow is once again neglected. Under this set of conditions, equation (1.4) reduces to

$$- J = \varepsilon\varepsilon_o \, v(E) \, \frac{dE}{dx} \quad . \tag{1.25}$$

The electric field and the potential are assumed zero at the emitter interface. Three empirical relations are considered for v(E), namely,

$$v(E) = v_s \tanh (E/E_o) \, , \tag{1.26}$$

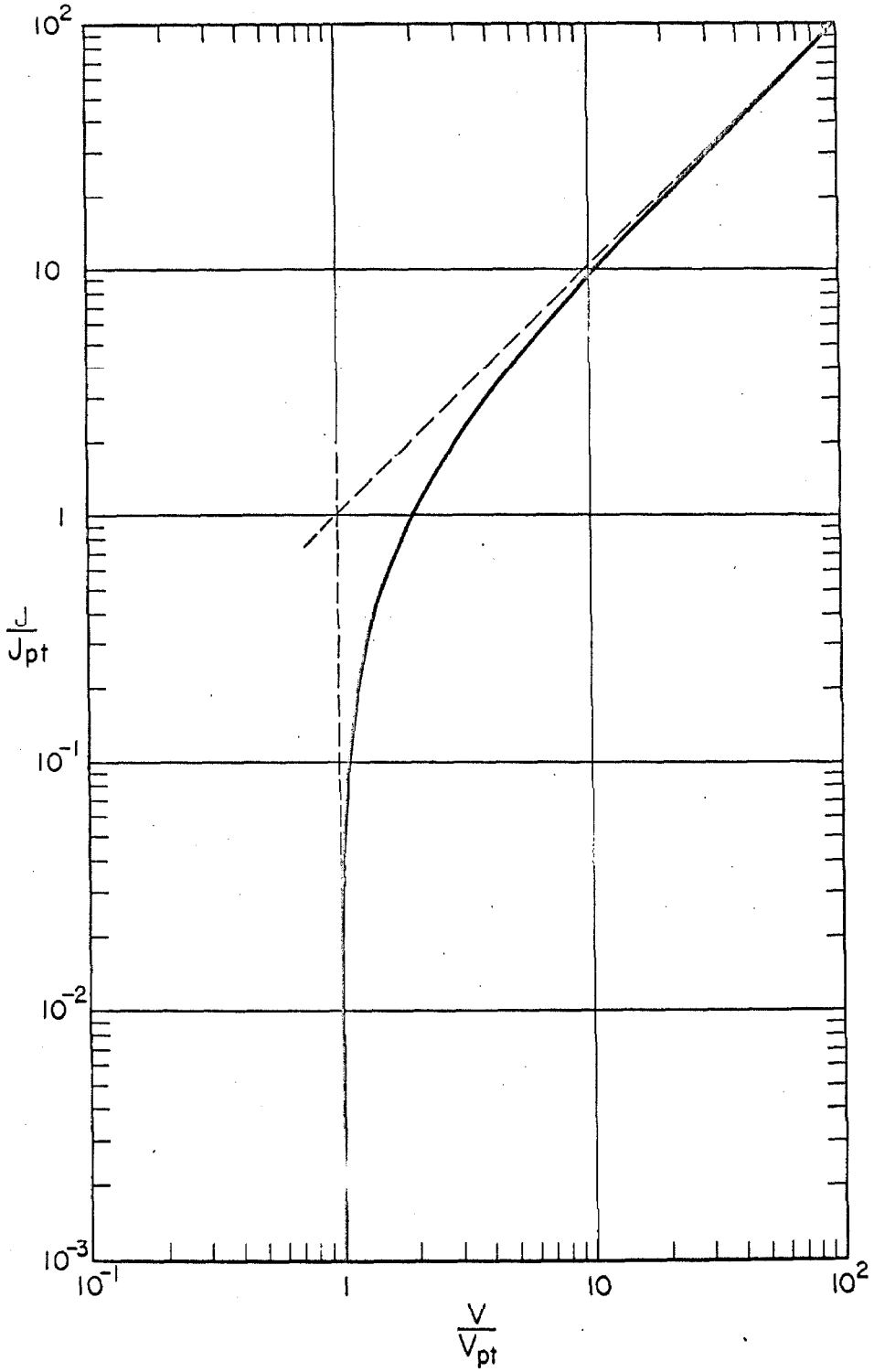

Figure 1.5

$$v(E) = v_s \left[1 - \exp\left(-E/E_o\right)\right] \quad , \tag{1.27}$$

and

$$v(E) = 2/\pi \; v_s \tan^{-1}\left(\pi/2 \cdot E/E_o\right) \tag{1.28}$$

E_o is the electric field intercept of the low and high field assymptotic to v(E). The previous relations are shown in figure (1.4). The solution of (1.25) cannot be accomplished analytically for any of the three cases, consequently, it is necessary to resort to a numerical evaluation of the differential equations[1.6]. The dc characteristics obtained in this fashion are shown in figures (1.6), (1.7) and (1.8). The three characteristics are very similar in appearance, as illustrated in figure (1.9). However, if the measurements of pure unipolar sclc exhibit well defined square and linear ranges, it should be possible to obtain a good determination of the actual field-velocity relationship by fitting various empirical relations to the experimental data. This is demonstrated in chapter 3. Moreover, if measurements can be carried out in a large number of identical structures, the statistical determination of the drift velocity as a function of the electric field should be in good agreement with the true relationship.

Finally, if the thermal concentration of electrons is high enough, a range exits in which hot carrier effects are observed before

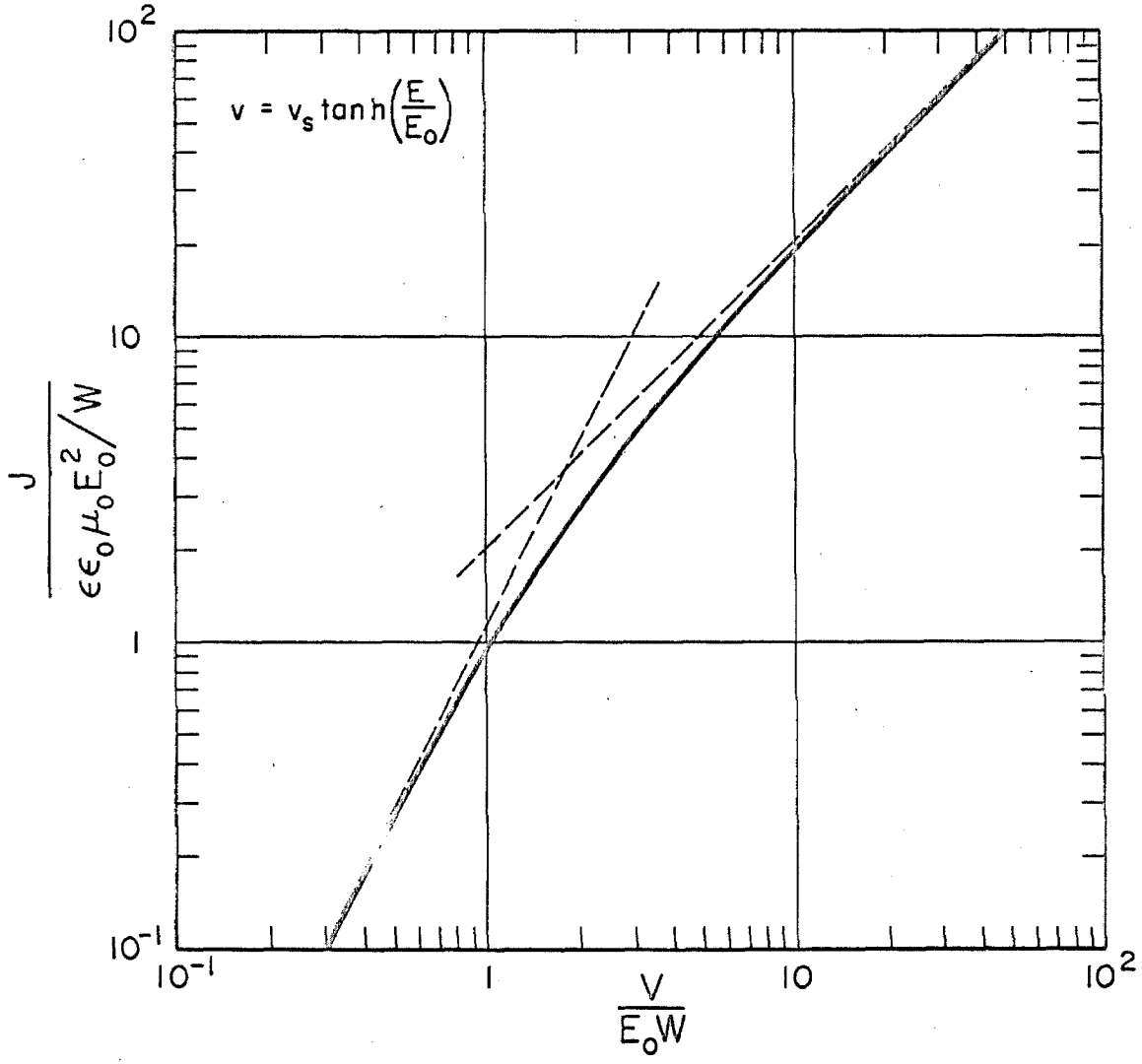
$v = v_s \tanh\left(\frac{E}{E_o}\right)$
10^2
10
1
10^{-1}
10^{-1}
1
10
10^2
$\frac{J}{\epsilon\epsilon_o\mu_o E_o^2/W}$
$\frac{V}{E_o W}$

Figure 1.6

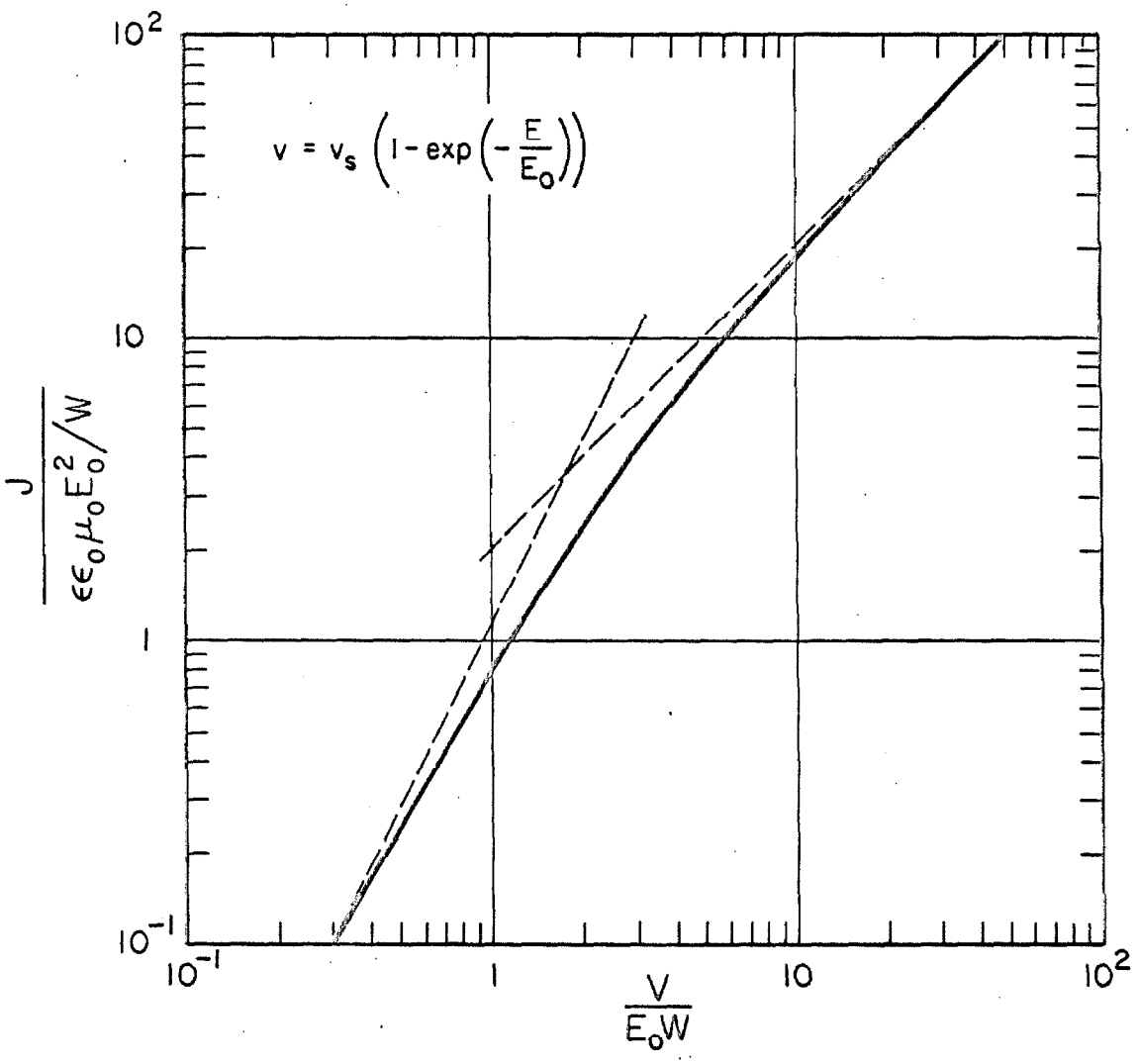
$v = v_s\left(1-\exp\left(-\frac{E}{E_0}\right)\right)$
10^2
10
1
10^{-1}
10^{-1}
1
10
10^2
$\frac{J}{\epsilon\epsilon_0\mu_0 E_0^2/W}$
$\frac{V}{E_0 W}$

Figure 1.7

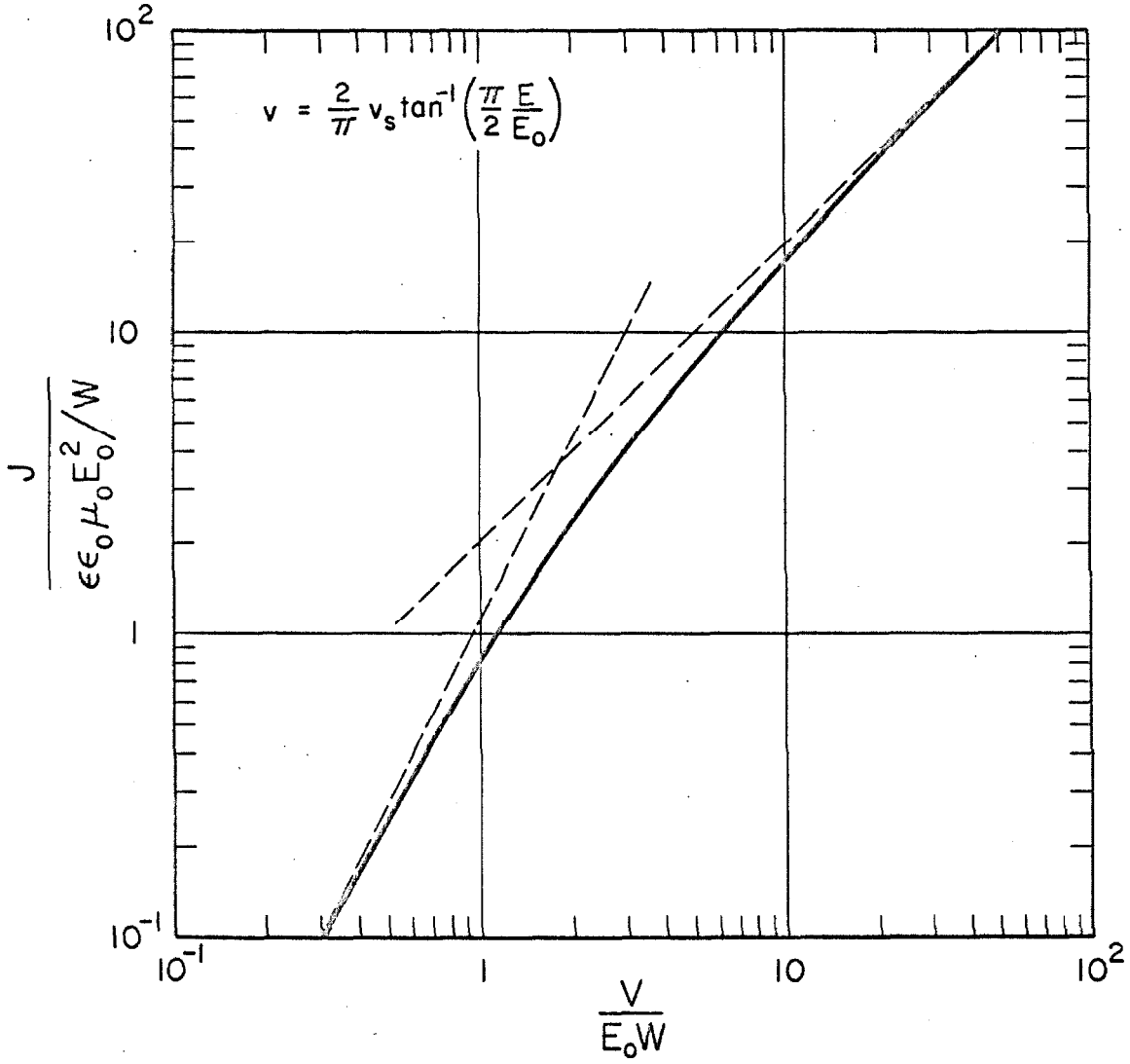
$v = \frac{2}{\pi} v_s \tan^{-1}\left(\frac{\pi}{2}\frac{E}{E_o}\right)$
10^2
10
1
10^{-1}
10^{-1}
1
10
10^2
$\frac{J}{\epsilon\epsilon_o\mu_o E_o^2/W}$
$\frac{V}{E_o W}$

Figure 1.8

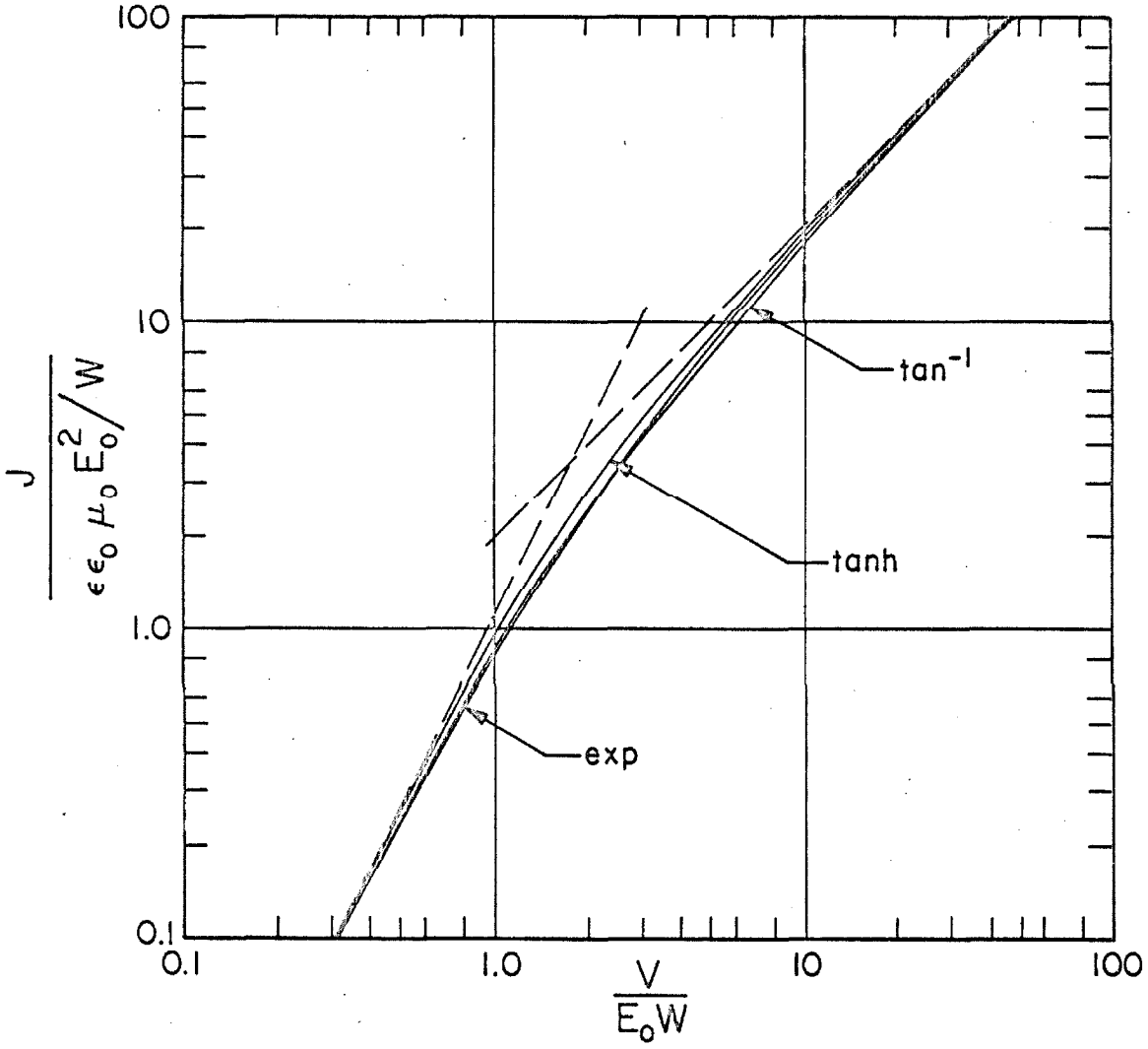
100
10
1.0
0.1
0.1
1.0
10
100
$\frac{J}{\epsilon\epsilon_0\mu_0 E_0^2/W}$
$\frac{V}{E_0 W}$
tan⁻¹
tanh
exp

Figure 1.9

the onset of unipolar sclc. In such a case, the current density is given by

$$J = n_o e v(E) + 2\varepsilon\varepsilon_o v_s V/W^2 \quad . \tag{1.29}$$

Figure (1.10) illustrates this relationship with $v(E) = v_s \tanh (E/E_o)$. The assumption is made that, in the thermal range, the drift velocity has reached the limiting value v_s before the injected carriers dominate the current flow. This model has relevance, primarily, in evaluating the field-velocity relationship obtained from measurements of ohmic flow in crystals, as will be seen in section 3.2.4.

We have now covered those models for pure unipolar sclc which are pertinent to the present investigation, except for trapping which will be dealt with - due to its complexity - in the context of the experimental V-I characteristics. It is unfortunate that a unified theory for unipolar sclc is impossible, but on the other hand, it is fortunate that a simple measurement of the dc characteristics of a crystal, provided with at least an ohmic contact, can yield so much information about its nature. The large number of models mentioned in this section to describe various aspects of the general phenomenon of sclc demonstrate the complexity of the general situation.

1.3 Temperature Dependence. Pure unipolar sclc depends upon lattice temperature through the variation of the material dependent parameters, i.e., the dielectric constant and the drift velocity of the carriers.

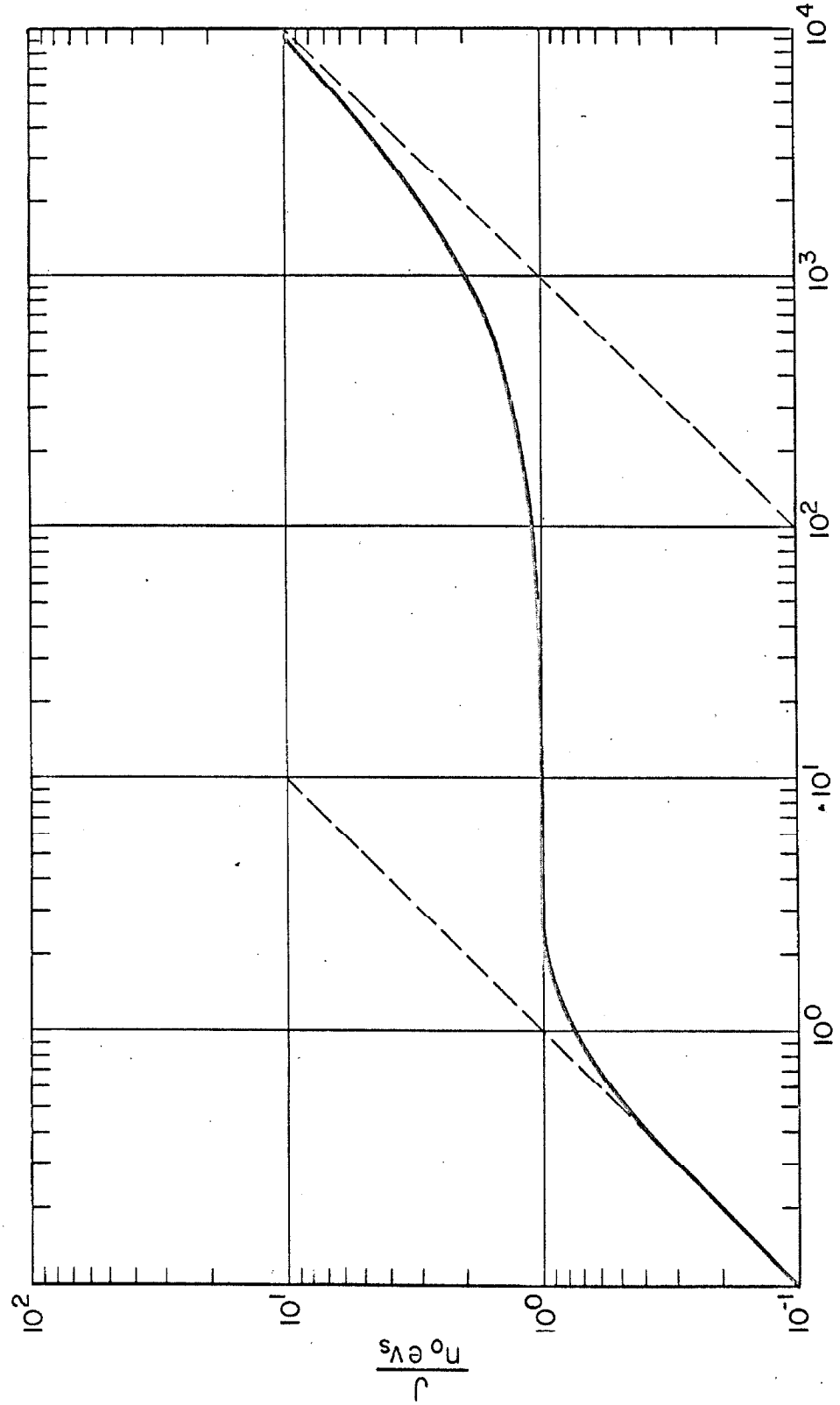

Figure 1.10

The dielectric constant is impervious to temperature variations in high purity materials.[1.7-8] Consequently, any change with temperature of pure unipolar sclc reflects the dependence of the field velocity relationship. If this relationship is such that a constant drift velocity is achieved beyond a critical field E_o, the dc characteristics of structures which exhibit the behavior prescribed by equation (1.24), will yield directly the temperature dependence of v_s. Breakdown phenomena are the only major experimental limitations of this technique. The low field mobility can also be easily obtained from any sclc structure which exhibits a V^2 dependence for J over the prescribed temperature range.

The present investigation establishes that, for silicon oriented along the [111] direction, a limiting drift velocity for electrons exists in the temperature range $4.2 \leq T \leq 300^{o}K$. On the other hand, Gunn et al.[1.9] have established that below $77^{o}K$ germanium oriented along the [100] direction exhibits a negative differential mobility for electrons at field strengths above 1 or 2 kilovolts/cm. In this instance, the dc characteristic of pure unipolar sclc should exhibit instabilities as observed in the Gunn effect. The remaining alternative is for the drift velocity to increase monotonically with increasing field strength, in which case, the dc characteristics always exhibit a voltage dependence larger than V. It follows that pure unipolar sclc provides quantitative

information on the temperature dependence of the drift velocity at high field strengths only when velocity saturation is present. Nevertheless, it also provides a simple method with which to establish the general behavior of the field velocity-relationship as a function of temperature.

CHAPTER II

STRUCTURE FABRICATION, EVALUATION AND METHOD OF MEASUREMENT

Two series of structures were used in this work, called here D- and R-structures. The procedure utilized to fabricate D-structures has been described elsewhere.[2.1] Information on the manufacturing process of R-structures follows, preceded by brief considerations on some general requirements these structures must meet.

The major problem to solve when unipolar sclc is to flow through a solid is that of finding a suitable injecting or ohmic contact. This contact, by definition, has a large reservoir of carriers which can be readily injected into the base under forward bias. The problem is aggravated if the contact is required to retain this property throughout the temperature range $4.2^{o} \leq T \leq 300^{o}K$. A nondegenerate diffused or alloyed contact is unsuitable because at low temperatures it becomes an extension of the insulating bulk and presents an energy barrier to the electrons at the metal contact. Degenerate material, on the other hand, behaves like a metal at low temperatures and presents a very small barrier to the electrons entering the base. This type of contact has been attained by diffusing phosphorus or boron, for an n^{+} or a p^{+} contact, respectively, into the bulk from a constant concentration at the surface well in excess of the solid solubility limit for silicon.

P-type silicon of 2000Ω - cm resistivity before diffusion and oriented along the [111] crystalographic direction has been employed to manufacture R-structures. Up to the diffusion step, the technique used is essentially the same that applies for the D-structures. A wafer is first cut from an ingot with a diamond saw, then lapped with silicon carbide 400, 800, 1600 and 3200 mesh to the desired thickness and finally polished with two diamond compounds 0.5, 0.2 microns. The wafer is etched immediately after it has been thoroughly cleaned to remove all residues of the lapping and polishing compounds and to eliminate the mechanically damaged layer. The surfaces must be essentially free of damage since the junctions are shallow and irregularities on the surface would be reflected in the junction profile. After this etching, the wafer is again cleaned thoroughly right before it is placed for two hours in a furnace with an oxygen atmosphere at 920°C. The thickness of the oxide grown is approximately 0.5 microns. One of the surfaces (top) is now masked with circular dots eight mils in diameter and twenty mils apart. The oxide is removed everywhere from the opposite side (bottom). The wafer is now ready for diffusion. This step is carried out at 1070°C. The carrier gas, N_2 or O_2, is allowed to flow through $POCl_3$ and the furnace where it is reduced at the surface of the wafer which is placed on its edge to expose both sides. The wafer is kept on the furnace for no longer than fifteen or twenty minutes. The resulting surface concentration of phosphorus exceeds

10^{20} cm^{-3} as determined by sheet resistivity (V/I approximately 0.75) and junction depth measurements.

To mask one side of the wafer only simplifies the procedure greatly. If both sides were masked, the circular openings in the oxide would have to be carefully aligned. Also, before testing, the structures would have to be scribed and broken into individual devices. The thin oxide grown on the surface during diffusion has to be removed before measurements can be performed on the structures. In the meantime, it serves as a protection against contamination from the environment during storage and transport which, otherwise, might change the characteristics of the device. The procedure outlined above applies equally well for $p^+p\ p^+$ structures. The carrier gas in the diffusion step is allowed to flow through BBr_3 instead of $POCl_3$, in order to dope the crystal p^+ at the surface. The furnace is preheated to 1150°C and the diffusion time is, again, of the order of 15 minutes.

The structures are not canned because: (1) it is complicated, (2) it is not essential, electrically and (3) it would spoil the thermal properties of the structures, as will be demonstrated in chapter 3. A pressure contact is used for testing. Since the surfaces are highly degenerate, no appreciable error is expected from the contact resistance. It is also advisable not to bond leads to such shallow doped layers because they could cause irregularities in and damage to the diffusion profile.

The thickness and area of the structures have been determined with a calibrated microscope. The junction depth, in the case of D-structures, has been measured by an angle lap and staining technique. Typical values vary from 2 to 3 microns. An accurate determination of the junction depth of the R-structures has not been carried out. However, from the diffusion time and the resistivity of the material, it is not expected to exceed that of the D-structures. Since the current flow in the R-structures is not unidirectional, it is only possible to prescribe the area of the masked circular dots in the top side which have a diameter equal to 200 microns.

The electrical characteristics are measured with a saw-tooth voltage of variable duty cycle and rise time. A visual display of the V-I characteristics is preferred as long as the power dissipated in the structures is not excessive. The alternative approach is to apply a square wave voltage and obtain the characteristics point by point. However, in this particular instance, that is not practical since, as will be described in the subsequent paragraph, the temperature of the sample cannot be kept constant for a reasonable length of time except at the extremes of the temperature range covered. A block diagram of the electrical apparatus used is given in figure (2.1). The circuit diagram of the saw-tooth amplifier is given in figure (2.2). The capacitance of the sample holder and its leads to the cryostat limits the acceptable minimum pulse width to approximately 2 microseconds.

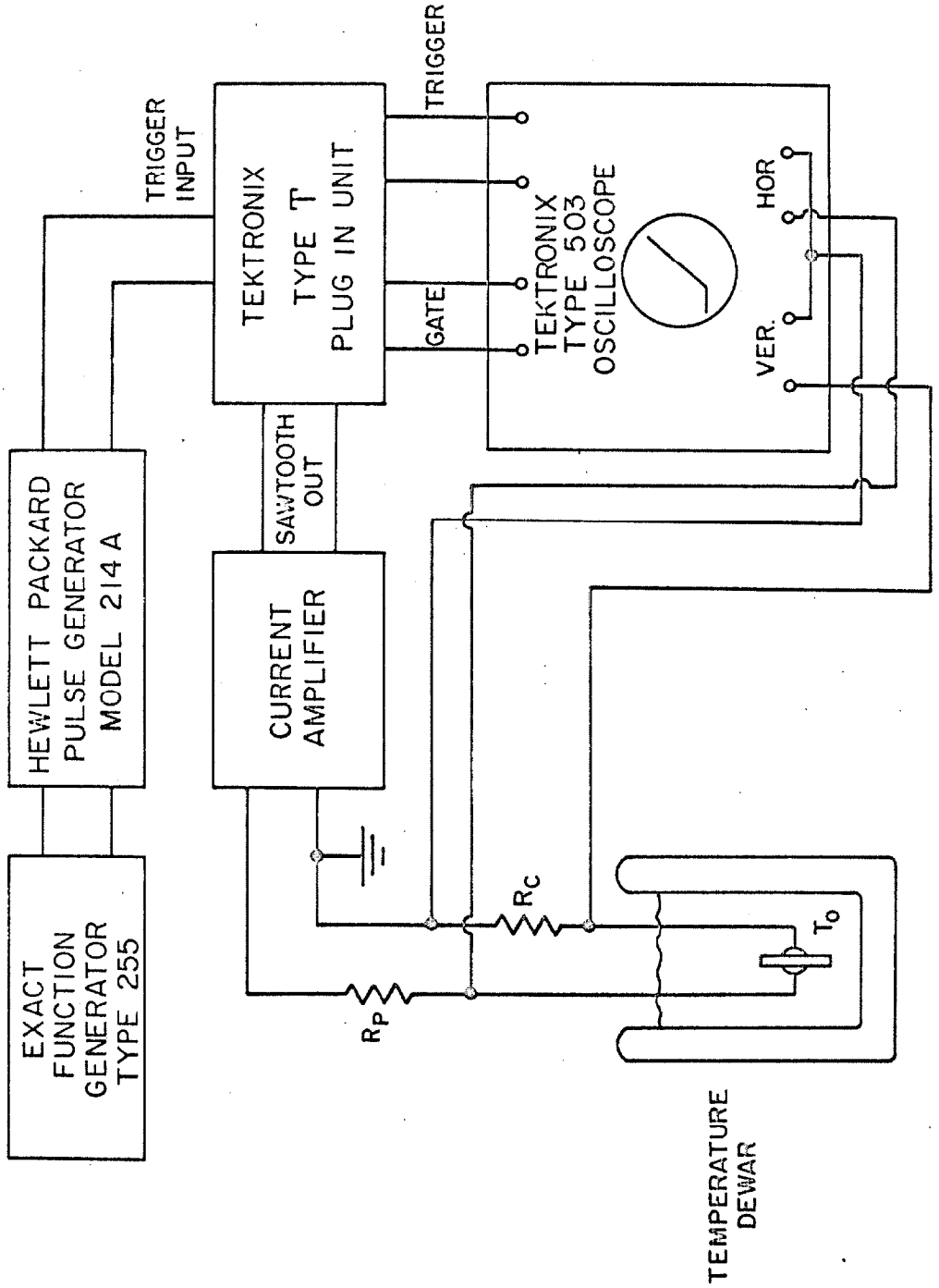
EXACT FUNCTION GENERATOR TYPE 255
HEWLETT PACKARD PULSE GENERATOR MODEL 214 A
TRIGGER INPUT
TEKTRONIX TYPE T PLUG IN UNIT
TRIGGER
GATE
SAWTOOTH OUT
CURRENT AMPLIFIER
TEKTRONIX TYPE 503 OSCILLOSCOPE
HOR
VER.
R_P
R_C
T_o
TEMPERATURE DEWAR

Figure 2.1

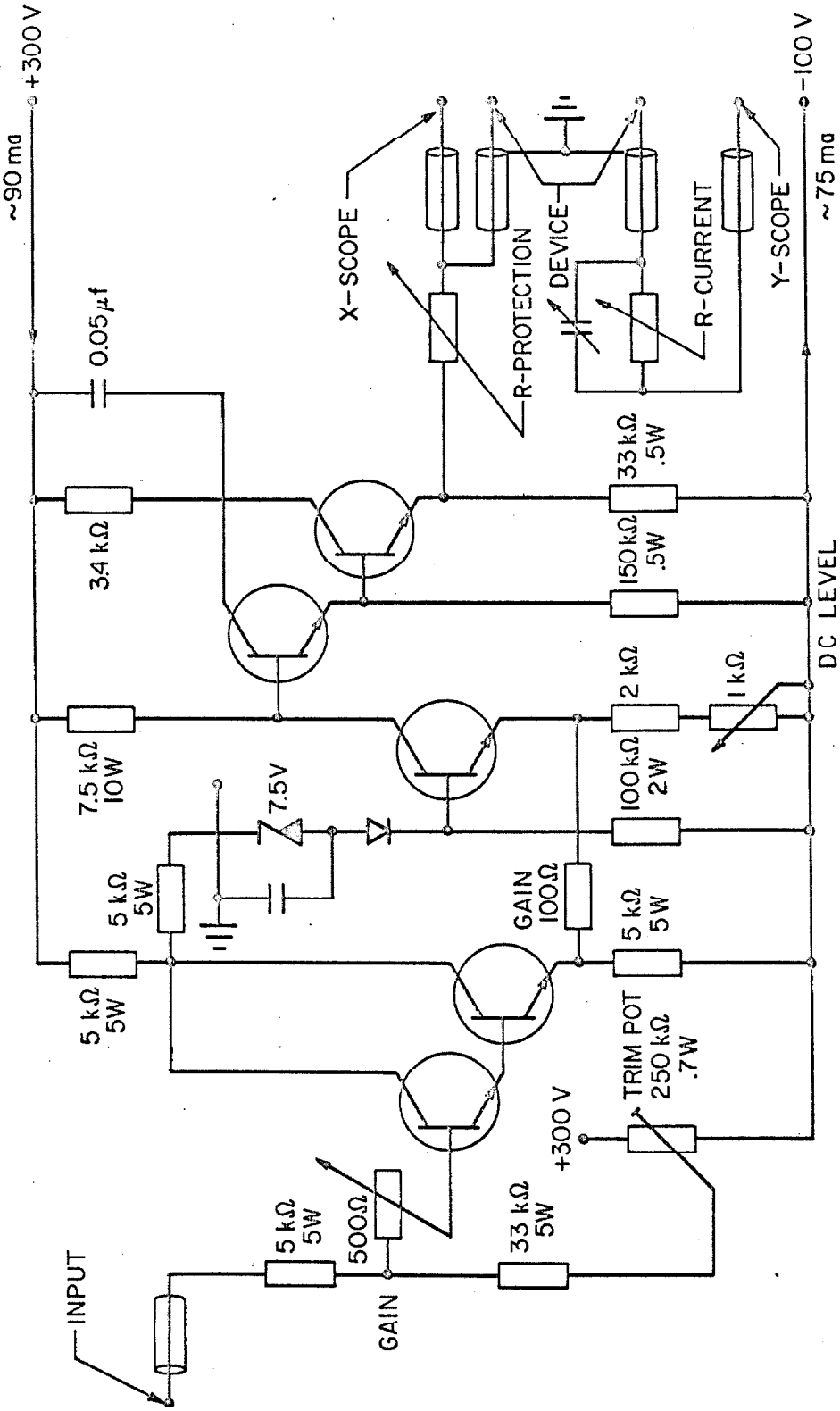
~90 ma
+300 V
0.05 μf
3.4 kΩ
7.5 kΩ 10W
5 kΩ 5W
5 kΩ 5W
INPUT
5 kΩ 5W
500Ω
GAIN
33 kΩ 5W
+300 V
TRIM POT 250 kΩ .7W
7.5V
GAIN 100Ω
5 kΩ 5W
100 kΩ 2W
2 kΩ
1 kΩ
DC LEVEL
33 kΩ .5W
150 kΩ .5W
X-SCOPE
R-PROTECTION
DEVICE
R-CURRENT
Y-SCOPE
-100 V
~75 ma

Figure 2.2

Single shot measurements were used, primarily, to check against excessive heating caused by the duty cycle. DC measurements were carried out with a Keithley 610 B electrometer up to 10^{-5} amps. From this current level up to 5.10^{-3} amps, a Hewlett-Packard Harrison 6207B DC power supply was used as a constant current source and the voltage and current were measured with two Dynamics D.C. Micro Volt-Ammeter Model 4072.

Measurements were performed over the range of environmental temperatures $4.2 \leq T \leq 300^{o}K$ in a double-dewar cryostat. The structures were mounted in a light tight, vacuum tight, and electrostatically shielded sample holder which consists of: (1) a top made of brass where the vacuum valve is mounted and through which the electrical connections are taken out; (2) a high-purity-copper block where the structure, the thermometer, and the thermocouple are mounted; (3) a copper cap which encloses (2); and (4) a stainless steel tubing which joins (1) and (2). An indium O-ring is used to vacuum seal the cap to the copper block. The sample enclosure is thermally isolated from the top (at room temperature) by (4) which has a very small thermal conductivity at any temperature. Also, the electrical connections are taken out of this enclosure through sapphire beads - sapphire has a relatively large thermal conductivity at all temperatures - in order to short thermally the leads coming out of the enclosure to the copper block. In general, the sample holder was designed to reduce heat leaks

to a minimum and the choice of materials used is such as to meet this requirement. The leads were fed from the enclosure to the top in tension provided by four springs on the top mount, and separated from each other and the stainless tubing by pierced plastic disks placed along the way to the top. Figure (2.3) illustrates a top view of the copper block and a cross-sectional view of the entire sample holder. The temperature was measured with a germanium thermometer manufactured by Solitron, good in the range from 1.5° to 100°K. Above this range and up to 300°K, a chromel-alumel thermocouple was employed. Data were taken at the lowest temperatures by filling the cryostat with liquid He and N_2. After evaporation of the liquids, the temperature of the sample increases by the natural heat leakage of the system, in about three hours from 4.2° to 77°K, and roughly the same time from 77° to 300°K. An active control of the temperature was not attempted.

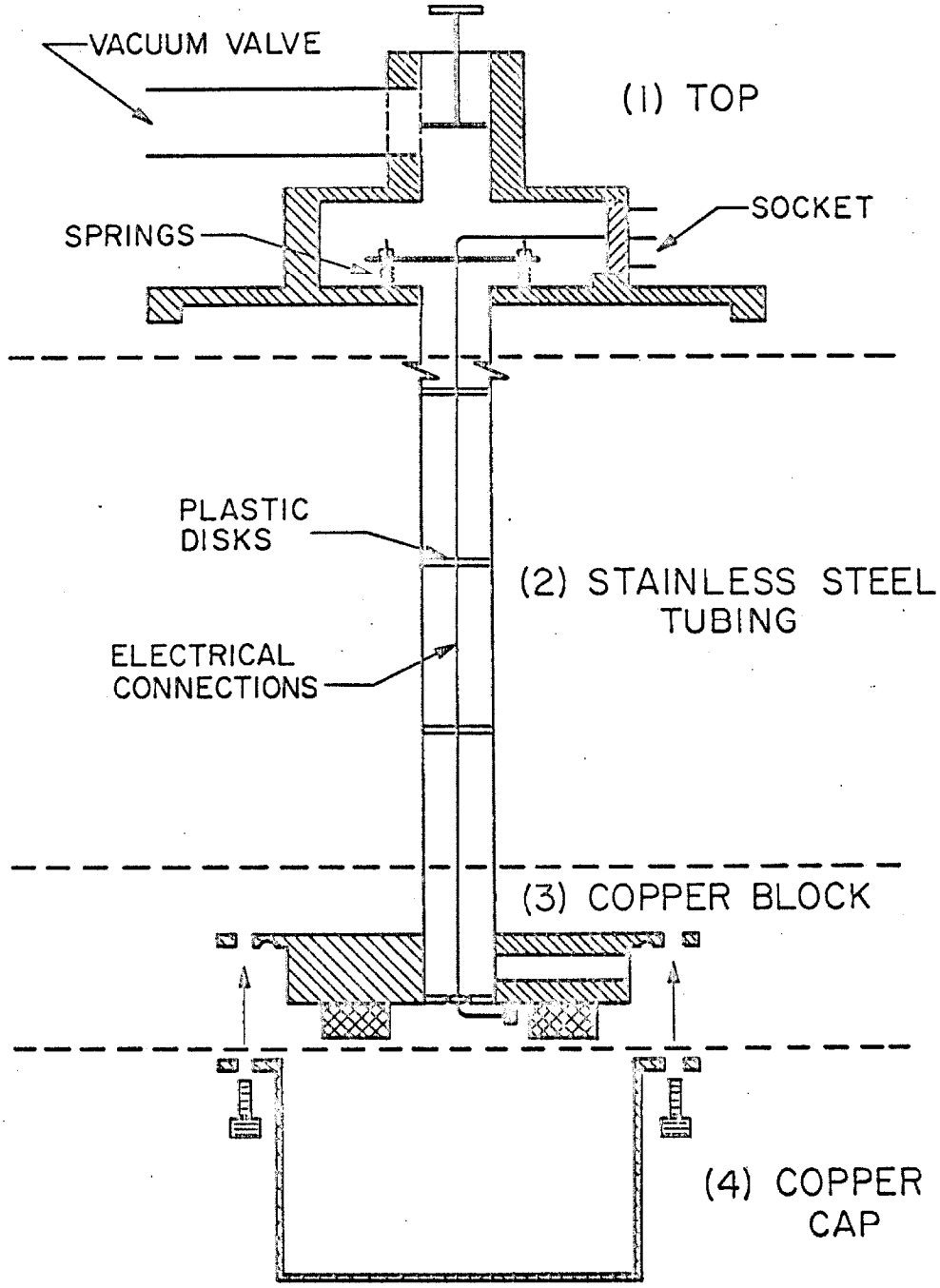
VACUUM VALVE
(1) TOP
SOCKET
SPRINGS
PLASTIC DISKS
(2) STAINLESS STEEL TUBING
ELECTRICAL CONNECTIONS
(3) COPPER BLOCK
(4) COPPER CAP

Figure 2.3a

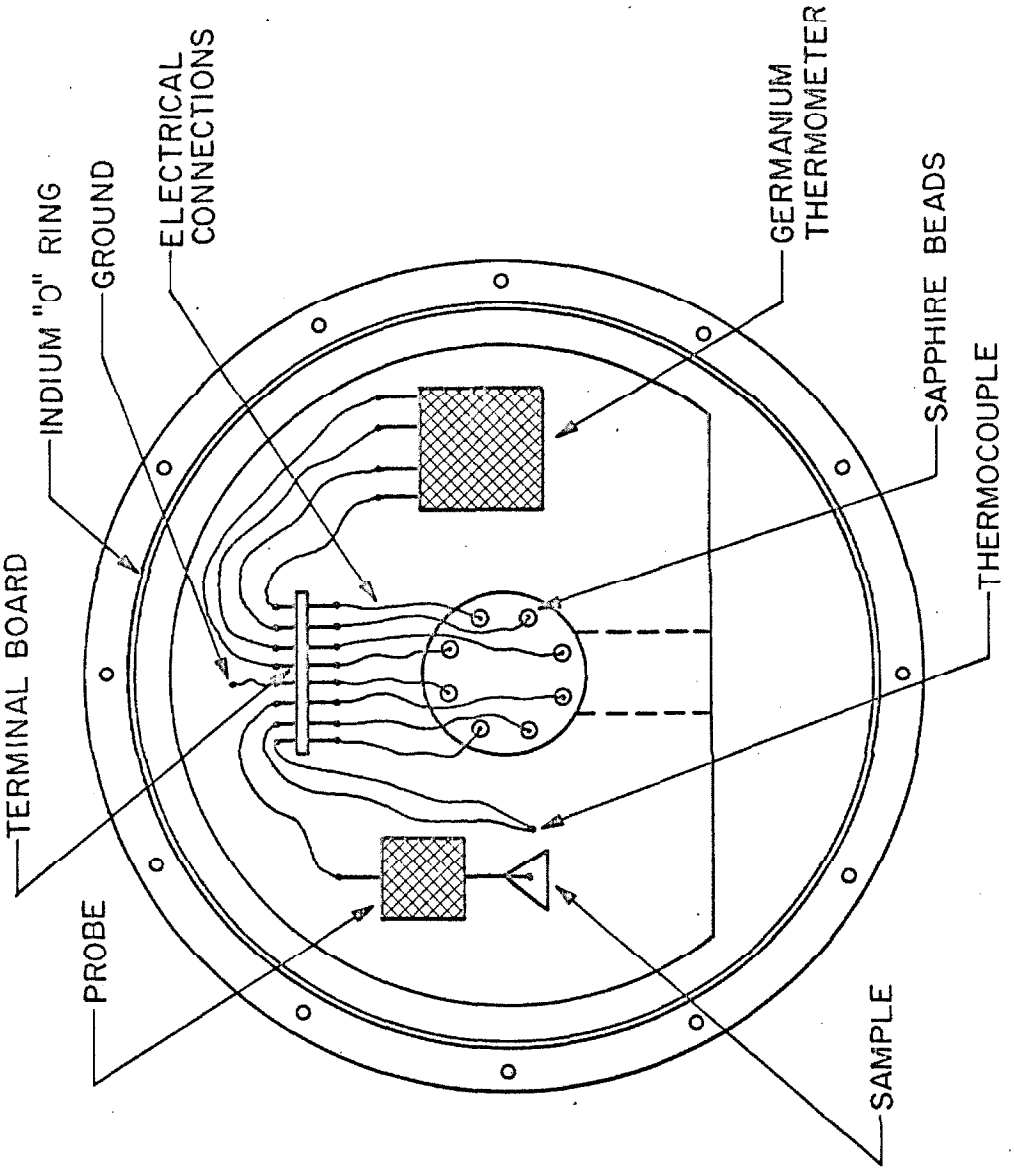
TERMINAL BOARD
INDIUM "O" RING
GROUND
ELECTRICAL CONNECTIONS
GERMANIUM THERMOMETER
SAPPHIRE BEADS
THERMOCOUPLE
PROBE
SAMPLE

Figure 2,3b

CHAPTER III

EXPERIMENTAL RESULTS

This chapter encompasses all the experimental results obtained from the three types of structures used in analyzing the flow of unipolar sclc in silicon, except for the temperature dependence of the limiting drift velocity which is presented in the next chapter. The emphasis is placed in understanding the underlying physical phenomena which determine the structure of the V-I characteristics. Little effort is made to provide quantitative treatments.

The V-I characteristics are covered through the entire range of applied voltages. The analysis is divided into two regimes, below and above threshold, and the influence of trapping and the field-velocity relationship are considered extensively. The threshold voltage is treated independently because of its remarkable content of information about the electronic properties of the material. Finally, the influence of the geometrical configuration and the thermal properties of the structures are reported and analyzed.

3.1 The threshold voltage. All V-I characteristics exhibit a threshold voltage at which the current density increases abruptly. Its value is in general dependent on the concentration of empty traps and ionized impurities in the crystal at a given temperature. (see section 1.1). D-structures have been manufactured from p-type

crystals whose resistivities are 200 and 2000 Ω-cm. before diffusion and 300 and 8000 Ω-cm., respectively, after diffusion. The thresholds observed for these structures are in accordance with what is expected theoretically for punch-through, as the analysis carried out with samples varying in thickness from 30 to 60 microns reveals. This, plus a few other tests performed - which are elaborated upon in relation with the R-structures - precludes the possibility of a large concentration of trapping centers for the injected charge carriers above 77°K. In this case, the threshold voltage is thus due to the doping of the crystal and is therefore punch-through.

R-structures have been manufactured from a p-type crystal whose resistivity is 2000 Ω-cm. before diffusion (the resistivity after diffusion has not been determined). In the same temperature range, $77^{o} \leq T \leq 300^{o}K$, these structures exhibit a clear threshold only in the vicinity of 77°K. There, its value is larger than what is expected for punch-through. The discrepancy can be explained by assuming a significant concentration of trapping centers in the bulk. Further evidence pointing towards their existence comes from the influence of illumination on the V-I characteristics.

Figure (3.1) depicts three characteristics measured in the same sample; (1) exposed to intense illumination, (2) exposed to room illumination, and (3) in the dark. It is observed that light reduces the threshold voltage. When trapped carriers are present, illumination

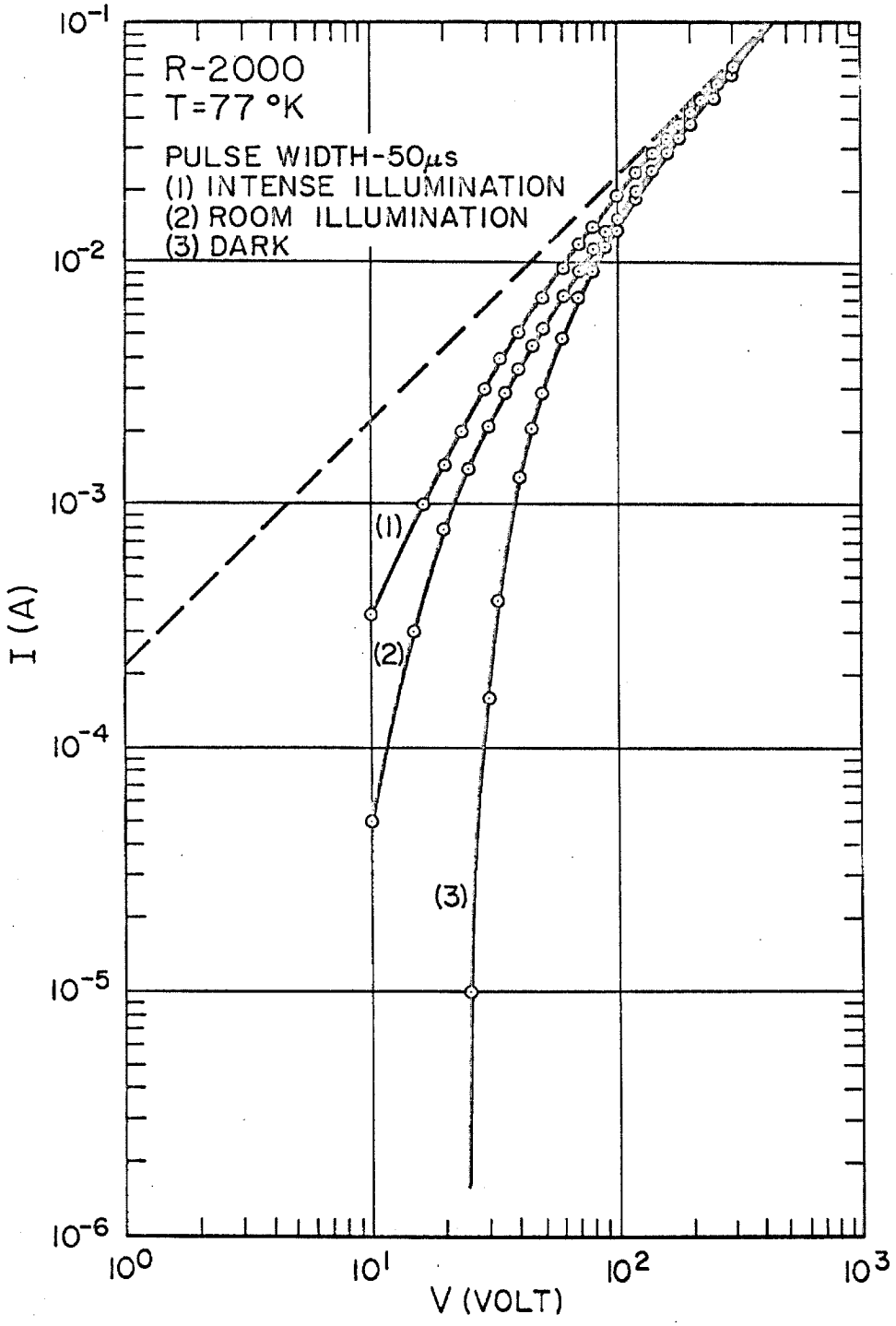
R-2000
T=77 °K
PULSE WIDTH-50μs
(1) INTENSE ILLUMINATION
(2) ROOM ILLUMINATION
(3) DARK
(1)
(2)
(3)
I (A)
V (VOLT)
10^-1
10^-2
10^-3
10^-4
10^-5
10^-6
10^0
10^1
10^2
10^3

Figure 3.1

will depopulate the traps and reduce the threshold voltage, as is observed. The effect is practically absent in D-structures, as figure (3.2) indicates. If the samples are illuminated through a silicon filter - to cut off wavelengths capable of causing band to band excitation - the effect is essentially the same for R-structures, while D-structures remain unaffected. Additional evidence is obtained when a double pulse, i.e., two voltage ramps whose separation in time is much smaller than their respective rise times, is applied to an R-structure. It is observed that the threshold voltage of the second pulse is larger than that of the initial pulse, similar to the result illustrated in figure (3.1). This cannot be accounted for by the temperature dependence of punch-through (see section 3.1.1), since heating of the sample would cause a change in the opposite direction. Also, as the repetition rate or the rise time of the pulses is increased, the effect diminishes and eventually disappears, as expected if traps are the cause of the effect.

Hence, enough evidence has been gathered to state conclusively that over the temperature range $77^{o} \leq T \leq 300^{o}K$, the threshold of D-structures is determined by punch-through and that of R-structures by trapping. Below $77^{o}K$, all structures exhibit giant trapping and the threshold voltage is determined by the density of ionized donors and neutral acceptors.

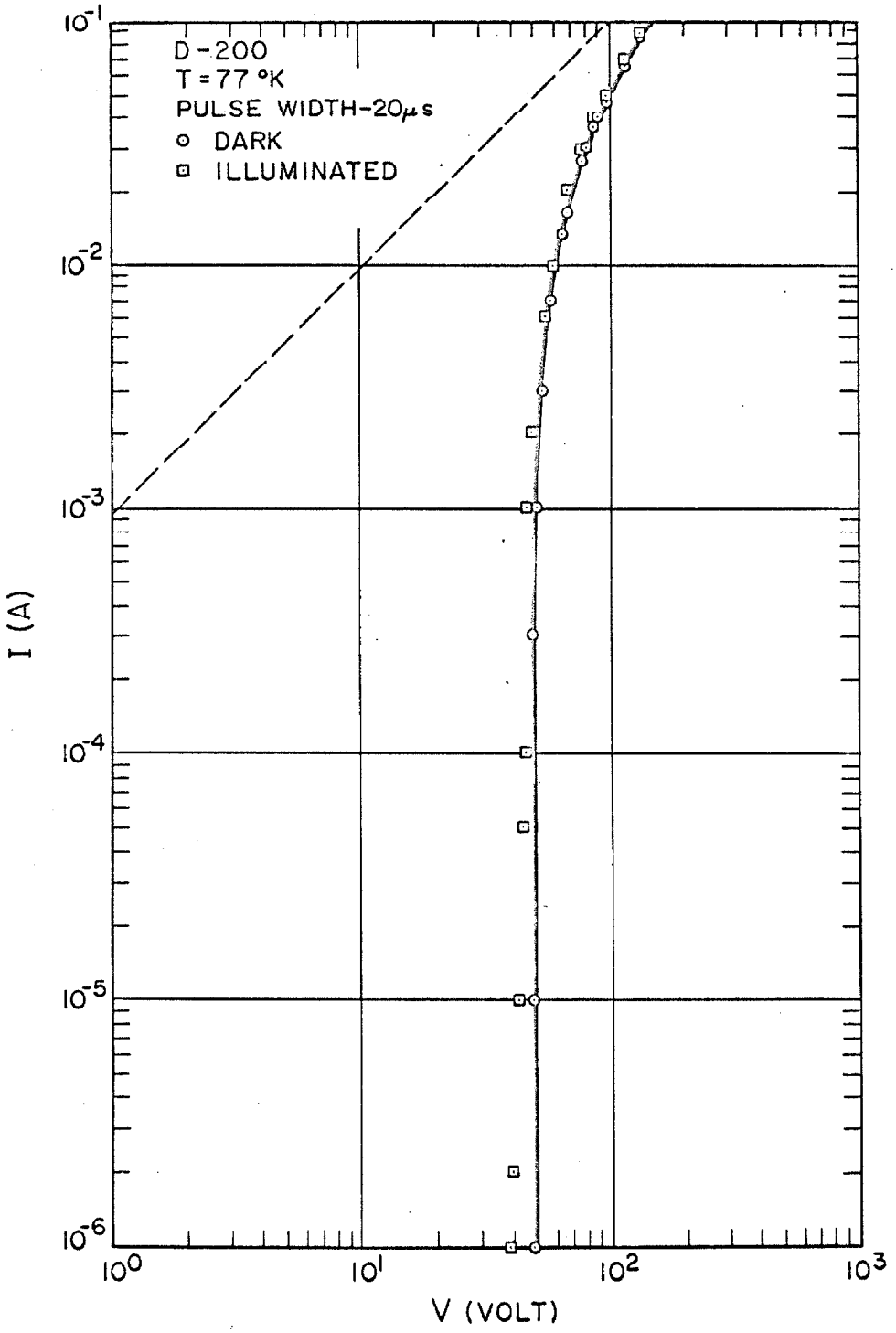
D-200
T=77 °K
PULSE WIDTH-20μs
DARK
ILLUMINATED
I (A)
V (VOLT)
10^-1
10^-2
10^-3
10^-4
10^-5
10^-6
10^0
10^1
10^2
10^3

Figure 3.2

3.1.1 Punch-through as a function of temperature. Different techniques are available for determining the value of punch-through. For instance: (1) capacitance-voltage measurements, (2) application of a sawtooth-voltage to either of the two junctions with the base grounded (only applicable when the base is provided with a contact of its own), (3) the V-I characteristics. In this work punch-through has been determined by feeding a constant current through the structure, whose value is in the regime of the V-I characteristics where the current density increases sharply, and measuring the resulting voltage as a function of temperature. As long as punch-through is well defined, this technique provides a good determination of its value.

Figure (3.3) illustrates the temperature dependence of punch-through for a D-2000 structure approximately 70 microns thick. A considerable error in its absolute value can be expected due to the measuring technique employed. However, its temperature dependence $T^{-1/2}$, should be quite accurate except at both extremes in temperature. Below 50°K, the threshold voltage increases rapidly, not due to punch-through but to giant trapping as will be demonstrated in the subsequent section. At high temperatures punch-through is not well defined. Consequently, at the high operating points the temperature dependence of the mobility becomes noticeable and at low operating points the temperature dependence of leakage and saturation

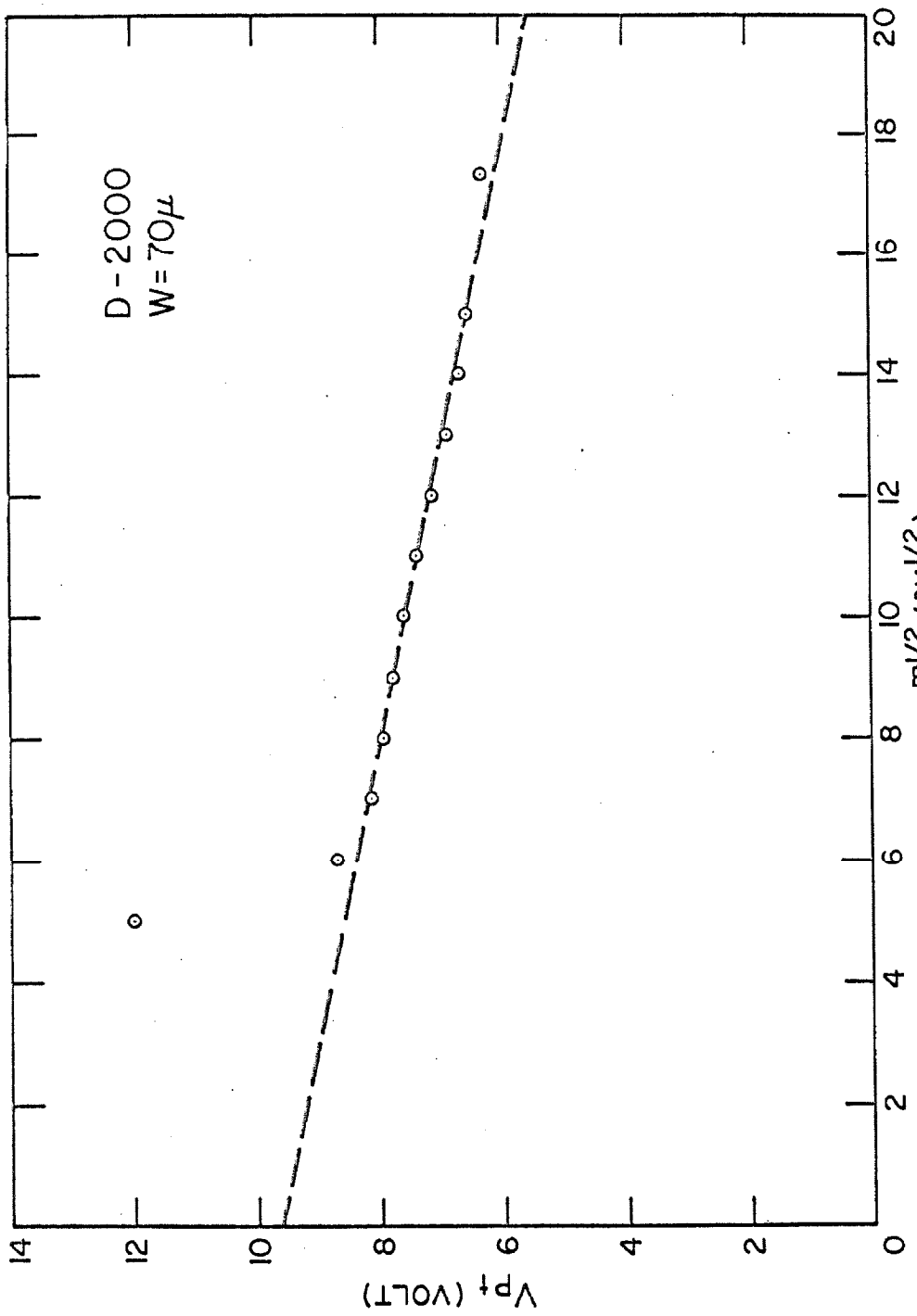

Figure 3.3

current dominate. The best determination of punch-through can be obtained by comparing the applicable theoretical model of unipolar sclc to the experimental V-I characteristics.

Punch-through has been found in section 1.2 as a function of the density of impurities by assuming that: (1) the junctions are abrupt and (2) the thermal equilibrium concentration of majority charge carriers extends up to the metallurgical junctions. In this section, we shall derive an expression for punch-through which, to a first approximation, takes into account the physical nature of the junctions. Figure (3.4) illustrates a floating base transistor at thermal equilibrium. The internal built-in voltage of the junctions is found by setting the algebraic sum of the drift and diffusion terms equal to zero[3.1], and it is given by

$$V_i = V_t \ln n_n/n_p \ , \tag{3.1}$$

where $V_t = kT/e$, and n_n and n_p are the densities of electrons at either side of the junction. Assuming complete depletion, the width of the transition region is given by

$$W_t = \sqrt{2}\ L_D\ (V_i/V_t)^{1/2} \ , \tag{3.2}$$

where

$$L_D = \frac{\sqrt{\varepsilon\varepsilon_o kT}}{e^2 N_A} \ . \tag{3.3}$$

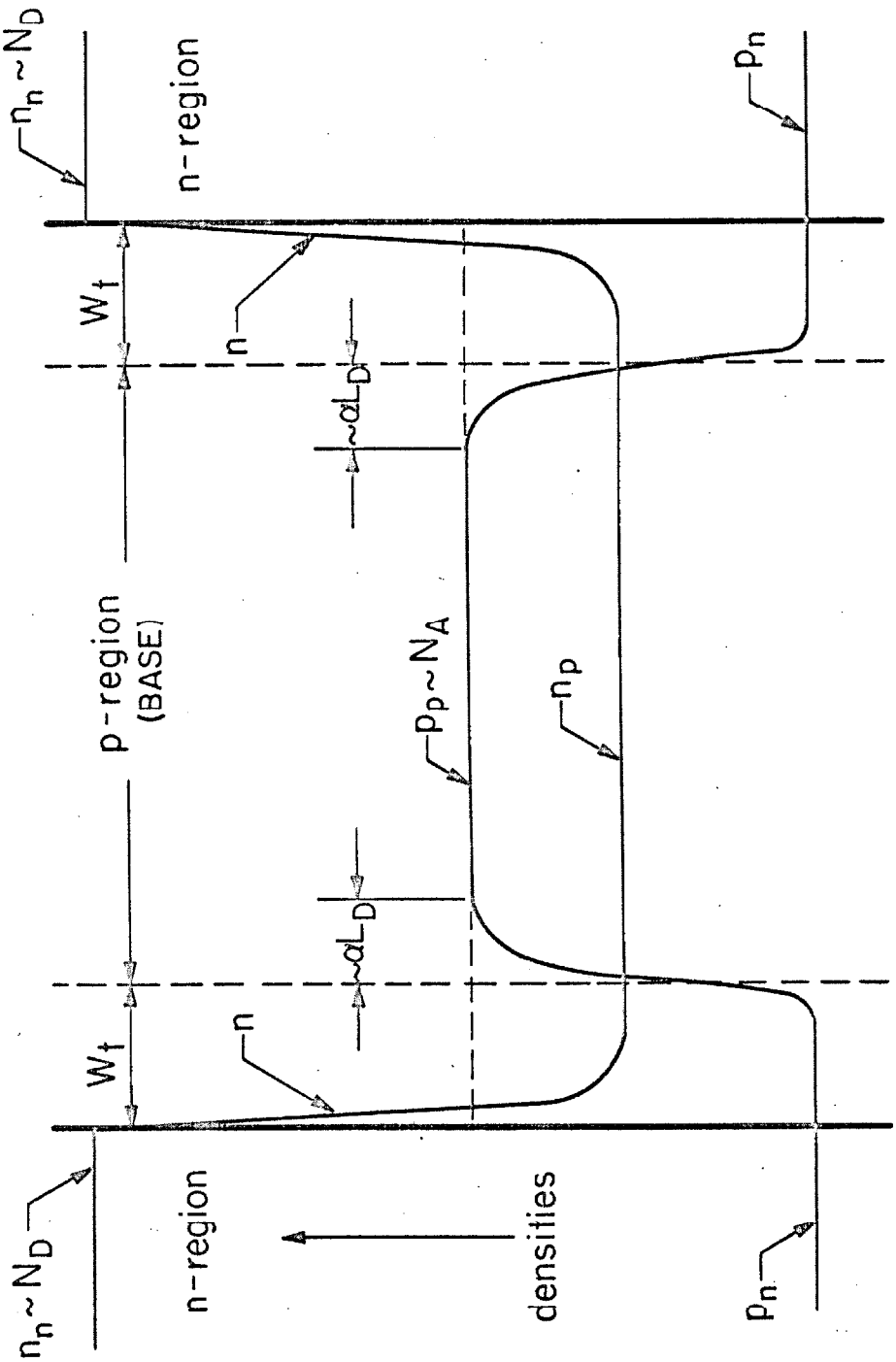
$n_n \sim N_D$
n-region
W_t
n
$\sim aL_D$
p-region
(BASE)
$p_p \sim N_A$
n_p
p_n
densities

Figure 3.4

L_D is the extrinsic Debye length. *If* W_t *and* L_D *are taken into account,* the effective width of the base region is

$$W_{eff} = W - 2\,W_t - 2\,L_D$$

According to this model, then, the voltage required to remove the remaining mobile holes from the base is given by

$$V_{pt} + V_i = \frac{e\,N_I}{2\varepsilon\varepsilon_o}\,[W - W_t - 2\,L_D\,]^2$$

$$V_{pt} = \frac{e\,N_I W^2}{2\,\varepsilon\varepsilon_o}\,[(1 - W_t/W - 2\,L_D/W) - (W_t/W)^2\,]$$

$$= V_o\,[\,1 - 2\,W_t/W - 4\,L_D/W + \ldots\,]\,, \qquad (3.4)$$

where V_o is the zero-order approximation for punch-through when the nature of the contacts is disregarded. V_o will, thus, hold in the limits of high impurity density and $W \gg L_D$. The ratio $\frac{2(W_t + 2\,L_D)}{W}$ essentially determines how much of an error is involved if V_{pt} is used to calculate either the resistivity or the thickness of the crystal.

The implicit assumption has been made that the forward biased junction is unaffected by the applied potential and, hence, that all

the voltage appears in the reverse biased junction. This is indeed the case since at V_{pt}, the built-in voltage at the emitter junction is approximately given by(3.2)

$$V_i' = V_i - kT \ln \{ 2 [1 + \exp (- e V_{pt}/kT)]\}^{-1} \qquad (3.5)$$

or

$$V_i' = V_i - kT \ln 2 \qquad (3.6)$$

for $V_{pt} >> kT/e$.

Expression (3.4) exhibits a temperature dependence directly related to the Debye length. If W_t is expressed in terms of the crystal parameters, one obtains

$$W_t = \left[\frac{2\varepsilon\varepsilon_o kT}{N_A e^2} \left(\ln \frac{N_D N_A}{N_c N_v} + E_g/kT\right) \right]^{1/2} , \qquad (3.7)$$

where E_g is the band gap energy, N_c and N_v the effective number of states in the conduction and valence bands, respectively, and N_D the density of electrons in the contacts. The first term within the parenthesis is relatively small and proportional to ln T. If the conditions are such that W_t is virtually independent of temperature, expression (3.4) plotted as a function of T yields a straight line whose slope is given by $\left[\frac{N_A W^2 k}{\varepsilon\varepsilon_o}\right]^{1/2}$ (higher order terms

have been neglected). This relation is only good in the extrinsic range of the material, but it can be extrapolated to intercept both coordinates which yields at 0°K, $V_{pt} = V_o \left[1 - \frac{2W_t}{W}\right]$ and at $V_{pt} = 0$, $W = 2(W_t + 2\ L_D)$. From these intercepts and the slope, it is possible to find the thickness and resistivity of the crystal. The model visualized to derive (3.4) seems to be in accordance with our experimental findings for the temperature dependence of punch-through, as will be demonstrated hereafter.

The resistivity of the sample, unfortunately, is not known accurately which makes a comparison of the experimental result with theory more difficult. It is known, however, to lie between 2000 and 8000 Ω-cm, corresponding to impurity densities of 7.10^{12} and 2.10^{12} cm^{-3}. An average value of $(4.5)\cdot 10^{12}$ will be used. The Debye length for this concentration is $(1.9)\cdot 10^{-4}$ cm at 300°K. The width of the transition region is about $17\cdot 10^{-4}$ cm. Thus, from (3.4)

$$V_{pt} \approx 18\ [5.2 \times 10^{-1} - 6.2 \times 10^{-3}\ T^{1/2}\ ] \quad . \qquad (3.8)$$

A comparison of this relation with experiment yields moderate agreement in the slope of figure (3.4). However, if L_D is replaced by $\alpha\ L_D$, one obtains instead of (3.4))

$$V_{pt} = V_o\ [1 - \frac{2}{W}\ (W_t + 2\ \alpha\ L_D)\ ] \quad , \qquad (3.9)$$

which provides an excellent fit to the experimental results for an α of about 1.5. This is indeed quite reasonable. The empirical factor α accounts, essentially, for the subtleties of junction theory left out in the model. It has been assumed that the junctions are abrupt, but the diffusion profile is an error function - diffusion was carried out from a constant concentration at the surface - dropping from a maximum concentration in the contacts (equal to the solid solubility limit for phosphorus in silicon) to the thermal concentration of holes in the crystal in about 3.10^{-4} cm. Also, at a distance L_D from thermal equilibrium in the base region, the concentration of mobile holes has only decreased by a factor e^{-1} and, consequently, it is logical to expect a non-negligible contribution passed this deviation.

To conclude, if punch-through is used to determine either, the density of impurities or the thickness of the crystal, its extrapolated value at $0^{o}K$ must be employed. The effect of W_t and L_D must be taken into consideration.

3.1.2 Trapping at low temperatures. It has been established experimentally [3.3-5] and subsequently formulated theoretically [3.6-8] that large capture cross-sections exist in compensated materials for temperatures in the vicinity of liquid helium. Mobile charge carriers are captured in one of the excited states of an ionized impurity atom by emitting either a phonon or a photon. Eventually, the trapped carrier cascades down to the ground level of the ionized impurity atom by subsequent emission of phonons or photons, or it is thermally reexcited into the conduction band. The carrier is considered to be trapped when it reaches an orbit more than kT below the conduction band. Lowering the temperature permits states of increasing radius to contribute to the capturing, thus, the strong temperature dependence of the capture cross-section [3.6]. Experimental results for n-type phosphorus and boron doped silicon have been obtained by Levitt and Honig[3.9] for the capture cross-section and the trapping time of conduction electrons as a function of temperature. Their results are illustrated in figures (3.5) and (3.6). The theoretical analysis presently available explains only partially the experimental results for "giant trapping" at low temperatures. The experimental capture cross-sections differ in some instances by as much as an order of magnitude from what is expected theoretically, and the effect of different degrees of compensation has not yet been accounted for satisfactorily. Those

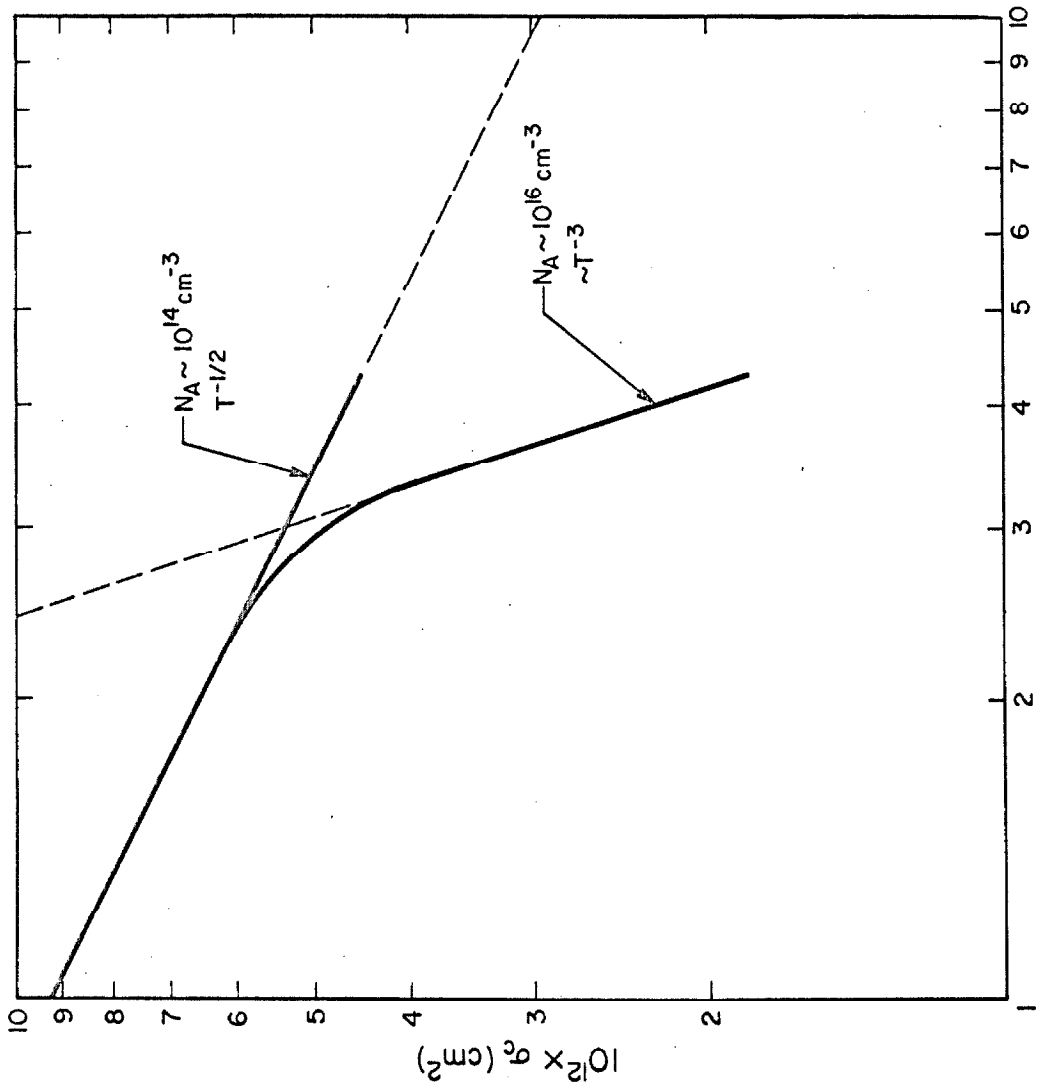

Figure 3.5

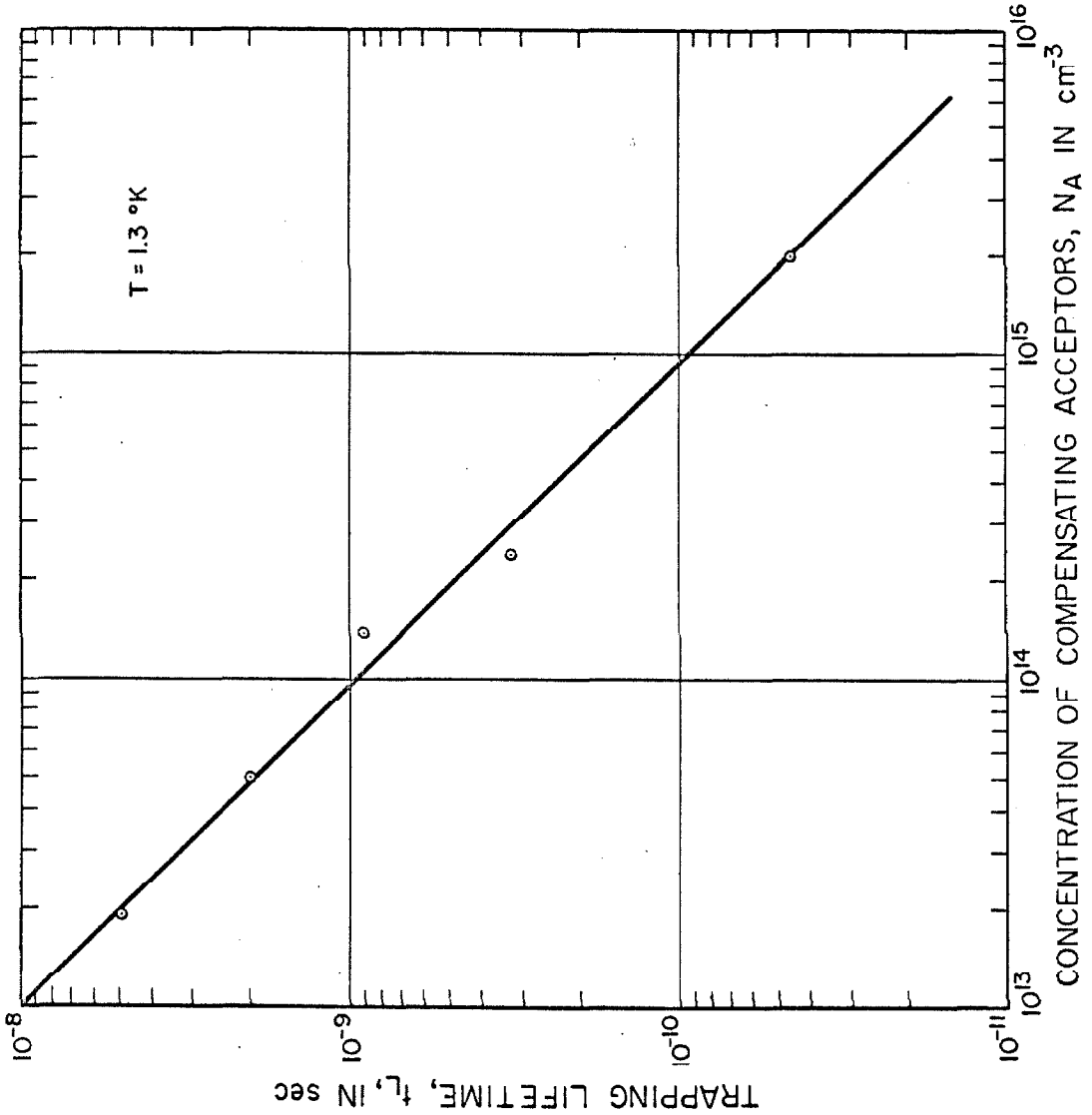
T = 1.3 °K
TRAPPING LIFETIME, t_L, IN sec
10^{-8}
10^{-9}
10^{-10}
10^{-11}
10^{13}
10^{14}
10^{15}
10^{16}
CONCENTRATION OF COMPENSATING ACCEPTORS, N_A IN cm^{-3}

Figure 3.6

authors explain the magnitude and the temperature dependence of the capture cross-section in terms of the available theories, namely, those by Lax[3.6] and Rodriguez and Ascarelli[3.7] The $T^{-1/2}$ power law dependence is attributed to the fact that, at very low temperatures, the capture rate constant α is independent of temperature and since the capture cross-section is given by $\sigma_c = \alpha / \langle v_{th} \rangle$, it will reflect the temperature dependence of the average thermal velocity.

Owing to the nature of this work, trapping at low temperatures would manifest itself through the variation with temperature of the threshold voltage. This parameter has been obtained over the temperature range $4.2^o \leq T \leq 77^oK$. Its dependence with temperature is given in figure (3.7) for three different types of structures, namely, D-200, D-2000 and R-2000. Lowering the temperature from approximately 50^oK, the threshold voltage first increases sharply and eventually levels off for temperatures of the order of 12^oK. The percentage change from 50^o to 4.2^oK is about the same for the R- and D-2000 structures and different for the D-200 structure. Measurement above 77^oK have been carried out for D-2000 structures which exhibit a threshold voltage whose only contribution is due to punch-through. The results in that range of temperatures were given and analyzed in the preceding section.

Illumination of the structures at 4.2^oK causes the observed increase in threshold voltage from its value at 77^oK to disappear

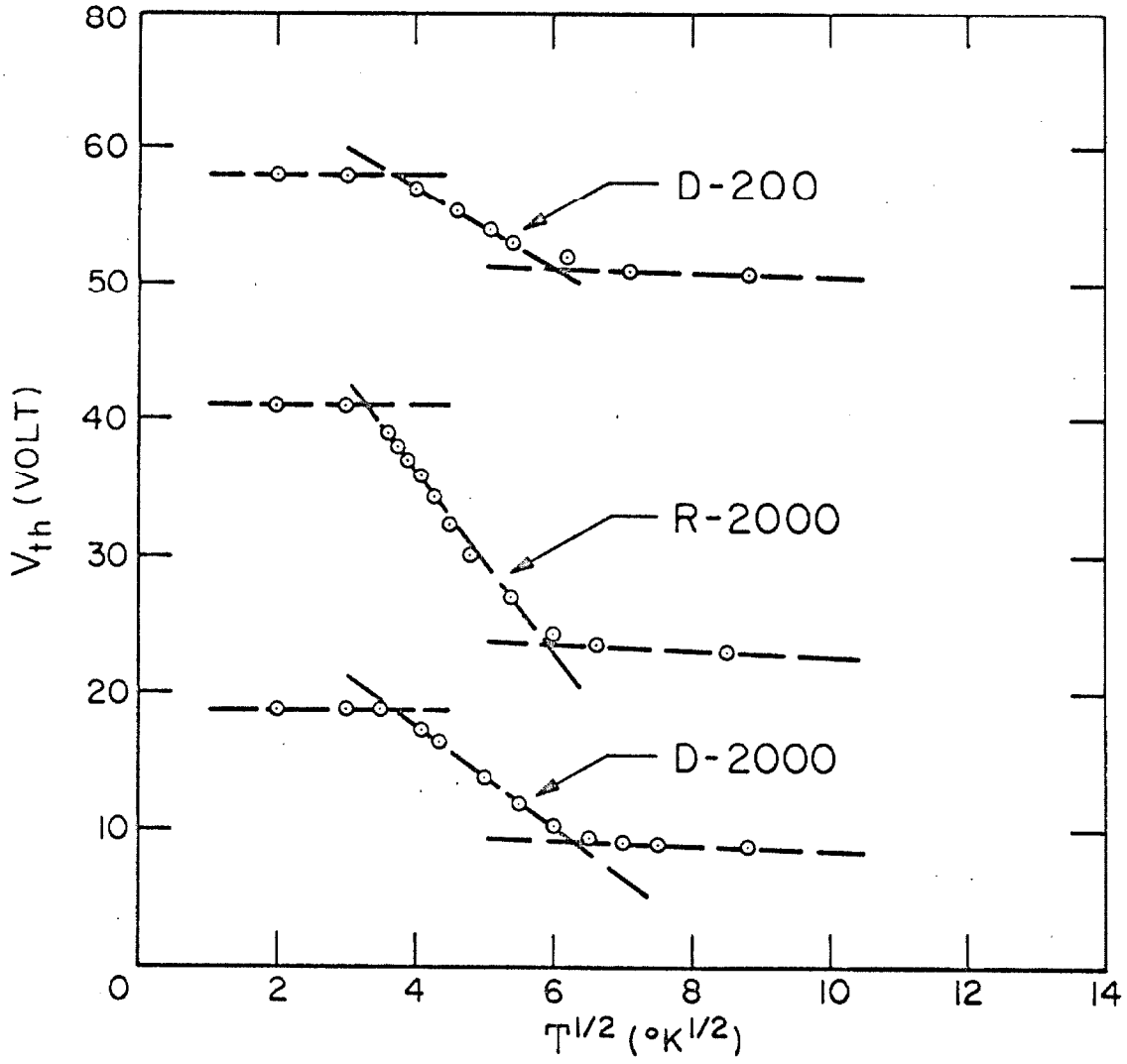
80
60
50
40
30
20
10
0
2
4
6
8
10
12
14
V_{th} (VOLT)
$T^{1/2}$ ($^{o}K^{1/2}$)
D-200
R-2000
D-2000

Figure 3.7

if the measurements are taken with a ramp pulse whose rise time is of the order of microseconds. No change is observed, however, if dc measurements are taken. The effect of increasing the repetition rate or the time width of the ramp is to gradually make the behavior conform with that observed at dc. Also, the return pulse of the ramp traces essentially the V-I characteristic with no illumination present. Typical V-I characteristics for D-200 and R-2000 structures measured with pulses and dc at 4.2°K, with and without illumination, are shown in figures (3.8) and (3.9).

These phenomena are indicative of trapping which is known to be closely related to the properties of the material. For this work, p-type compensated silicon has been used. The energy band scheme is illustrated in figure (3.10). N_a and N_d are the total concentrations of acceptors (boron) and donors (phosphorus). $N_a - N_d$ represents the total number of holes available for conduction in the extrinsic range of the material. At low temperatures, the density of holes in the valence band is given by the expression[3.10]

$$p = \left(\frac{2\pi m^* T}{h^2}\right)^{3/2}\left(\frac{N_a - N_d}{2 N_d}\right) \exp(-E_a/kT) \quad , \qquad (3.10)$$

where E_a is the acceptor activation energy. In the limit, as T approaches 0°K, the neutral acceptor concentration becomes equal to $N_a - N_d$.

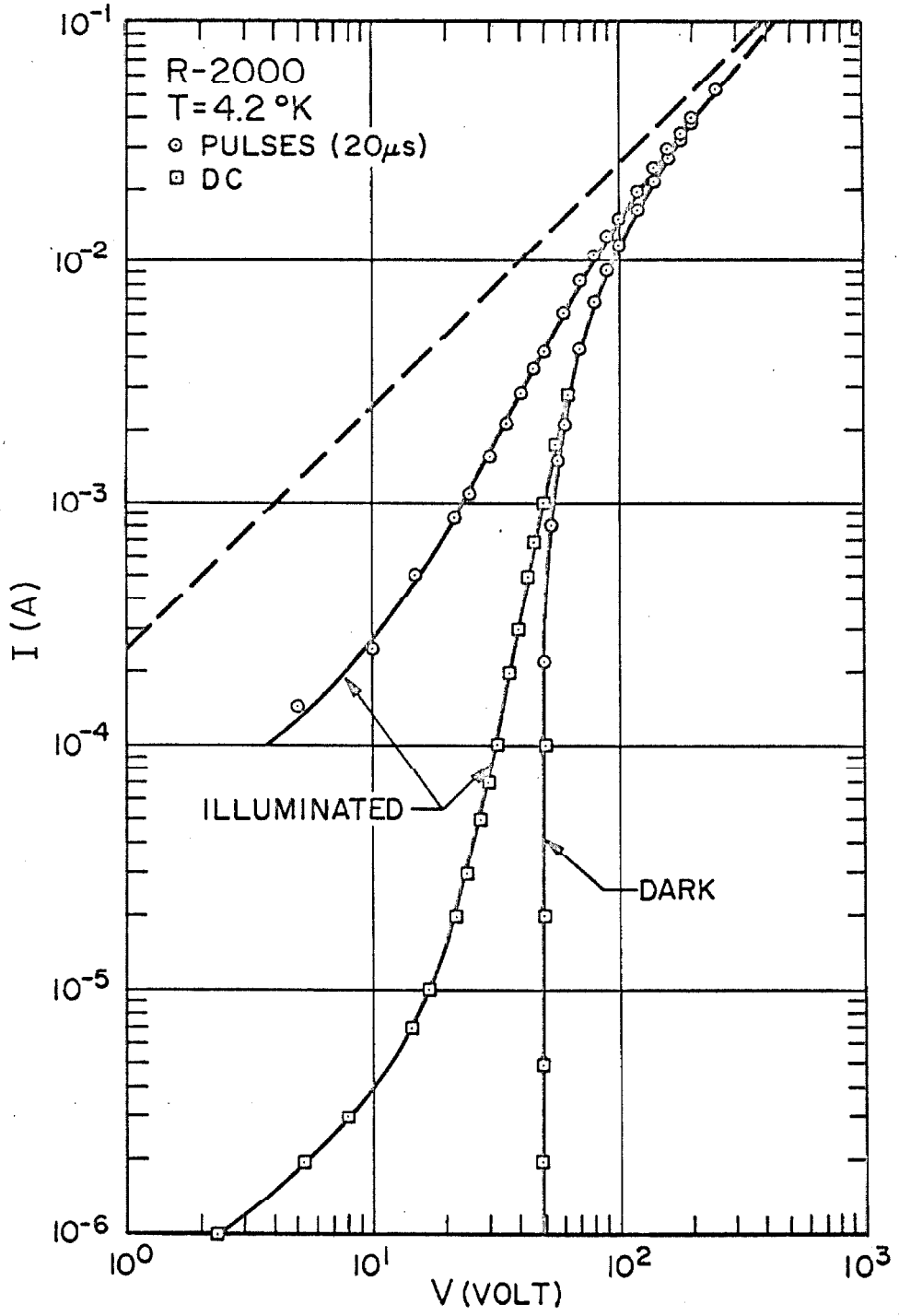
R-2000
T=4.2 °K
⊙ PULSES (20μs)
⊡ DC
ILLUMINATED
DARK
I (A)
V (VOLT)
10^-1
10^-2
10^-3
10^-4
10^-5
10^-6
10^0
10^1
10^2
10^3

Figure 3.8

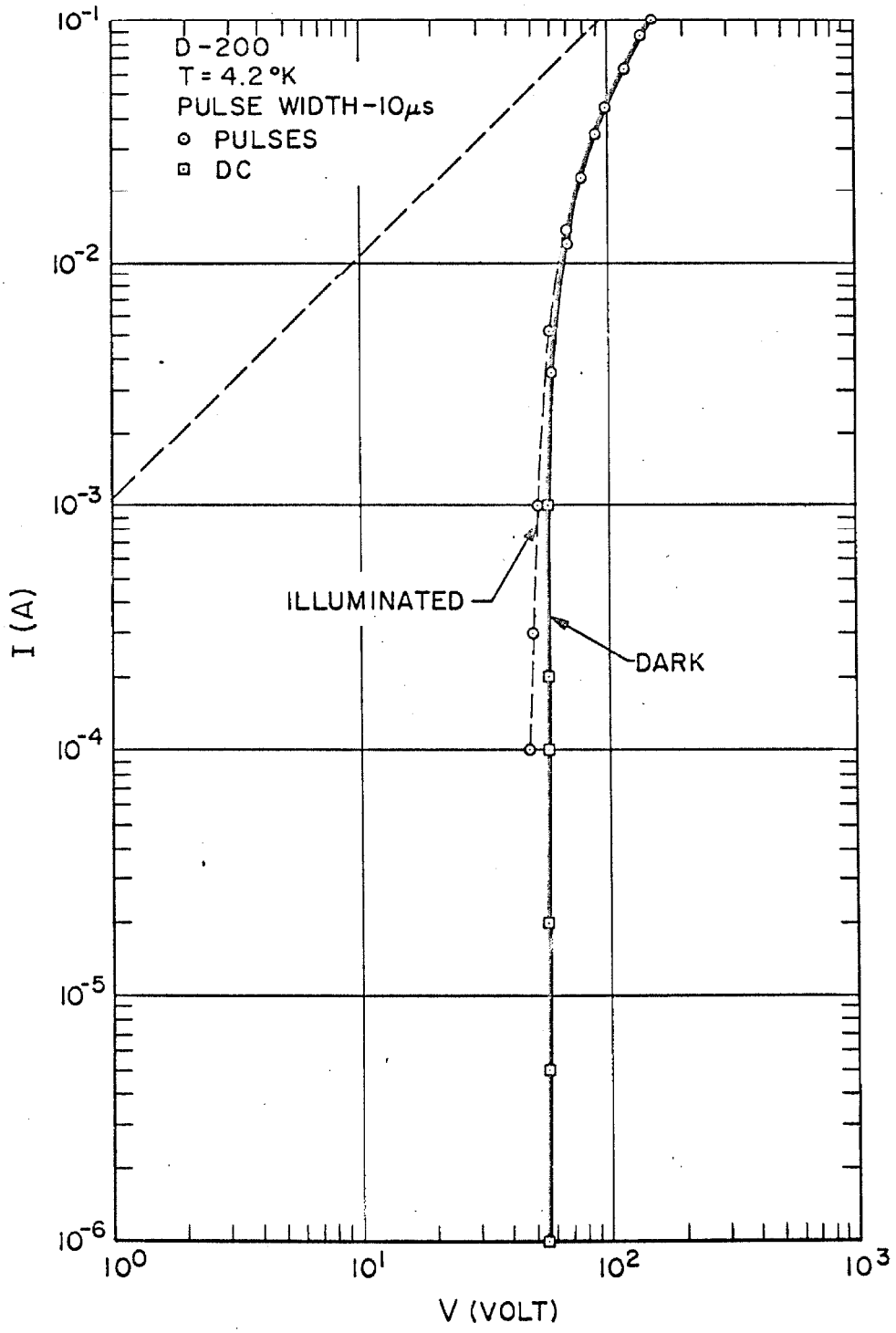
D-200
T = 4.2 °K
PULSE WIDTH-10μs
PULSES
DC
ILLUMINATED
DARK
I (A)
V (VOLT)
10^-1
10^-2
10^-3
10^-4
10^-5
10^-6
10^0
10^1
10^2
10^3

Figure 3.9

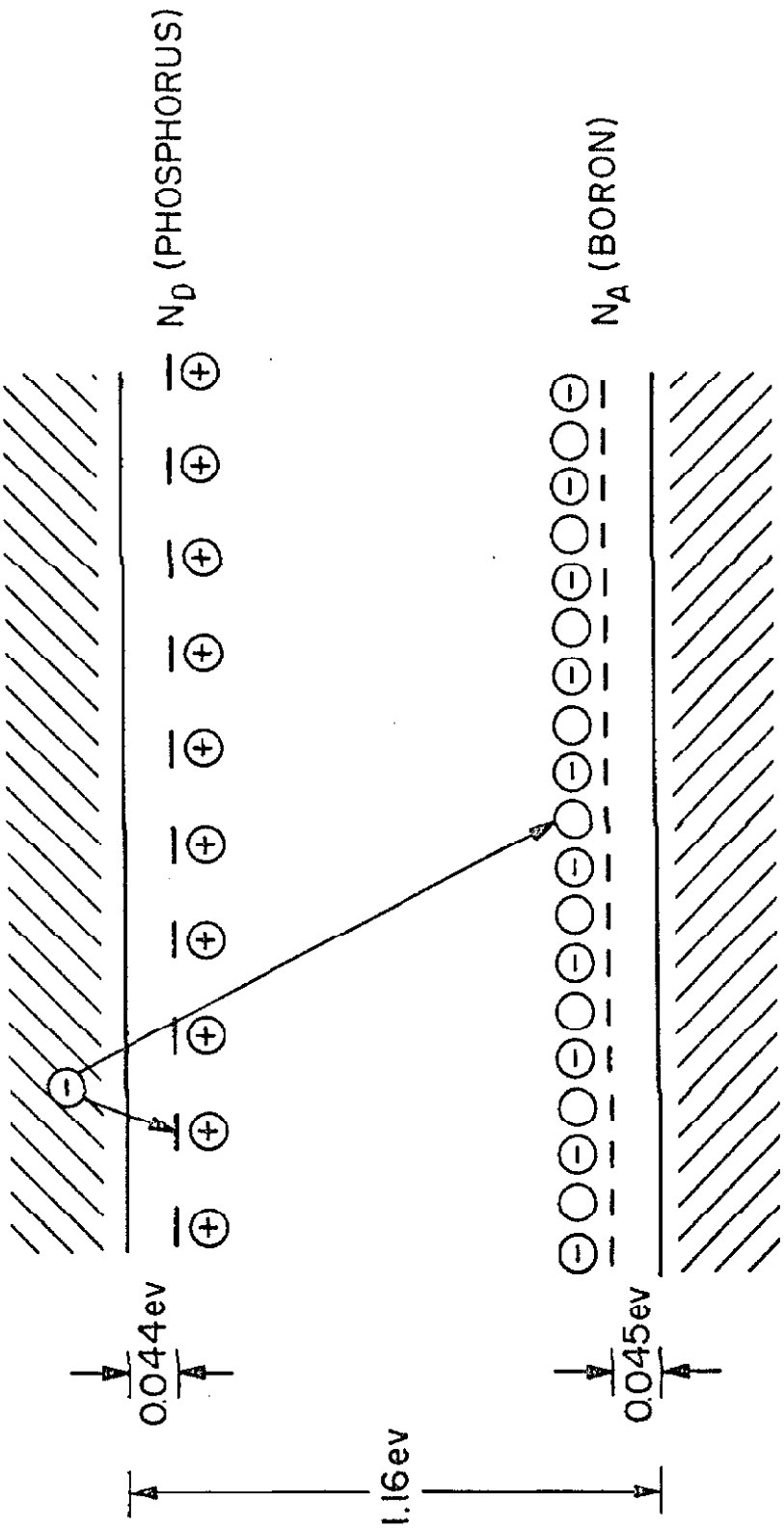

Figure 3.10

The D- and R-2000 structures have been manufactured from the same ingot. The resistivity of the 2000 Ω-cm wafers changed during diffusion. Punch-through and capacitance measurements carried out after diffusion for the D-structures, in a sample not diffused but placed on the furnace for the same length of time, indicated the resistivity of the bulk to be of the order of 8000 Ω-cm. The R-2000 structures were oxidized for two hours at 920°C, and diffused for 15 or 20 minutes at 1050°C, as opposed to thirty minutes total time for the D-structures at 1150°C and, consequently, the resistivity is expected to be somewhat higher. No attempt was made to determine the actual resistivity of the R-structures except for punch-through measurements. However, these are not to be trusted since the behavior is mostly dominated by traps also introduced during the oxidation step. The increase in resistivity is believed to be caused by outgassing of the acceptor impurities, and the appearance of traps by contaminants present on the furnace.

The phenomena observed experimentally at very low temperatures can be explained satisfactorily by invoking trapping of injected electrons at the ionized donor and neutral acceptor atoms. Consider a structure which exhibits punch-through at high temperatures and giant trapping at low temperatures. The expected temperature dependence of threshold is illustrated in figure (3.11). The dependence at high temperatures has already been analyzed for the

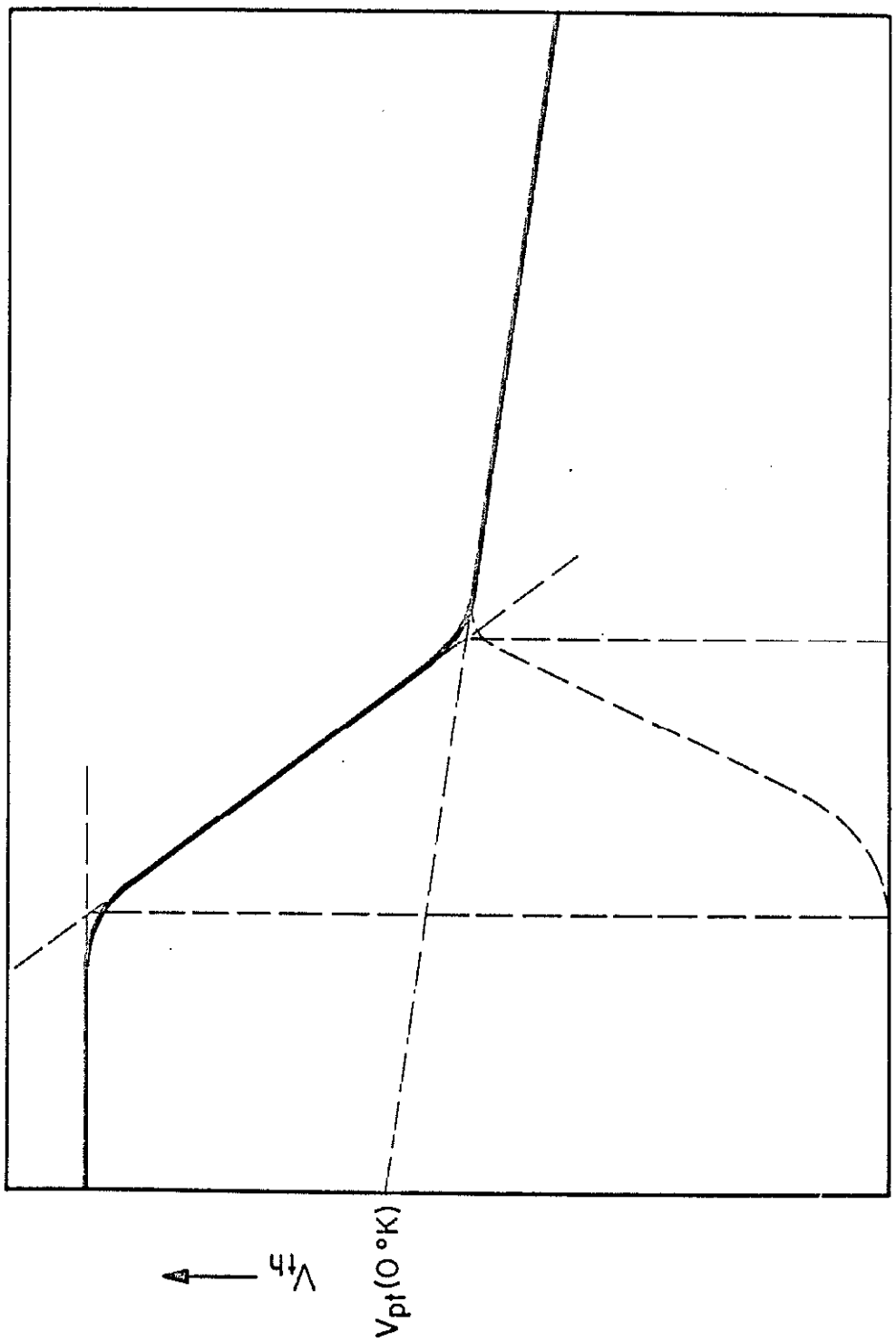

Figure 3.11

case of punch-through in the preceding section. This analysis yields the concentration of uncompensated acceptors $N_a - N_d$. Lowering the temperature below T_i, the threshold increases and eventually levels off at about T_c'. The difference between the value of threshold below T_c' and the extrapolated value of punch-through at 0^oK is attributed to trapping in the donor level. Between T_c' and T_i, the threshold voltage essentially reflects the variation with temperature of the capture cross-section (see figure 3.9), and consequently of the trapping time. According to Brown[3.11] the temperature T_c, at which the capture cross-section deviates from the $T^{-1/2}$ power law and attains a very strong dependence with temperature (approximately T^{-3}), should occur somewhere between 7^oK and 17^oK for lowly doped materials. This is in agreement with the temperature T_c' at which the threshold voltage starts deviating appreciably from its saturation value at 4.2^oK. Thus, as the temperature is increased above T_c, the donor level gradually ceases to behave like a trapping level since its trapping time is becoming longer and the release time is diminishing. Eventually, the injected electrons cannot be considered to be captured in any of the excited states of the Coulomb potential since the sticking probability - the probability for an electron not to be reexcited into the conduction band - is negligibly small. The temperature at which this occurs is about 40^oK (see figure (3.10)). This is also the temperature at which the uncompensated donor atoms

become almost totally ionized. Whether this correlation is of deeper significance is unclear.

Theoretically, one should expect the contribution from punch-through to decrease and eventually disappear since the concentration of mobile holes in the valence band diminishes exponentially with temperature. However, as the holes freeze in, the neutral centers are believed to behave as deep traps for injected electrons with a fairly small trapping time and long release time. This conclusion has been reached from the effect of illumination on the samples. Lax theoretically[3.6] and Honig experimentally[3.12], have found trapping cross-section for neutral centers about two orders of magnitude smaller than those of ionized donor centers with a shallow temperature dependence. They concluded that, at low temperature, these two types of centers dominate the capture process, in agreement with our findings. Our experimental evidence is, nevertheless, not sufficient to stipulate this with certitude. An independent measurement of the compensation at low temperatures would clarify the situation. This could be accomplished by performing Hall effect measurements below 50°K. From expression (3.10), a plot of $\ln(pT^{-3/2})$ versus $1/T$ results in a straight line of slope $-E_a/k$ which yields the activation energy for the acceptors. The intercept of the extrapolated linear range at $1/T = 0$ gives the quantity $(N_a - N_d)/N_d$. Since $N_a - N_d$ is known from punch-through measurements in the high

temperature range, the compensation N_d can be readily obtained. However, this procedure is complicated by the fact that the compensation of the material varies during the manufacturing steps and, consequently, the measurements have to be obtained in a sample which has been exposed to the same procedure except for the actual doping of the contacts.

The effect of illumination can be readily explained in terms of the previous model. D C measurements with and without light yield the same threshold because the trapping time is much smaller than the release time and consequently, on the average, the donor trapping level is filled with injected electrons. On the other hand, pulse measurements with and without illumination result in different V-I characteristics. If Levitt and Honig results for the trapping time (see figure (3.11)) are extrapolated to a concentration of about 10^{12} cm^{-3}, which is what is expected in this particular case, the trapping time is of the order of microseconds. This extrapolation is perhaps questionable but it indicates the order of magnitude to be expected. When a ramp with a few microseconds rise time is initially applied to the structure in the dark, the donor level is not totally filled with injected electrons, since the duration of the pulse is of the order of the trapping time. If the repetition rate is increased sufficiently, electrons will accumulate in the donor level for each ramp and, eventually, the V-I characteristic exhibits the same threshold

voltage as for dc measurements. This is indeed observed. When the structures are illuminated, however, the release time is decreased and, in between ramps, the trapped electrons are reexcited. The structures will, thus, exhibit a threshold voltage approximately equal to that observed at 77°K in accordance with the results obtained.

The D-2000 and D-200 structures exhibit essentially the behavior prescribed above. At 77°K, illumination has little effect because the threshold voltage is mostly caused by punch-through. Pulse and dc measurements yield identical V-I characteristics in the range of interest. At 4.2°K, illumination removes most of the contribution to V_{th} due to trapping in the donor level when the samples are pulsed with a ramp whose duration is a few microseconds. DC measurements are identical with or without illumination. The R-2000 structures, however, have a threshold voltage at 77°K which is partly due to punch-through and partly due to trapping. Since the R- and D-2000 structures were manufactured from the same ingot, the discrepancy in behavior must be a direct consequence of contamination. A trapping level due to contaminants present on the furnace - most probably nickel or gold - was probably introduced during the oxidation step for the R-2000 structures. Hence, pulse measurements with the sample illuminated at 77°K also cause the threshold voltage to decrease. Illumination at 4.2°K removes most of the contributions

to V_{th} due to trapping in the donor level and in the impurity level introduced during processing. The remaining V_{th} is mostly due to trapping in the neutral acceptor atoms.

In conclusion, the existence of giant trapping at low temperatures has been established. A more exhaustive analysis of pure unipolar sclc, in the temperature range below 77°K, will yield information about the magnitude and temperature dependence of the capture cross-section. Gregory and Jordan[3.13] analyzed the transient response of pure unipolar sclc under the influence of giant trapping, and obtained the capture cross-section of holes in the ionized acceptor atoms. The value gotten with this technique applied to hot carriers, since the energy gained by the carriers from the electric field is much greater than their thermal energy. A more extensive analysis of the threshold voltage can clarify the trapping mechanisms present at low temperatures. However, enough information has been gathered to ascertain that its temperature dependence yields directly the concentration of donors and acceptors in the material. The density of acceptors is given by the value of V_{th} at 4.2°K and, the density of donors, by the extrapolated value of punch-through at 0°K. This technique eliminates the necessity of conducting Hall measurements in a sample carried through the same manufacturing steps as the structures.

3.2 The V-I characteristics. This section emphasizes the dependence of pure unipolar sclc upon the field-velocity relationship. The analysis provides an exhaustive treatment of pure unipolar sclc from low to values of electric field strengths as high as 10^5 v/cm over the temperature range $4.2^o \leq T \leq 300^oK$. An n^+ p n^+ structure - or its counter part p^+ n p^+ - is ideally suited to study segments of the field-velocity relationship. The width and doping of the p-region can be tailored to cover either the range of thermal or hot charge carriers. In some instances, the entire field-velocity relationship can be studied with just one structure, provided heating and breakdown phenomena are absent. The two possibilities have been considered in this work. A determination of the field-velocity relationship is made from pure unipolar sclc over the above mentioned temperature range. The experimental results obtained from this analysis about the drift velocity at high field strengths are discussed in more detail in the subsequent chapter.

Trapping phenomena below 50^oK have already been investigated through their effect on the threshold voltage. In this section, the trapping phenomena observed in the R-2000 structures above 50^oK will be analyzed. The discussion will be limited to presenting the V-I characteristics in the context of unipolar sclc. Also, the usefulness of the subject to gather information about the electronics properties of solids is demonstrated.

3.2.1 The effect of punch-through and trapping in limiting the current density. Below threshold, the current density is either suppressed by the reverse biased junction (punch-through), by trapping, or a combination of both. This regime of the V-I characteristics has been covered superficially, and the analysis is by no means exhaustive. However, a few of the observations made are presented.

In the case of punch-through, the behavior for applied voltages below threshold is that of a floating base transistor. At very low applied voltages, only saturation and leakage current - caused by generation and recombination centers, diffusion, surfaces and junction irregularities - flows through the structure (J_{FBT}). This is essentially the current density expected to flow in a reverse biased junction. An increase in applied potential causes the depletion region to extend closer to the forward biased junction. The effective width of the base region is reduced and, consequently, the amplification factor of the transistor β increases. For values of applied potential very close to but lower than punch-through, the current density is enhanced by a large β since the effective width of the base region is very small. Thus, the V-I characteristics exhibit a transition region where the current density increases rapidly with applied voltage even though punch-through has not yet been reached. Figure (3.12) illustrates the experimental results obtained

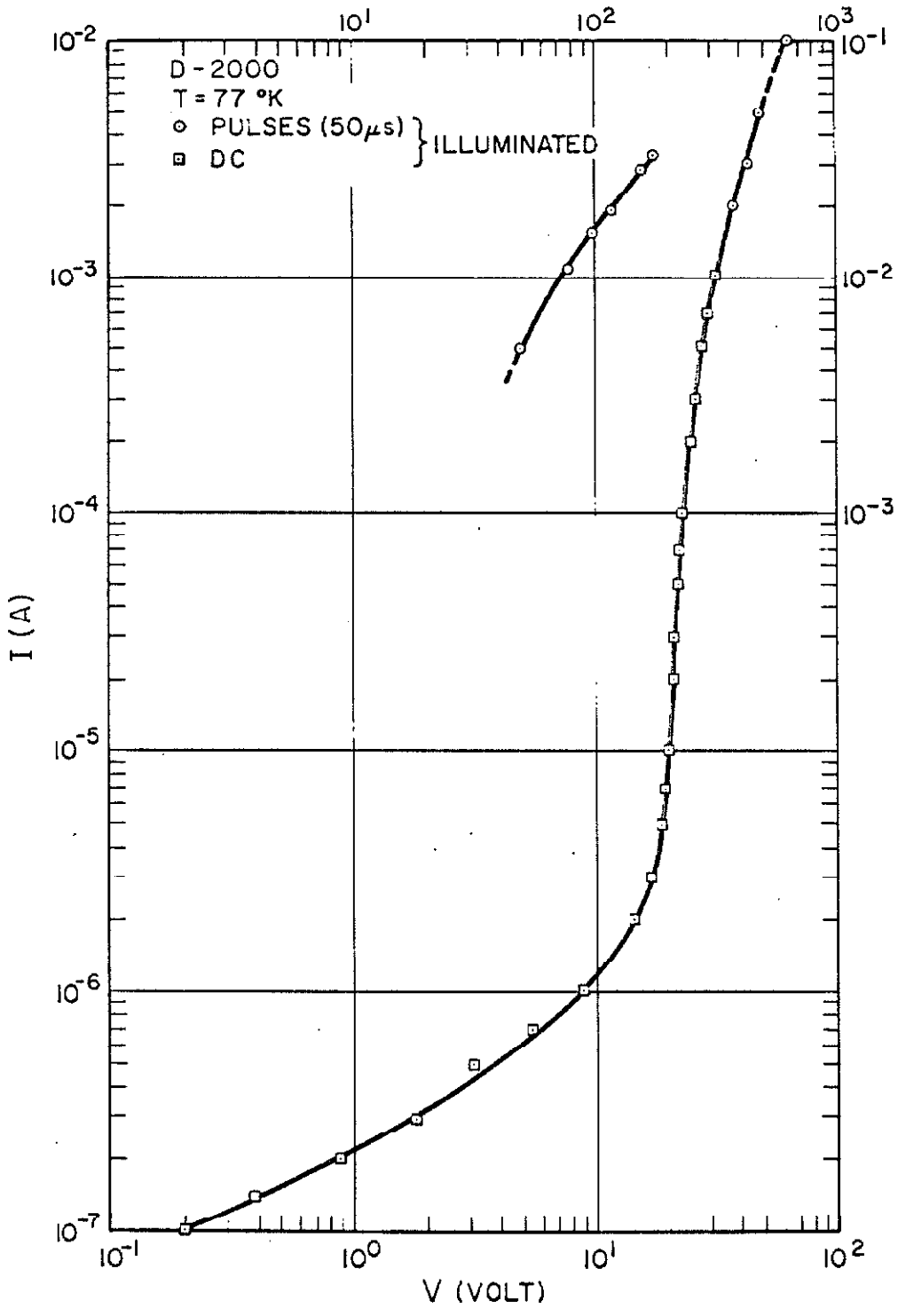
D - 2000
T = 77 °K
PULSES (50μs)
DC
ILLUMINATED
I (A)
V (VOLT)
10^-2
10^-3
10^-4
10^-5
10^-6
10^-7
10^-1
10^0
10^1
10^2
10^3

Figure 3.12

from a D-2000 structure which exhibits punch-through under the influence of illumination. When the structure is illuminated, the generation current is increased considerably and, consequently, the structure of the current density in this range can be more easily perceived. The behavior conforms with the previous description.

Trapping phenomena above 77°K have only been observed in the R-2000 structures. To explain the V-I characteristics of these structures, the energy band model of figure (3.13) is proposed. It is characterized by the presence of both hole and electron trapping levels. However, reference is made to one of these trapping levels only in the forthcoming analytical treatment. The relevance of the model will become apparent when the type of contaminant responsible for the observed behavior is determined. For simplicity the analysis is divided into the two regimes according to the location of the quasi fermi energy level with respect to E_t. The two regimes correspond to the two regions where the Fermi-Dirac distribution can be approximated by simple exponentials.

When $(E_t - E_F)/kT >> 1$, the Fermi-Dirac distribution can be approximated by

$$f = 1/g \exp - (E_t - E_F)/kT \quad , \tag{3.11}$$

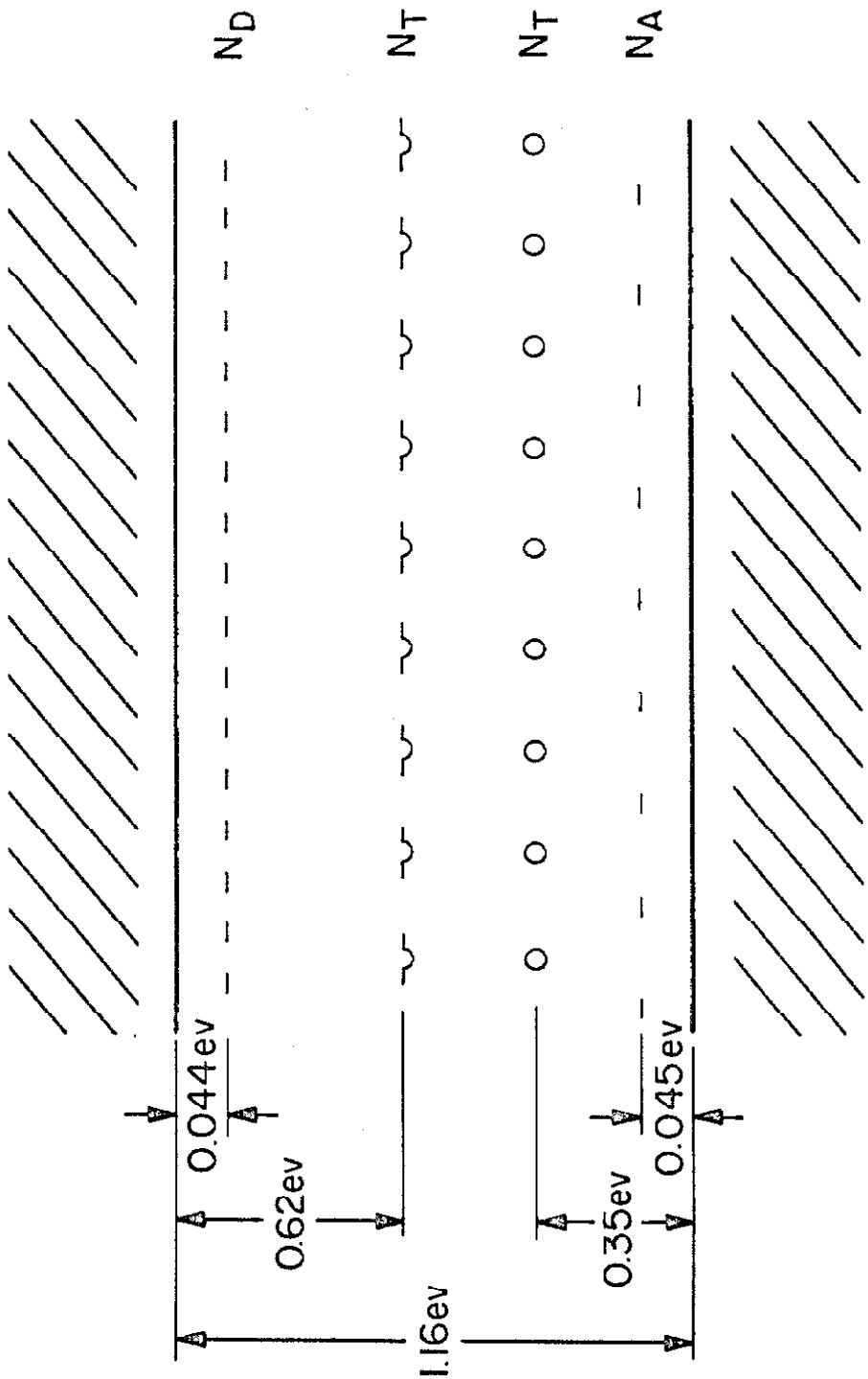

Figure 3.13

where g is the degeneracy factor of the traps.

At the onsent of injection, a number of the injected carriers determined by f are trapped. This leads to a current suppression factor θ[3.14], given by

$$\theta = N_c/gN_t \exp -(E_c - E_t)/kT \quad , \tag{3.12}$$

where N_t is the density of trapping states located at E_t in energy. In the limit of $\theta << 1$, the current density is given by the expression

$$J = 9/8\ \varepsilon\varepsilon_o \mu\ \theta\ V^2/W^3 \quad . \tag{3.13}$$

When the quasi fermi energy level (determined by the number of injected carriers) crosses E_t, the density of free carriers increases rapidly and the current density approaches the limit of pure unipolar sclc. The voltage required to fill all the traps, V_{TFL}, is given by

$$V_{TFL} = \frac{N_t\ e\ W^2}{2\ \varepsilon\varepsilon_o} \quad . \tag{3.14}$$

For the particular case of an n^+ n n^+ structure, the dc characteristic is given as a normalized log-log plot in figure (3.14). The cross-over voltage from the ohmic to the square range is now given by

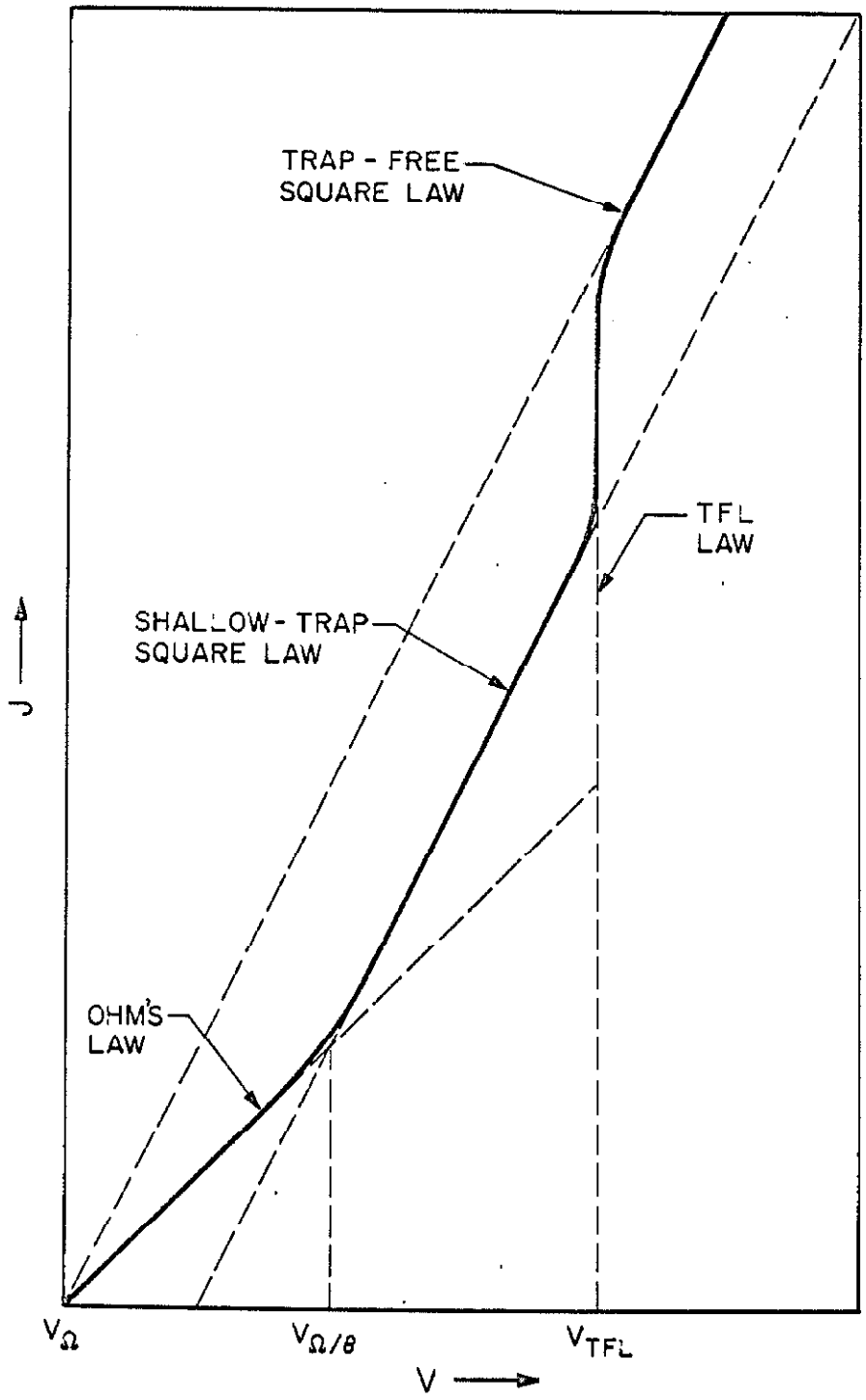
TRAP - FREE
SQUARE LAW
TFL
LAW
SHALLOW - TRAP
SQUARE LAW
OHM'S
LAW
J
V_Ω
$V_{\Omega/\theta}$
V_{TFL}
V

Figure 3.14

$$V_\Omega' = V_\Omega/\theta = 8/9 \cdot \frac{n_o e W^2}{\varepsilon\varepsilon_o} \frac{1}{\theta} \qquad (3.15)$$

When $(E_F - E_t)/kT \gg 1$,

$$1 - f = 1/g \exp (E_t - E_F)/kT \quad . \qquad (3.16)$$

Thus, at thermal equilibrium, the number of empty traps is(3.15)

$$\rho_o = N_t/g \exp (E_t - E_F)/kT \quad . \qquad (3.17)$$

At the onset of injection, practically all the injected carriers go into filling up ρ_o and their contribution to the current density is negligible. When the applied voltage reaches the value

$$V_{TFL} = \frac{e \rho_o W^2}{2 \varepsilon\varepsilon_o} \quad , \qquad (3.18)$$

all the traps have been filled and the contribution of the injected carriers to the current density increases rapidly to the limit of pure unipolar sclc. Once again, for the particular instance of an n^+ n n^+ structure, the dc characteristic is given as a normalized log-log plot for two values of V_{TFL} in figure (3.15).

The V-I characteristics of an R-2000 structure, taken at 300° and 77°K, are given in figures (3.16) and (3.17). These structures should exhibit a threshold dominated by punch-through. However, it

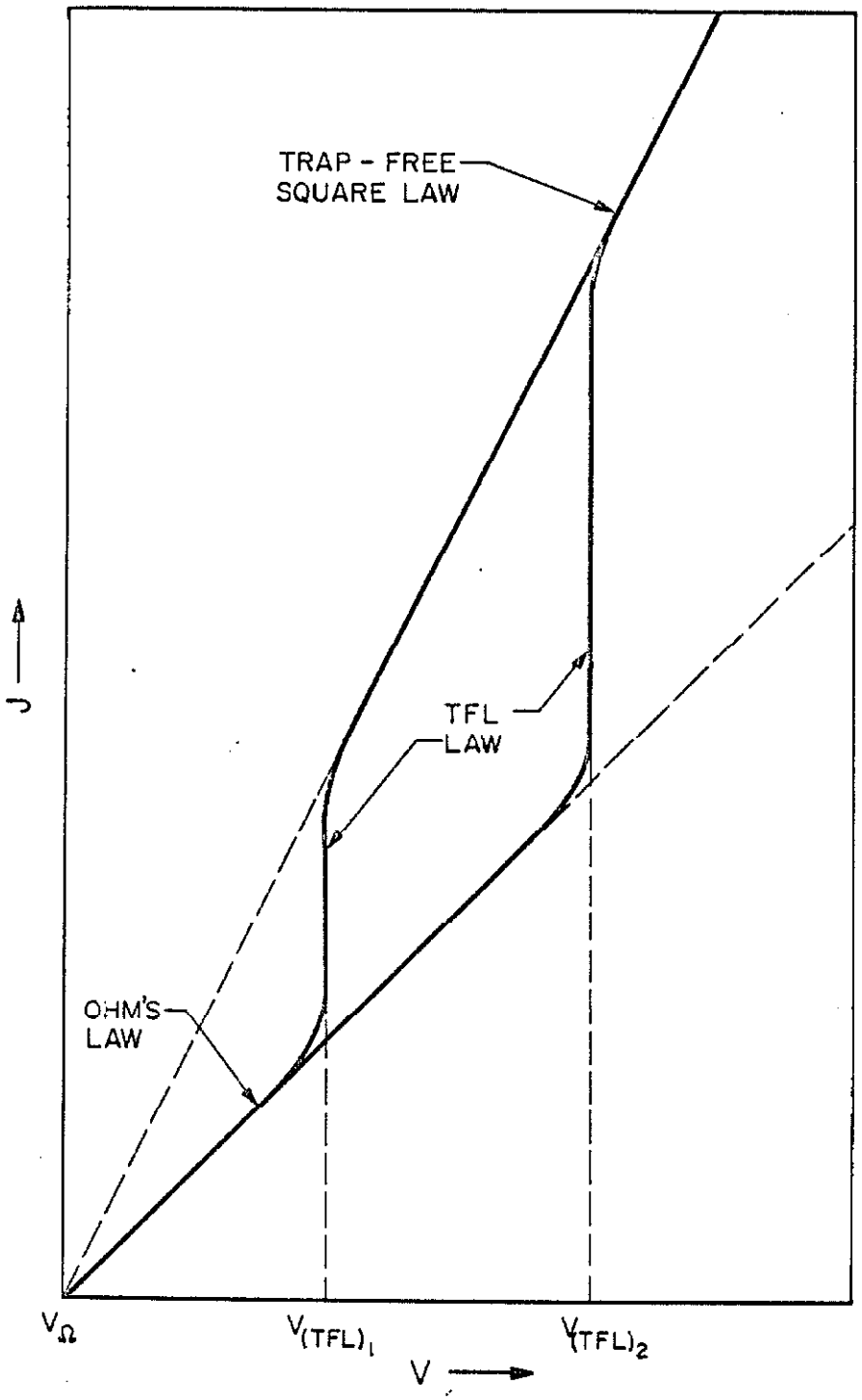

Figure 3.15

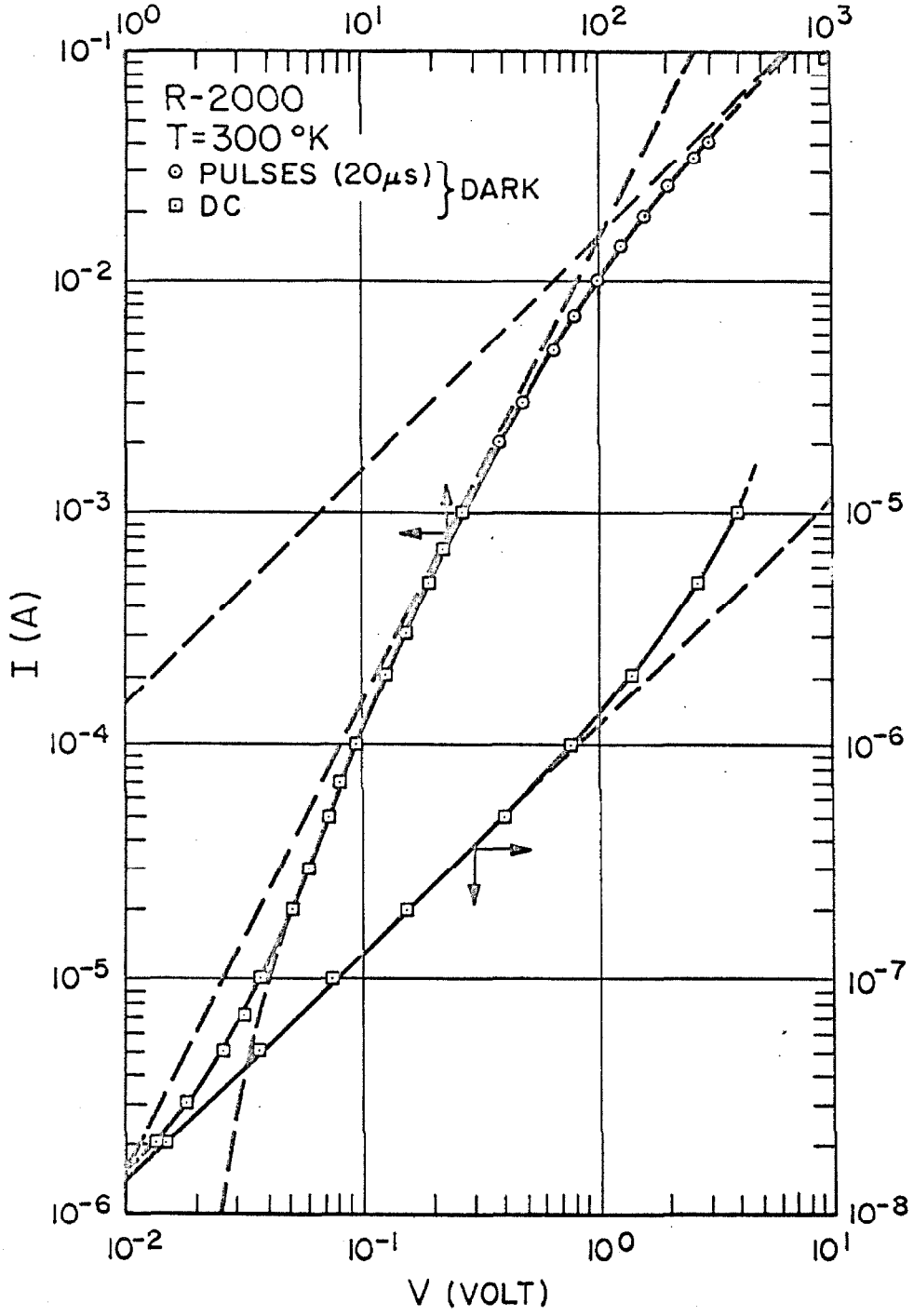
R-2000
T=300 °K
⊙ PULSES (20μs)
⊡ DC
DARK
I (A)
V (VOLT)
10^0
10^1
10^2
10^3
10^-1
10^-2
10^-3
10^-4
10^-5
10^-6
10^-5
10^-6
10^-7
10^-8

Figure 3.16

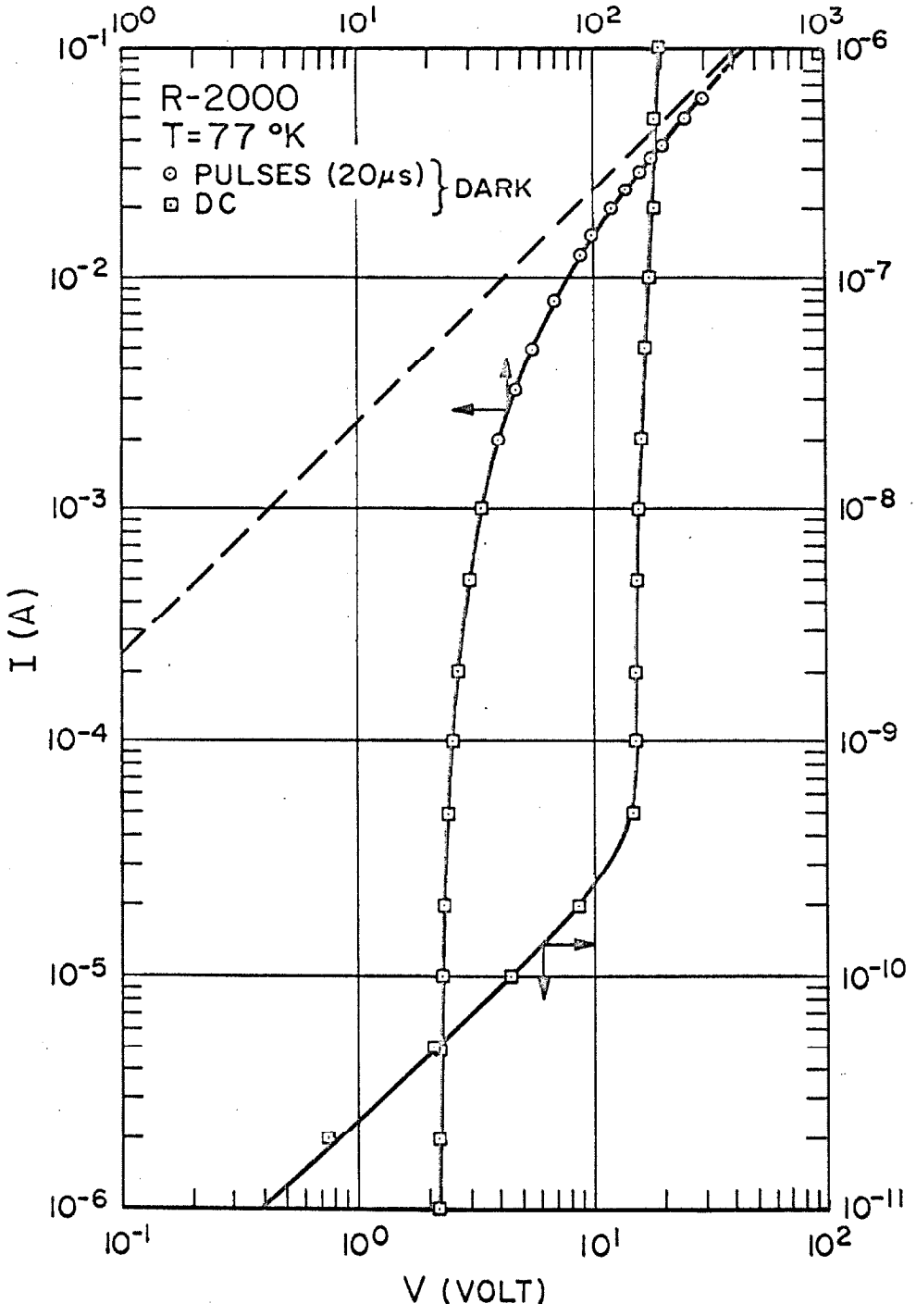
R-2000
T=77 °K
⊙ PULSES (20μs)
⊡ DC
DARK
I (A)
V (VOLT)
10^-1
10^0
10^1
10^2
10^3
10^-2
10^-3
10^-4
10^-5
10^-6
10^-7
10^-8
10^-9
10^-10
10^-11

Figure 3.17

is our contention that during the oxidation and diffusion steps, the p-region inverted to an n-region and, consequently, the structures are actually of the type n^+ n n^+; hence, the ohmic behavior at low applied voltages. At 300°K, the behavior is ohmic for three decades of applied voltage and no range is found where the current density has a square dependence for low applied voltages. This rules out the possibility of a shallow trap ($(E_t - E_F)/kT >> 1$) and, thus, the experimental characteristics are compared with that obtained for a deep trapping level ($(E_F - E_t)/kT > 1$). This comparison yields an effective value of approximately 1 volt for threshold, which is of the same order of magnitude as the cross-over voltage V_Ω. The thermal concentration of electrons in the conduction band has been determined from V_Ω and the magnitude of the current density in the ohmic range. The two values agree within 20%, and their average is about 9.10^{11} cm^{-3}. This is scarcely two orders of magnitude above the intrinsic concentration of silicon at 300°K. From the relation

$$n_o = N_c \exp - (E_c - E_F)/kT \quad , \tag{3.19}$$

the quasi fermi energy level is found to be located about 0.45 ev below the conduction band. At 77°K, the V-I characteristics exhibit a definite threshold of approximately 15 volts. The current density below threshold has only been measured for a decade of voltage and it is orders of magnitude smaller than at 300°K. The increase in

threshold from its value at 300°K. is unpredictable from the simple trapping models developed previously. The superficial coverage of the range below threshold and the lack of information for temperatures in between 300° and 77°K make the analysis difficult. It is feasible, nevertheless, to explain the temperature dependence of V_{TFL} in terms of a temperature dependent capture cross-section, as was done in relation with giant trapping. It is also plausible that since the material is almost intrinsic, the Debye length is long and the density of electrons in the conduction band is determined by the contacts. At 300°K. this density is enough to fill up most of the traps, but at 77°K the average density of electrons decreases which results in a higher V_{TFL}.

The location in energy of the traps has been inferred indirectly. The R-2000 and D-2000 structures have been manufactured from the same ingot and,consequently, their behavior should be identical. However, as has been demonstrated in this chapter,that is not the case. The difference in behavior can only be correlated to the different diffusion steps and the added oxidation step for the R-2000 structures in the manufacturing procedure employed. The wafers used to manufacture the R-2000 structures were probably contaminated in the diffusion furnace. The most probable contaminant is gold which is used for gettering transistors in order to improve their V-I characteristics. Further evidence pointing toward gold

as the contaminant comes from measurements taken with p^+ p p^+ structures manufactured from the same ingot. These structures also exhibit trapping phenomena for temperatures above 77°K, indicating that the contaminant is introducing at least two trapping levels capable of capturing holes and electrons. Gold is known[3.16] to introduce an acceptor and a donor level in silicon, as illustrated in figure (3.13), which is in agreement with what has been observed experimentally. Thus, even though the evidence gathered is not sufficient to establish this with certitude, it is feasible that gold is responsible for the trapping phenomena observed in the R-2000 structures.

3.2.2 The regime of pure unipolar sclc. Above threshold, the structure of the V-I characteristics is solely determined by the field-velocity relationship. A theoretical analysis was developed in chapter 1 for pure unipolar sclc which encompasses the effect of a field dependent mobility. Models were proposed to consider different segments of the field-velocity relationship. These models cover only combinations of limiting cases, but there is enough overlap among them to account for most real cases, if a definite square dependence on applied voltage is observed above threshold. If not, a graphical analysis can always be carried out. The following is a comparison of the above mentioned analytical models with the experimental V-I characteristics.

At 300°K, the R- and D-2000 structures exhibit V-I characteristics which reflect the entire field-velocity relationship (see figures 3.16 and 3.18). At low field strengths, after the effect of threshold has been overcome, a definite square voltage dependence for the current density is observed. At high field strengths, the current becomes linear with applied voltage. The experimental characteristic is compared with that obtained analytically by approximating the field-velocity relationship with the expression $v = v_s \tanh (E/E_o)$ (see figure 1.6). The agreement is excellent for both R-2000 and D-2000 structures. The effect of lowering the temperature from 300°K is to decrease the range where the current density

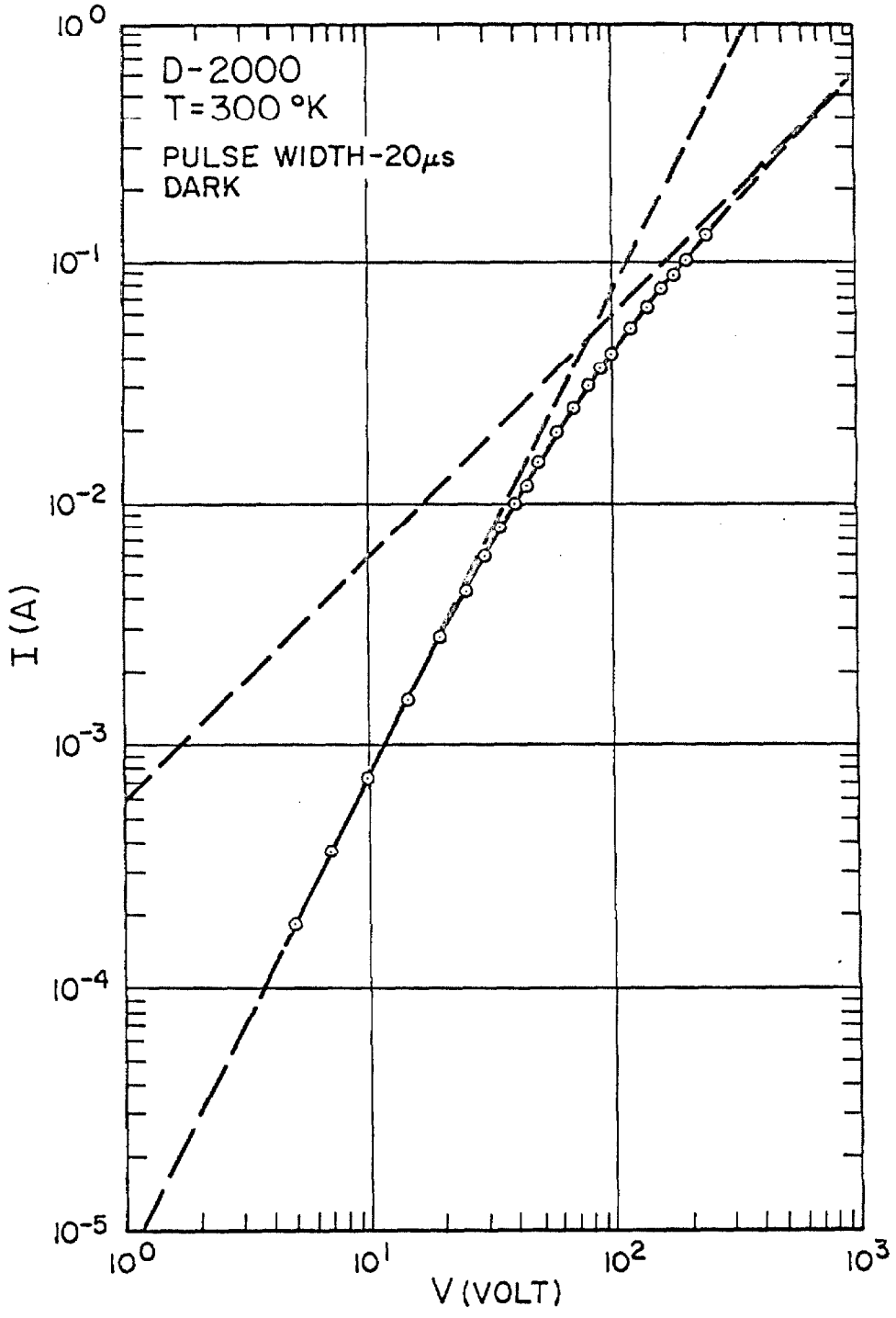
D-2000
T=300 °K
PULSE WIDTH-20μs
DARK
I (A)
V (VOLT)
10^0
10^-1
10^-2
10^-3
10^-4
10^-5
10^0
10^1
10^2
10^3

Figure 3.18

increases as the square of the applied voltage, and to increase the linear range. This is caused by a decrease with decreasing temperature of the critical field. Lowering the temperature causes the electrons to gain energy from the electric field at a faster rate since their interactions with the lattice decrease almost exponentially with temperature. Consequently, the low field mobility increases rapidly as a function of decreasing temperature, and the field at which the electrons deviate appreciably from thermal equilibrium with the lattice decreases. The fact that an extension of the linear range is observed implies not only that a limiting velocity exists, but also that it extends to lower fields as the temperature is increased. The V-I characteristics for R- and D-2000 structures at 77°K are shown in figures (3.17) and (3.19). A graphical analysis at this temperature is a difficult task, since the models available from chapter 1 assume that at threshold the electric field is either low or high enough for the V-I characteristics to clearly exhibit a square or linear dependence on applied voltage. Thus, the transition region from threshold to the linear range cannot be fully covered with one or a combination of models.

The threshold voltage of the D-200 structures is of such a magnitude at all temperatures as to create a built-in field in most of the base region bigger than the critical field. Consequently, in these structures the current density never exhibits a square

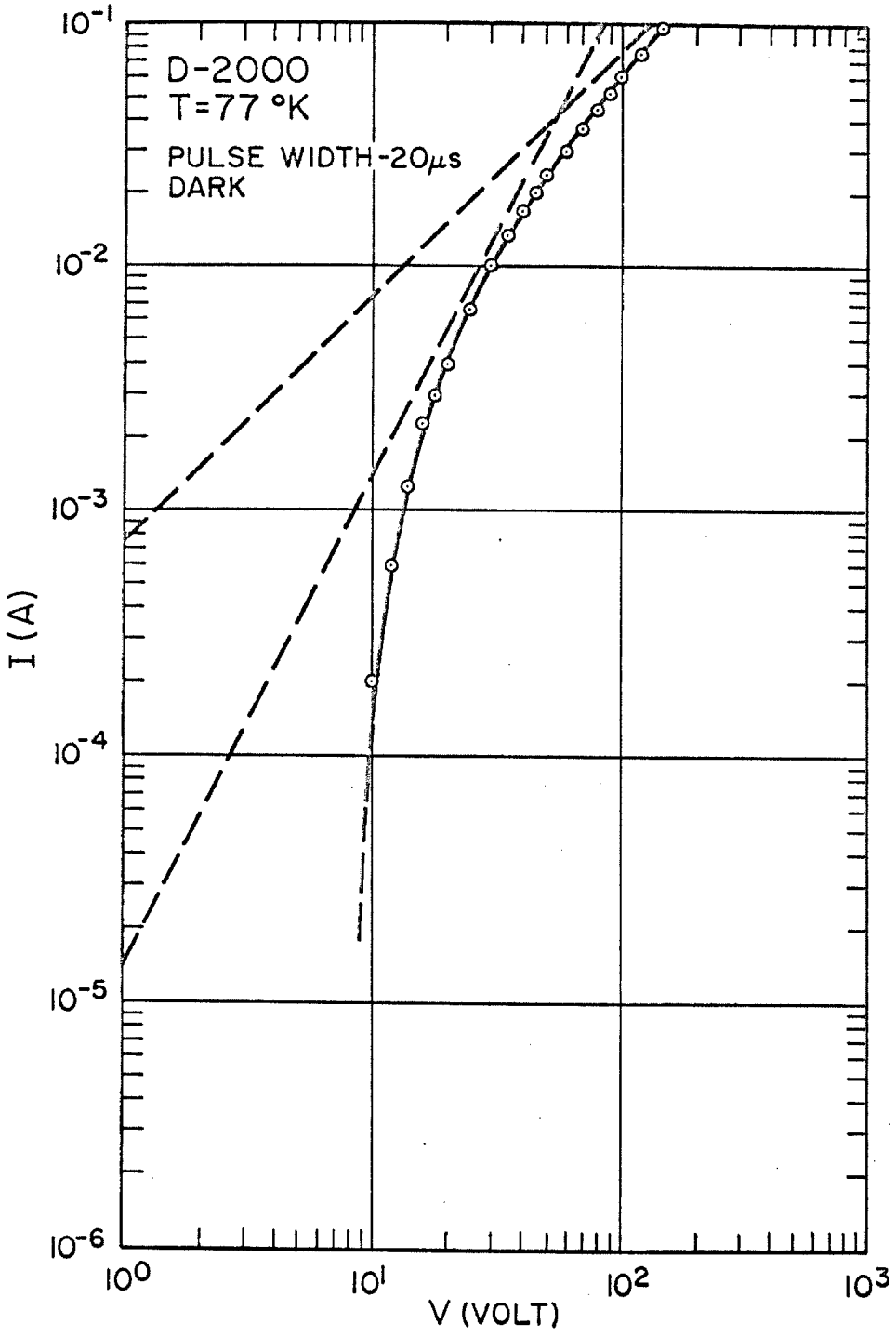
D-2000
T=77 °K
PULSE WIDTH-20μs
DARK
I (A)
V (VOLT)
10^-1
10^-2
10^-3
10^-4
10^-5
10^-6
10^0
10^1
10^2
10^3

Figure 3.19

dependence on applied voltage. The effect of a field dependent velocity is only noticeable in the range right after threshold at high temperatures. At 300°K (see figure (3.20)), a sizable deviation from a linear dependence is observed, due partly to a field dependent velocity and partly to J_{FBT}. Both tend to smooth out the abrupt jump in current density at threshold. As the temperature is lowered, the critical field and J_{FBT} decrease, hence, the deviation from a linear dependence diminishes, and at 77°K it is almost unnoticeable (see figure (3.21)).

Lowering the temperature below 77°K, causes the transition region from threshold to the linear range of the V-I characteristics to gradually disappear in all structures. Finally, over the temperature range $4.2^{o} \leq T \leq 50^{o}K$, the characteristics are independent of temperature. This behavior is a consequence of the variation with temperature of the limiting velocity, the critical field, and threshold. The limiting velocity is independent of temperature below 50°K, and the electrons deviate from thermal equilibrium at field strengths well below the built-in field established by the presence of a threshold. Also, the built-in field increases with decreasing temperature due to the increase in threshold caused by giant trapping. Over that temperature range, then, the V-I characteristics exhibit a linear dependence at any applied voltage above threshold. The

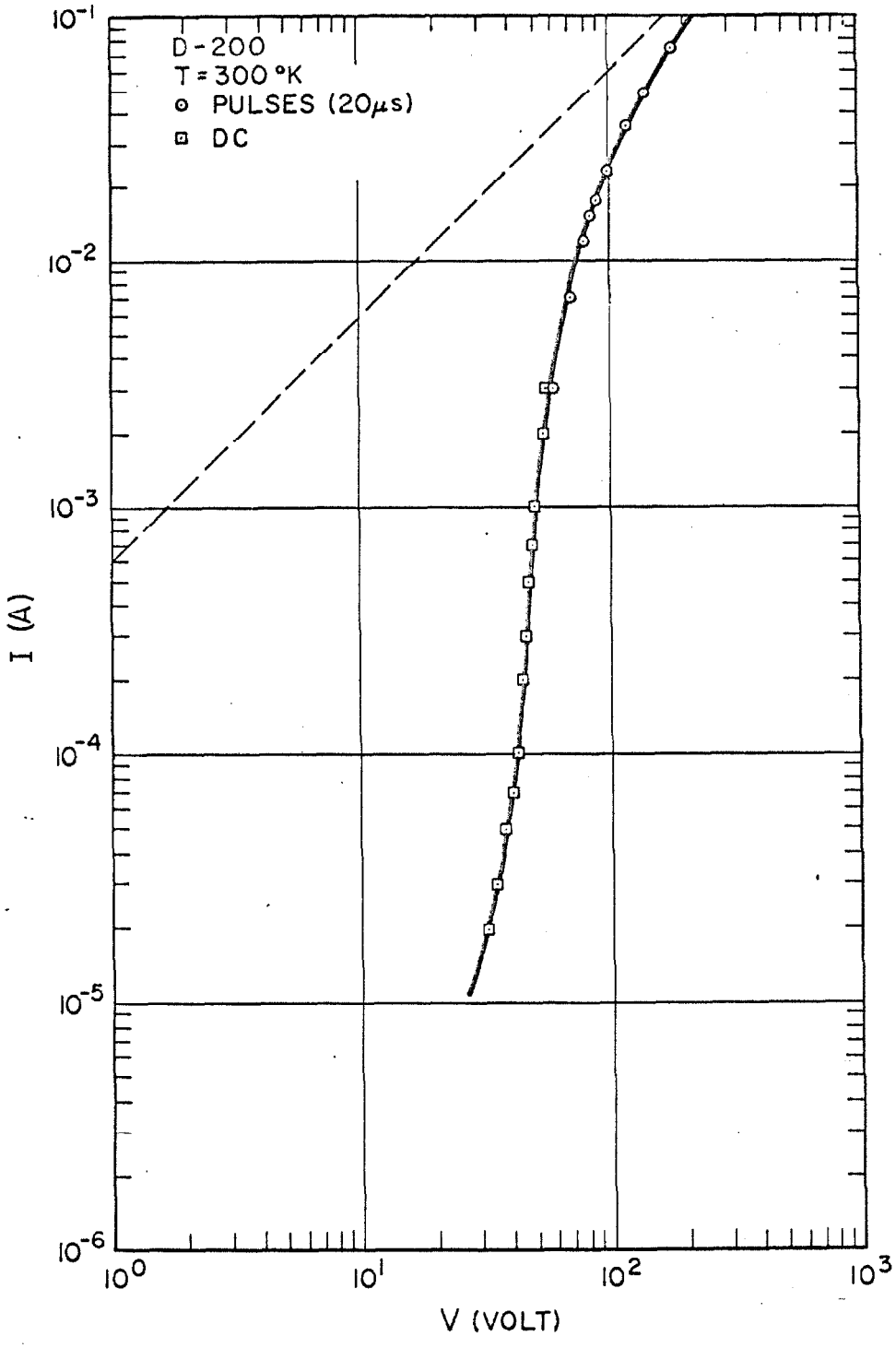
D-200
T = 300 °K
PULSES (20μs)
DC
I (A)
V (VOLT)
10^-1
10^-2
10^-3
10^-4
10^-5
10^-6
10^0
10^1
10^2
10^3

Figure 3.20

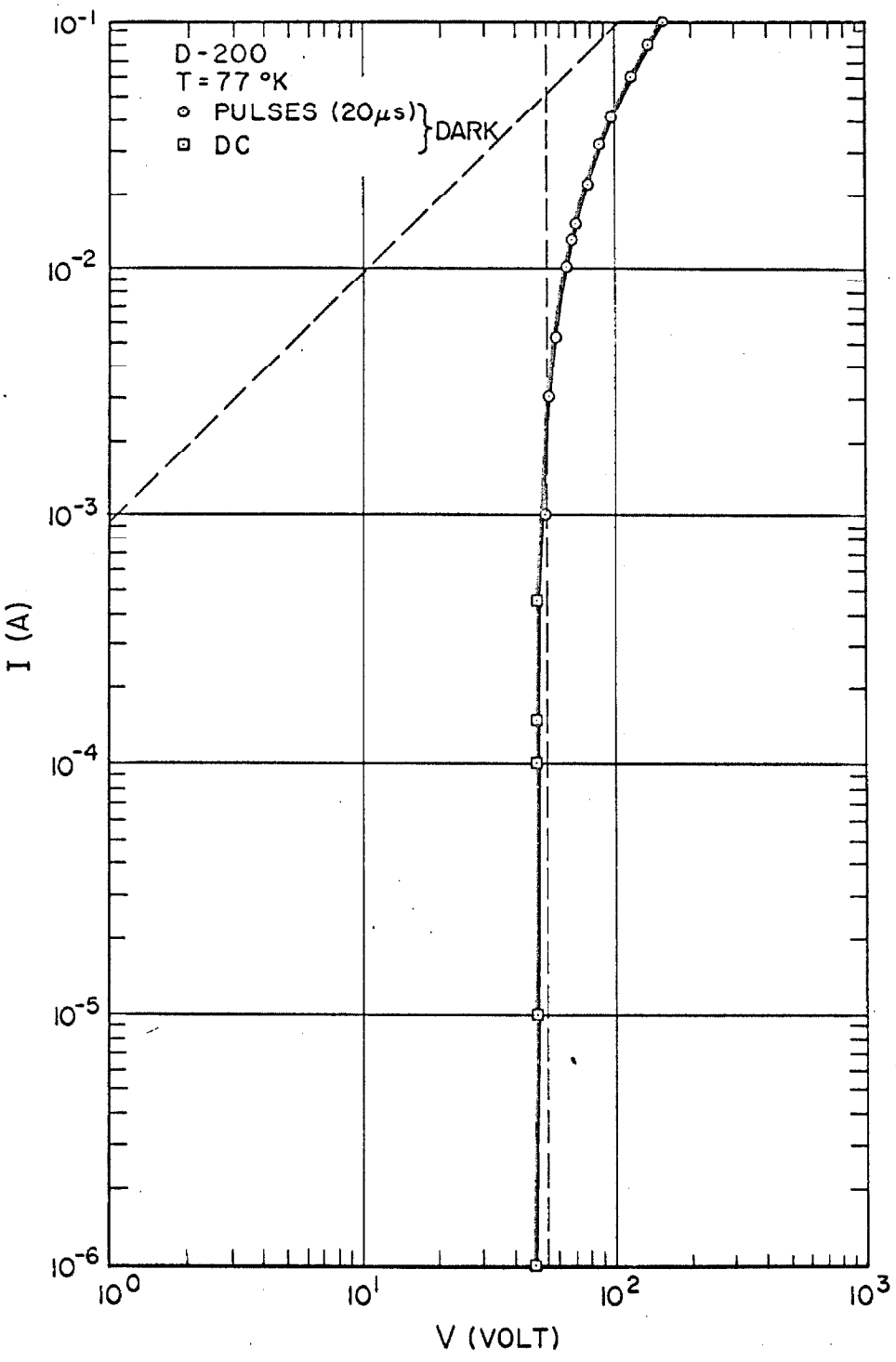
D-200
T=77 °K
PULSES (20μs)
DC
DARK
I (A)
V (VOLT)
10^-1
10^-2
10^-3
10^-4
10^-5
10^-6
10^0
10^1
10^2
10^3

Figure 3.21

experimental characteristics at 4.2°K are shown in figures (3. 8), (3.9) and (3.22) for the three types of structures. The agreement with the analytical model for pure unipolar sclc with a limiting velocity is remarkable. The current increases at threshold by five orders of magnitude without an appreciable increase in applied voltage.

To the author's knowledge, the only other measurement of pure unipolar sclc in silicon with hot electrons at 4.2°K was performed by Brown and Jordan[3.17]. These authors employed structures of the type n^+ n n^+. At that temperature, however, the type of impurity in the base region is irrelevant since the crystal becomes an ideal insulator. According to their evaluation of the V-I characteristics, the mobility as a function of the electric field is given by

$$\mu_n = 2.1 \times 10^6 \, E^{-0.8} \ (cm^2 \, V^{-1} \, sec^{-1}) \quad . \tag{3.20}$$

This relation was obtained from a comparison of the experimental V-I characteristics with an analytical model for pure unipolar sclc which assumes a field dependent mobility of the type

$$\mu_n = K_o E^{-\alpha} \quad , \tag{3.21}$$

and which yields the following expression for the dc characteristic,

$$J = \left(\frac{3 - \alpha}{2 - \alpha} \right) \left(\frac{\varepsilon \varepsilon_o K_o}{2 - \alpha} \right) \frac{V^{2-\alpha}}{W^{3-\alpha}} \quad . \tag{3.22}$$

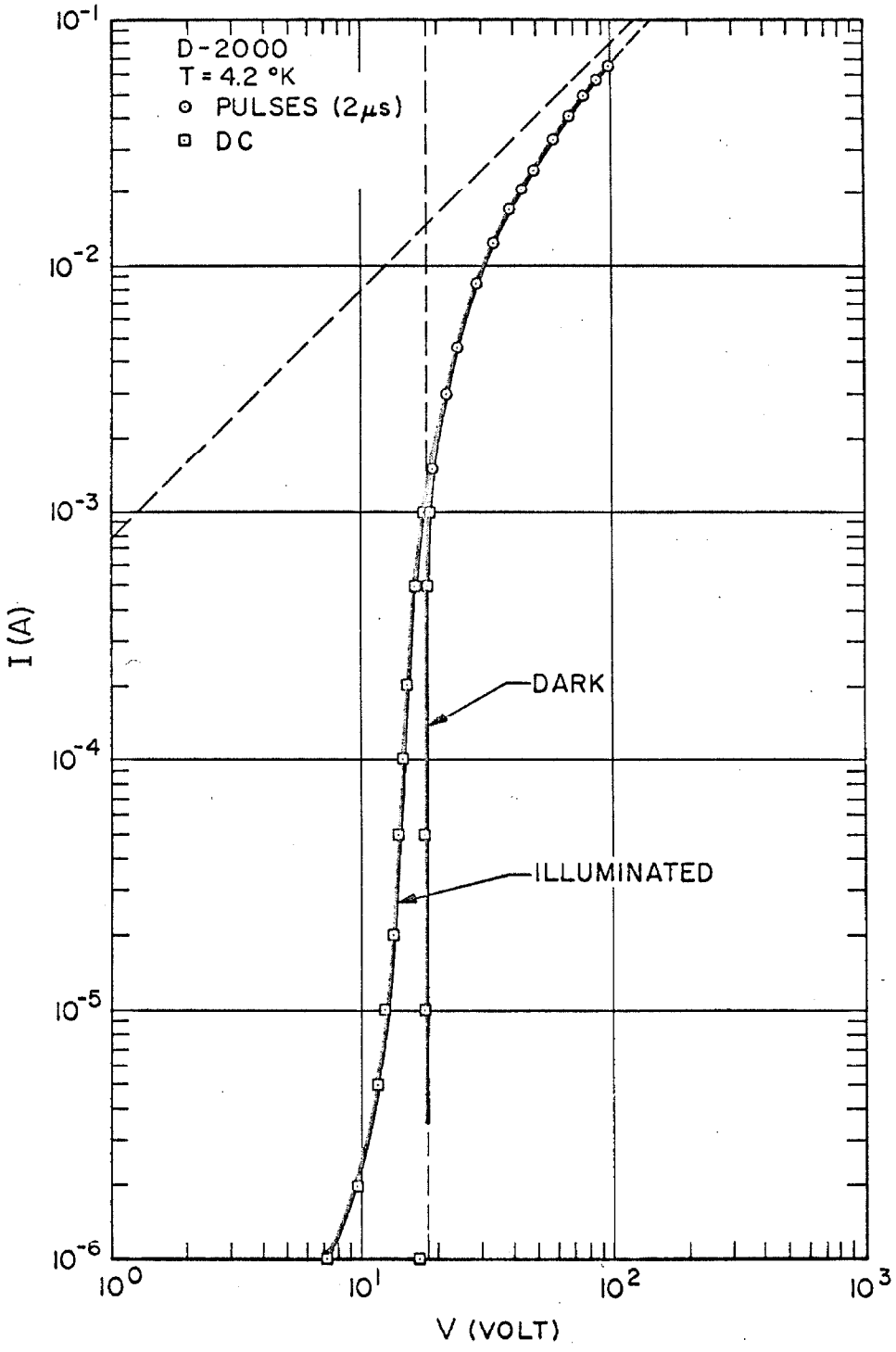
D-2000
T = 4.2 °K
o PULSES (2μs)
□ DC
DARK
ILLUMINATED
I (A)
V (VOLT)
10^-1
10^-2
10^-3
10^-4
10^-5
10^-6
10^0
10^1
10^2
10^3

Figure 3.22

Expression (3.20) does not agree with our experimental observations at 4.2°K. Our analysis of their data reveals, however, that the slope of the V-I characteristics is not 1.2 but 1.0, as our results would indicate. Figure (3.23) illustrates their results. The dots correspond to the experimental points and the smooth curve to the theoretical model for pure unipolar sclc with a limiting velocity. The agreement is excellent. Moreover, if a straight line is drawn through all the experimental points for currents above 10^{-1} amp., as was done in reference (3.17), the slope obtained is 1.25. It seems that the authors failed to realize that when the V-I characteristic is plotted in log-log paper, the true slope is observed only for voltages orders of magnitude above threshold. Their thickness dependence of the current density has also been replotted in figure (3.24). A straight line of slope 2.0 seems to fit the data as well as one with slope 2.2. This re-evaluation of Brown and Jordan data indicates that indeed a limiting velocity is present at 4.2°K in their case also. The magnitude of the limiting velocity was calculated from their data to be approximately 1.7×10^7 cm/sec., which is in very good agreement with our result. Thus, this analysis provides an independent check for our findings at this temperature. Brown and Jordan did not have a visual display of the V-I characteristics and a mistake in evaluating the data from a log-log plot is quite plausible.

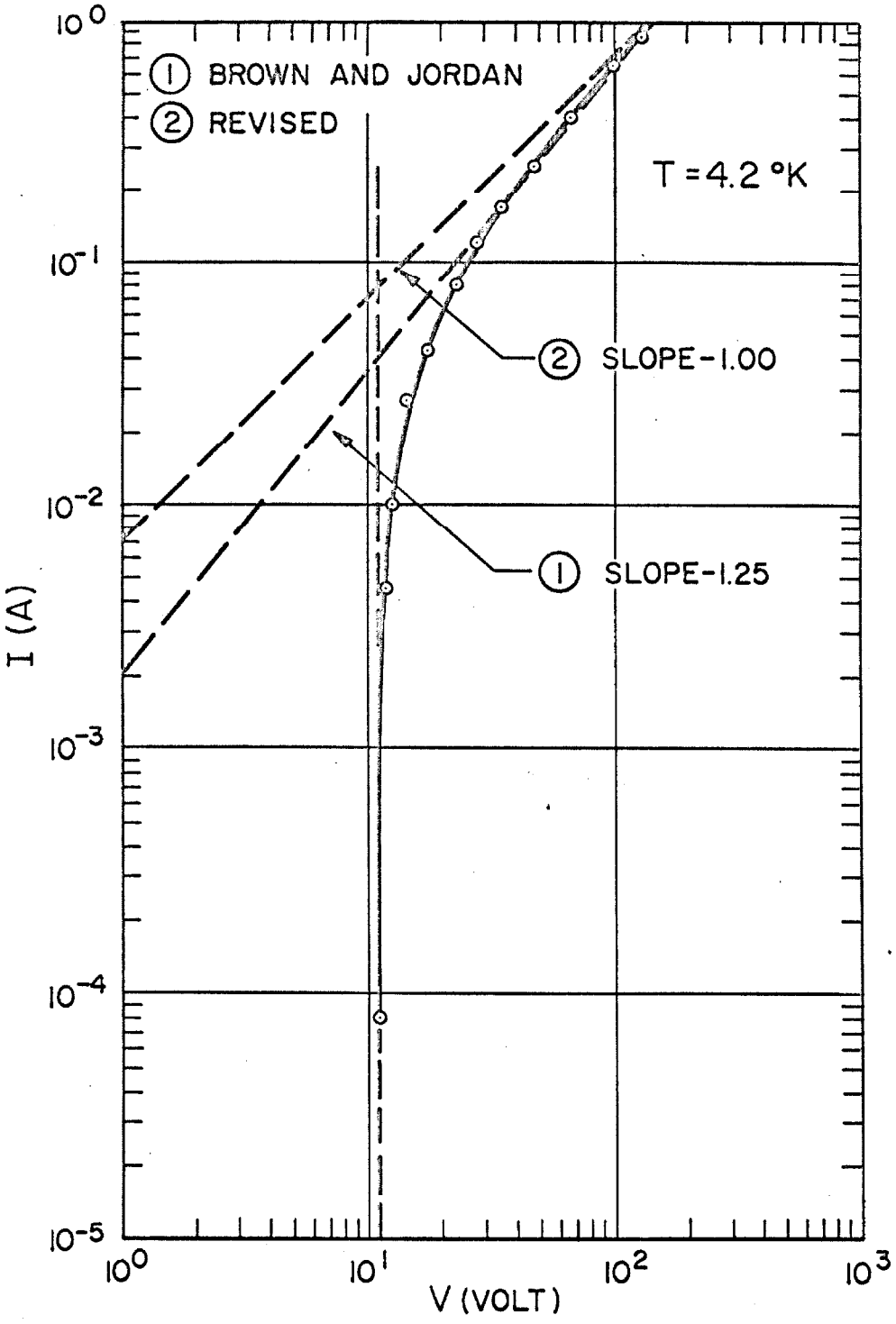
① BROWN AND JORDAN
② REVISED
T = 4.2 °K
② SLOPE-1.00
① SLOPE-1.25
I (A)
V (VOLT)
10^0
10^-1
10^-2
10^-3
10^-4
10^-5
10^0
10^1
10^2
10^3

Figure 3.23

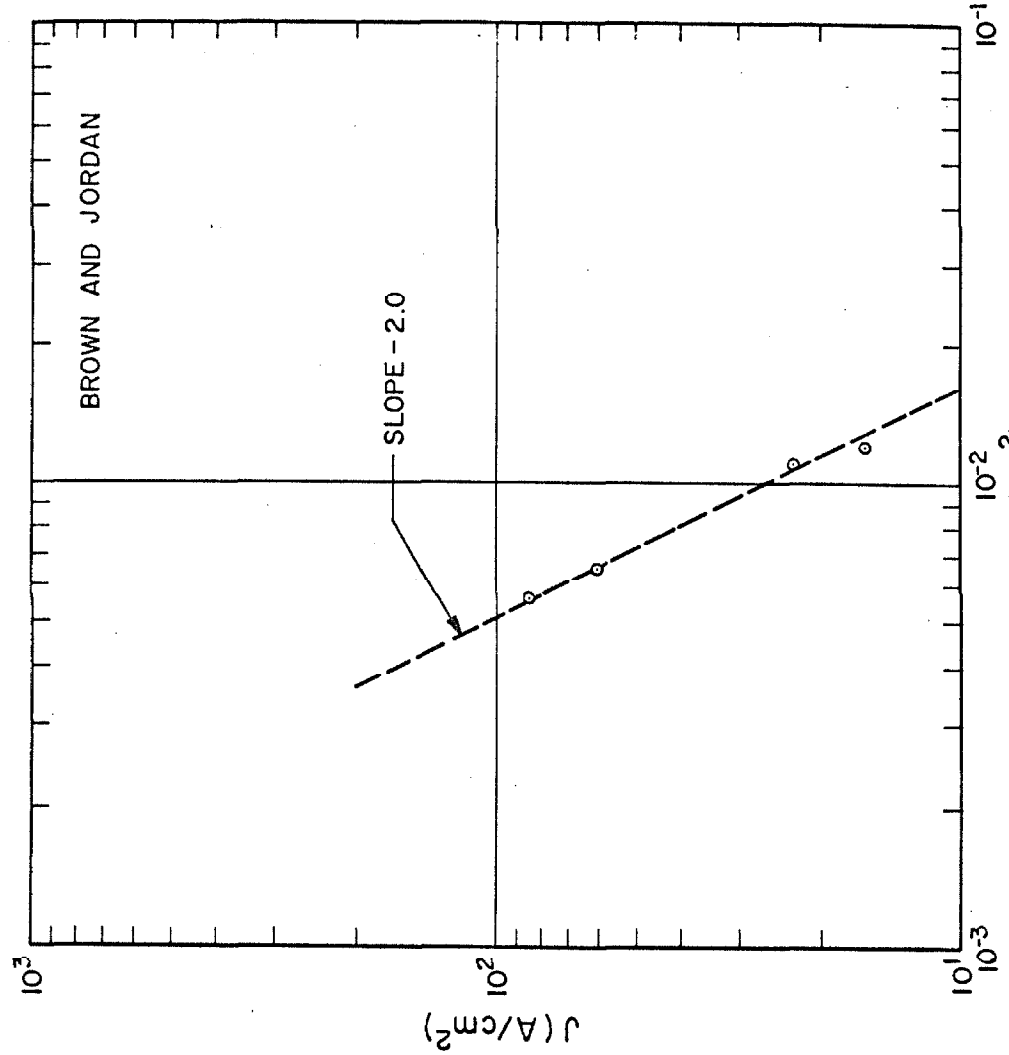

Figure 3.24

In the range of pure unipolar sclc, the V-I characteristics should be essentially independent of illumination except when trapping is present below threshold. In this instance, illumination causes the trapped electrons to be excited back into the conduction band in between ramps, if the repetition rate is small as compared to the release time. This tends to increase the range of pure unipolar sclc toward lower operating points. This extension could otherwide be accomplished only by taking single shot measurements and recycling the sample from T_o - temperature at which the measurements are taken - to 300°K and back to T_o, in order to thermally re-excite the electrons into the conduction band after each pulse. With light of the proper frequency and fast enought pulses, the range of pure unipolar sclc can be extended to very low voltages at low temperatures. Figures (3.1) and (3.9) illustrate the effect on an R-2000 structure at 77° and 4.2°K. A noticeable increase in the range of pure unipolar sclc is observed at both temperatures.

3.2.3 The effect of geometry. The geometrical configuration of the R and D-structures has been designed to conform with the assumption of a planar geometry. Nevertheless, for the sake of simplifying the manufacturing procedure, this has not been fully accomplished. The D-structures approach very closely the ideal case and current flow is symmetrical for both polarities if the resulting chip, after dicing, has the same area for both sides. The R-structures, however, are physically unsymmetrical. One side of the wafer is diffused throughout the entire area (bottom) while the opposite side (top) is masked to yield a large number of circular dots. When the bottom side is reverse biased, the depletion region will move uniformly toward the top throughout the wafer until threshold is reached. If the thickness is uniform, at least within one circular dot, the whole area of the emitter will start conducting at the same applied voltage. The current flow will be unidirectional since the equi-potential lines run parallel with respect to the surface of the wafer, except at the outer perimeter of the dots (see figure (3.25)). The contribution from the surrounding dots is negligible. When the top side is reverse biased, the depletion region will not only expand in depth, but also in width. When it finally reaches the bottom junction, current flow will not be unidirectional (see figure (3.26)). As the applied potential is increased above the value at which appreciable current is observed, the conducting area will tend to

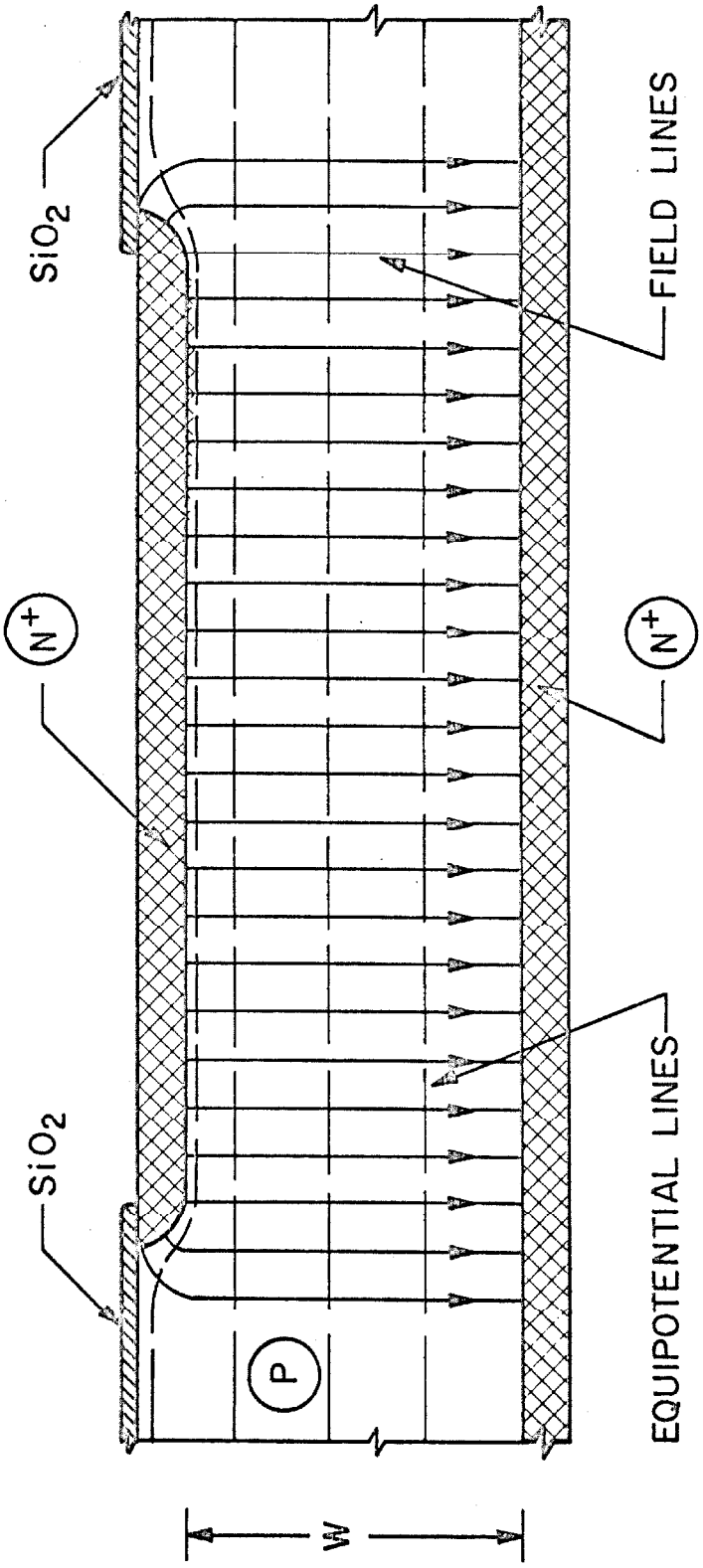

Figure 3.25

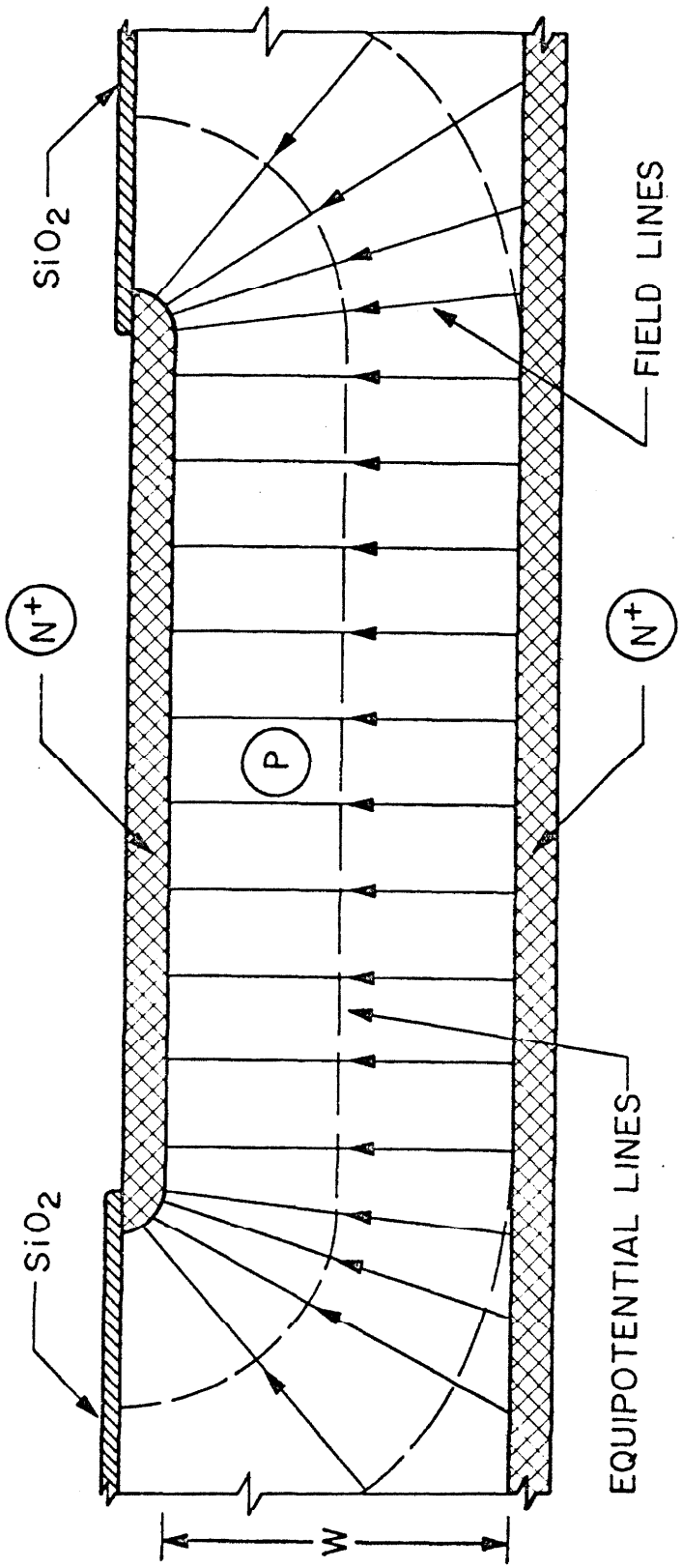

Figure 3.26

increase further significantly. R-structures, thus, are electrically non-symmetrical.

Rodriguez and Nicolet[3.18] solved the problem of pure unipolar sclc in three geometrical configurations - planar, cylindrical and spherical - and concluded that the current density would have the same voltage dependence regardless of geometry if the configuration is independent of applied voltage. The V-I characteristics are, in general, described by the relation

$$I = \delta_T \, (\bar{x}) \, V^2 \tag{3.23}$$

for thermal carriers, and

$$I = \delta_H \, (\bar{x}) \, V \tag{3.24}$$

for hot carriers, where $(\bar{x})$ is determined by the geometrical configuration. In particular, for a planar configuration,

$$\delta_T = 9/8 \cdot 1/W^3 \cdot A \tag{3.25}$$

and

$$\delta_H = 2 \cdot 1/W^2 \, A \quad , \tag{3.26}$$

where A is the area of the contacts.

The D-2000 and D-200 structures have the same geometry and, as expected, their behavior conforms with the analysis of pure unipolar sclc for a planar configuration. The R-structures also conform with

the analysis carried out in chapter 1, but an effective geometrical factor is found empirically different from that of a planar configuration and different for both biasing modes. When the top junction is forward biased, the V-I characteristics can be analyzed and made to conform with theory by employing (3.25) and (3.26) with an effective area equal to 5.5×10^{-4} cm^2 which is bigger than the area of the dot in the top side. Hence, the current flow is unidirectional as anticipated from the discussion of the field distribution for this polarity (see figure (3.25)). When the bottom junction is forward biased, the V-I characteristics cannot be described with the geometrical factor for a planar configuration with an effective area. Again, this is in agreement with the field distribution obtained for this polarity (see figure (3.26)). Figure (3.27) illustrates the V-I characteristics obtained for this biasing mode at 77°K. The experimental characteristic is compared with theory as was done in the previous sections, and the agreement is excellent. The deviation from linearity at high applied voltages is caused by impact ionization. Along the periphery of the circular area in the top side, there is a large gradient in the concentration of ionized impurities present. Consequently, by Gausses law, a large electric field results which causes microplasma breakdown at lower applied voltages than expected. $\delta(\bar{x})$ is then fairly insensitive to applied voltage since the current density follows the voltage dependence

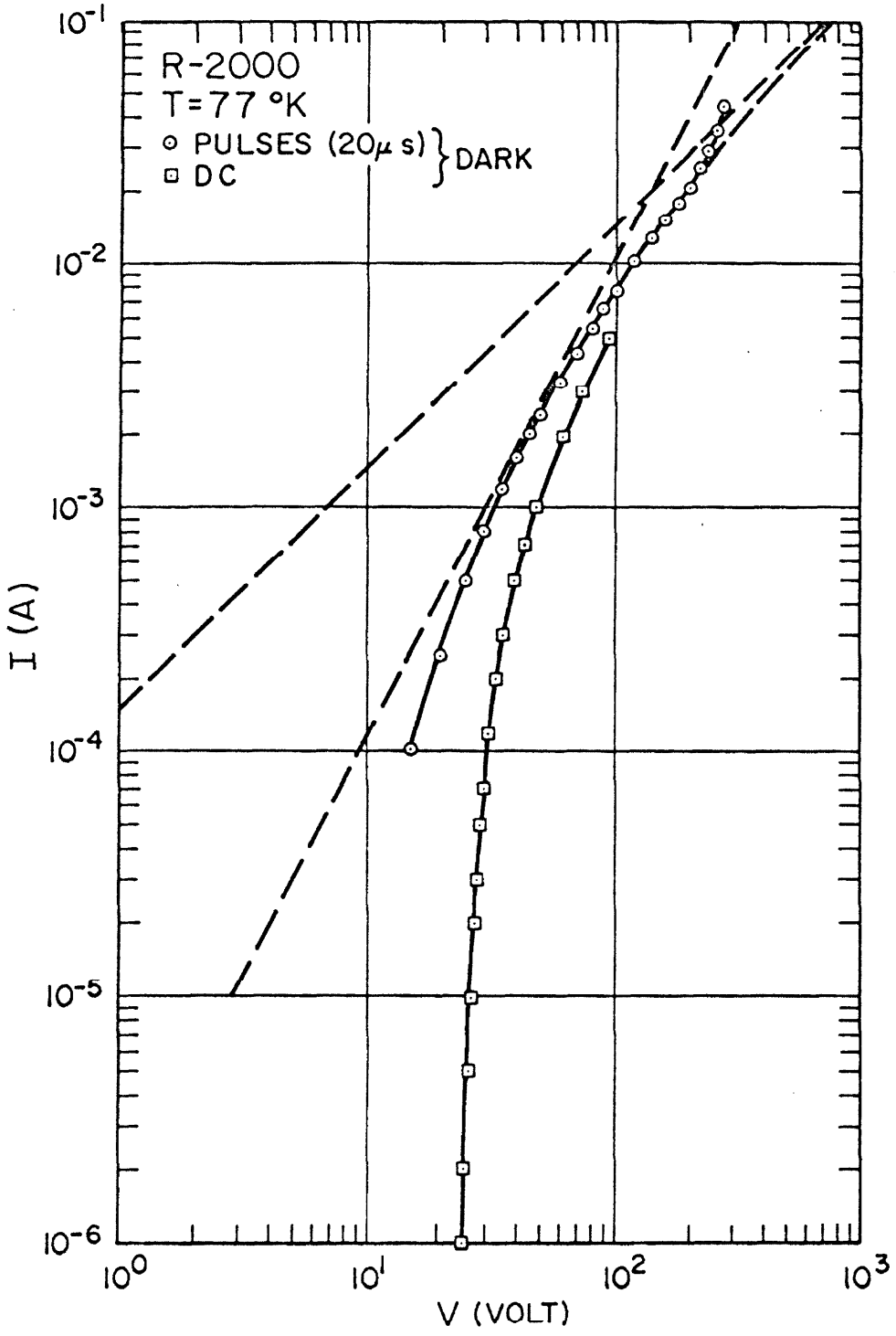
R-2000
T=77 °K
⊙ PULSES (20μ s)
□ DC
DARK
I (A)
V (VOLT)
10^-1
10^-2
10^-3
10^-4
10^-5
10^-6
10^0
10^1
10^2
10^3

Figure 3.27

predicted theoretically for a constant geometrical configuration. We know, however, that the emitting area is a function of applied voltage. The discrepancy can be explained by realizing that the predominant contribution to the current density comes from the emitting area below the collector, where the equipotential lines run parallel to the surfaces of the crystal. Carriers emitted from any other place in the bottom surface must transverse a larger path to reach the collector and, consequently, their contribution to the current flow is not as great and decreases as the path increases. Thus, the added contribution due to an increase with applied voltage of the emitting area is negligible and does not affect $\delta(\underline{x})$.

The geometrical factors found empirically for both polarities are bigger than the corresponding one for a planar geometry. It is seen that this must be the case by glancing at figures (3.25) and (3.26), since the planar case is included for both polarities.

3.2.4 The field-velocity relationship. We shall now discuss the possibility of using pure unipolar sclc to determine the drift velocity for all field strengths and at any temperature. Consider an R- or D-2000 structure at 300°K. From the square and the linear ranges of the V-I characteristic the low field mobility and the limiting drift velocity are obtained. The transition region is best approximated by an empirical relation of the form (1.26). Substituting the experimental values for v_s and E_o, this yields

$$v = 1.0 \times 10^7 \tanh E/7.5 \times 10^3 \qquad (3.27)$$

In figure (3.28), this dependence is compared with Norris and Gibbons' field-velocity relationship obtained by a time-of-flight technique[3.19]. The agreement is excellent at all field strengths. A comparison with determinations made by other authors[3.20-23] reveals that our relationship gives higher values at all field strengths and a better defined limiting velocity range (see figure (3.29)).

Prior's results[3.21] are in remarkable disagreement with all available determinations of the field velocity relationship because of an undue variation with the resistivity of the material. A possible explanation for this discrepancy is as follows. Some of his data can readily be interpreted with a model mentioned in chapter 1 where it is assumed that a field dependent mobility exists for the electrons present at thermal equilibrium, and that injection is

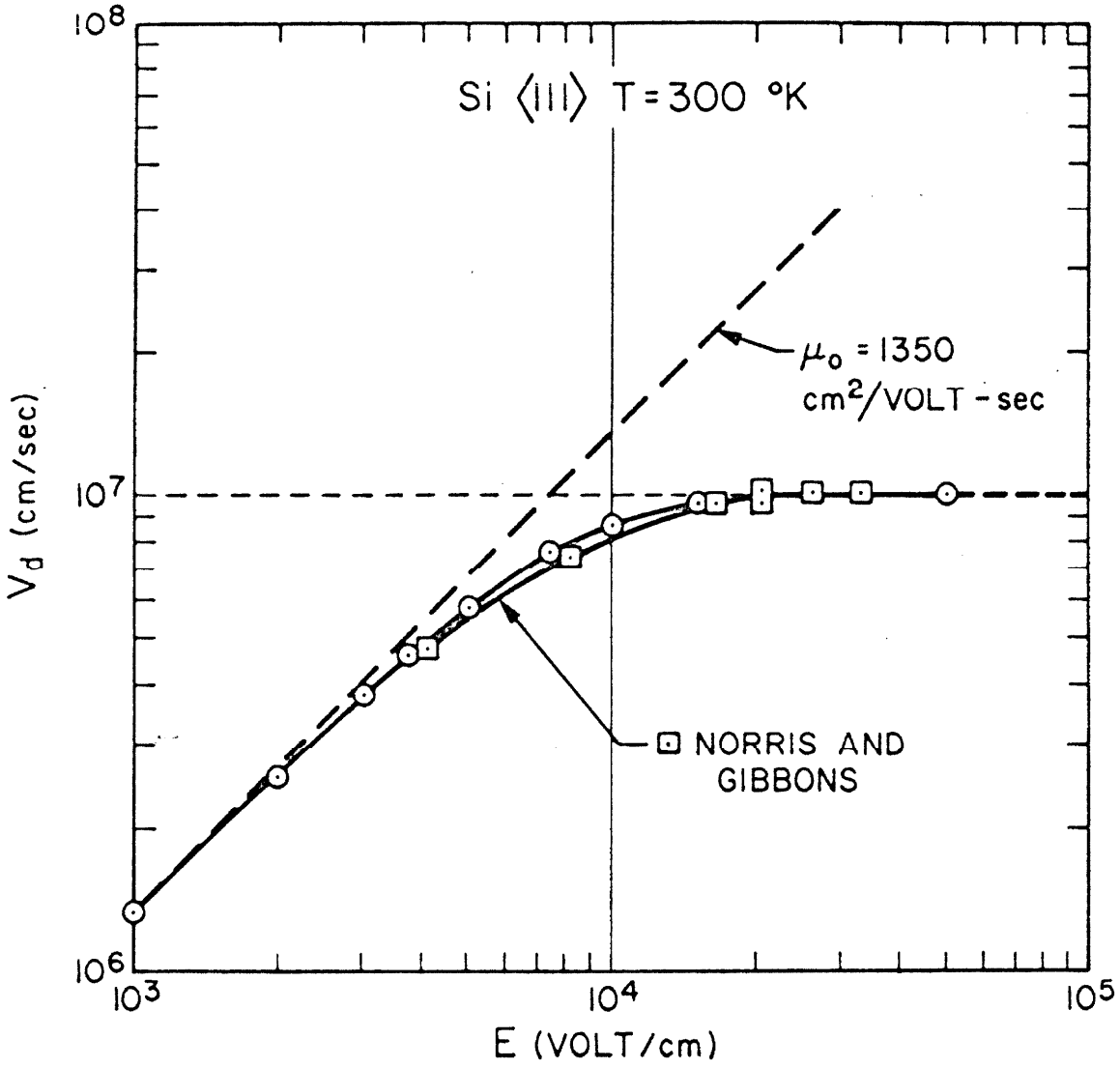
Si ⟨111⟩ T = 300 °K
μ_o = 1350
cm²/VOLT - sec
NORRIS AND
GIBBONS
V_d (cm/sec)
E (VOLT/cm)
10^8
10^7
10^6
10^3
10^4
10^5

Figure 3.28

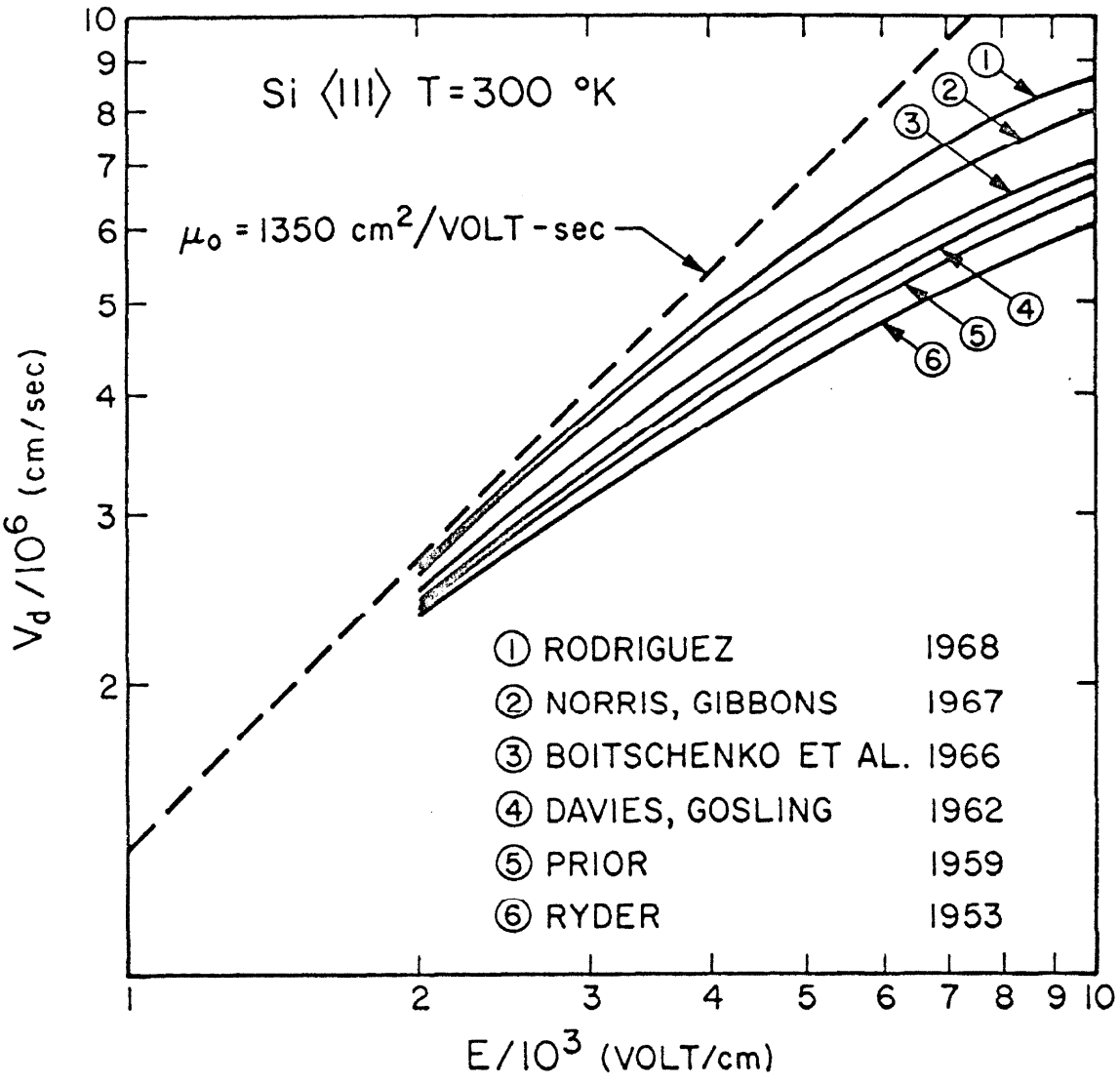
Si ⟨111⟩ T=300 °K
μ_o = 1350 cm²/VOLT-sec
① RODRIGUEZ 1968
② NORRIS, GIBBONS 1967
③ BOITSCHENKO ET AL. 1966
④ DAVIES, GOSLING 1962
⑤ PRIOR 1959
⑥ RYDER 1953
$V_d/10^6$ (cm/sec)
$E/10^3$ (VOLT/cm)
10
9
8
7
6
5
4
3
2
1
2
3
4
5
6
7
8
9
10

Figure 3.29

significant only at high field strengths (see figure 1.10). Of all the cases considered by Prior, the variation of the current density with electric field for a 34 Ω-cm n-type germanium sample is best explained in terms of the previous model. Unfortunately, Prior does not specify the thickness of the sample. But, if a width of 500 microns is assumed - which is within the specified crystal lengths -, one finds that the thermal and space charge contributions are equal at a field strength of the order of 5.10^4 v/cm. This agrees with his experimental result. If the same type of calculation is carried out for a 300 Ω-cm n-type silicon sample 500 microns thick, the electric field at which the two contributions are equal is 1.0×10^5 v/cm, again in fairly good agreement with what is observed experimentally as illustrated in figure (3) of Prior's publication. Our model also explains the variations in the field velocity relationship with crystal thickness observed in some of Prior's results since the contribution of the injected carriers to the current density has a stronger dependence on thickness than the ohmic contribution. A more accurate re-evaluation of Prior's data would require a numerical analysis encompassing the effect of injection at any field strength. The previous arguments are sufficient, however, to strongly suggest that Prior's erratic results were caused by electron injection at the negative contact. This also demonstrates the advantage of using, rather than suppressing, pure unipolar sclc to obtain the field velocity relationship. Prior's results at low field strengths may have been affected by

impurity scattering as well, since the resistivity of his base material varies by two orders of magnitude. This possibility is explored next.

In general and chronologically, from 1953 to 1968, the determinations of the field-velocity relationship for n-type silicon yielded increasingly higher values for the drift velocity at a fixed field strength. This coincides with the period of great progress in silicon technology. Two decades ago, the quality of the silicon crystals was low. The highest resistivities possible were of the order of ohm cm. Presently, it is possible to achieve resistivities as high as 100 kΩ - cm. In chronological order, the resistivity of the silicon crystals used to obtain the results illustrated in figure (3.27) are, in Ω-cm: (1) Ryder $\sim 10^{(3.20)}$, (2) Prior$^{(3.21)}$ 5-300, (3) Davies 70$^{(3.22)}$, (4) Boitschenco 20$^{(3.23)}$, (5) Norris $23 \times 10^{4(3.19)}$, (6) Rodriguez 20×10^4. Thus, the impurity concentration, as determined from resistivity values, has been reduced by four orders of magnitude within this time interval.

It has been established theoretically and experimentally$^{(3.24,25)}$ that impurity scattering is a dominant mechanism of the mobility at low field strengths. For intermediate fields strengths (the warm electron range), the mobility should be well approximated by$^{(3.26)}$

$$\mu = \mu_o (1 + \beta E^2) \qquad (3.27)$$

where μ_o is the low field mobility and β is independent of the field, but dependent on the impurity concentration. The variation of β with impurity concentration, as obtained by Gunn[3.27], for n-type germanium at 77°K is illustrated in figure (3.30). At high field strengths, impurity scattering is expected theoretically to be ineffective. Consequently, the high field mobility should be the same for pure and impure samples. As the field is increased from low values, the contribution of impurity scattering decreases and the mobility increases. Simultaneously, the carrier temperature increases and lattice scattering by acoustical and optical phonons reduces the mobility. The two effects oppose each other. Experimentally, an increase in mobility with electric field has been observed, but it is much smaller than expected theoretically[3.28]. Contradictory results have been reported at high field strengths[3.27,28]. In general, impurity scattering decreases the low field mobility and shifts the point of dominating lattice scattering to higher field strengths.

It is seen in figure (3.29) that the variation of the drift velocity at a fixed field strength is opposite from what is expected from impurity scattering, i.e., the deviation from linearity occurs at higher field strengths for purer samples. A plausible explanation for this discrepancy is the fact that the various determinations were obtained with samples of different crystallographic orientations and,

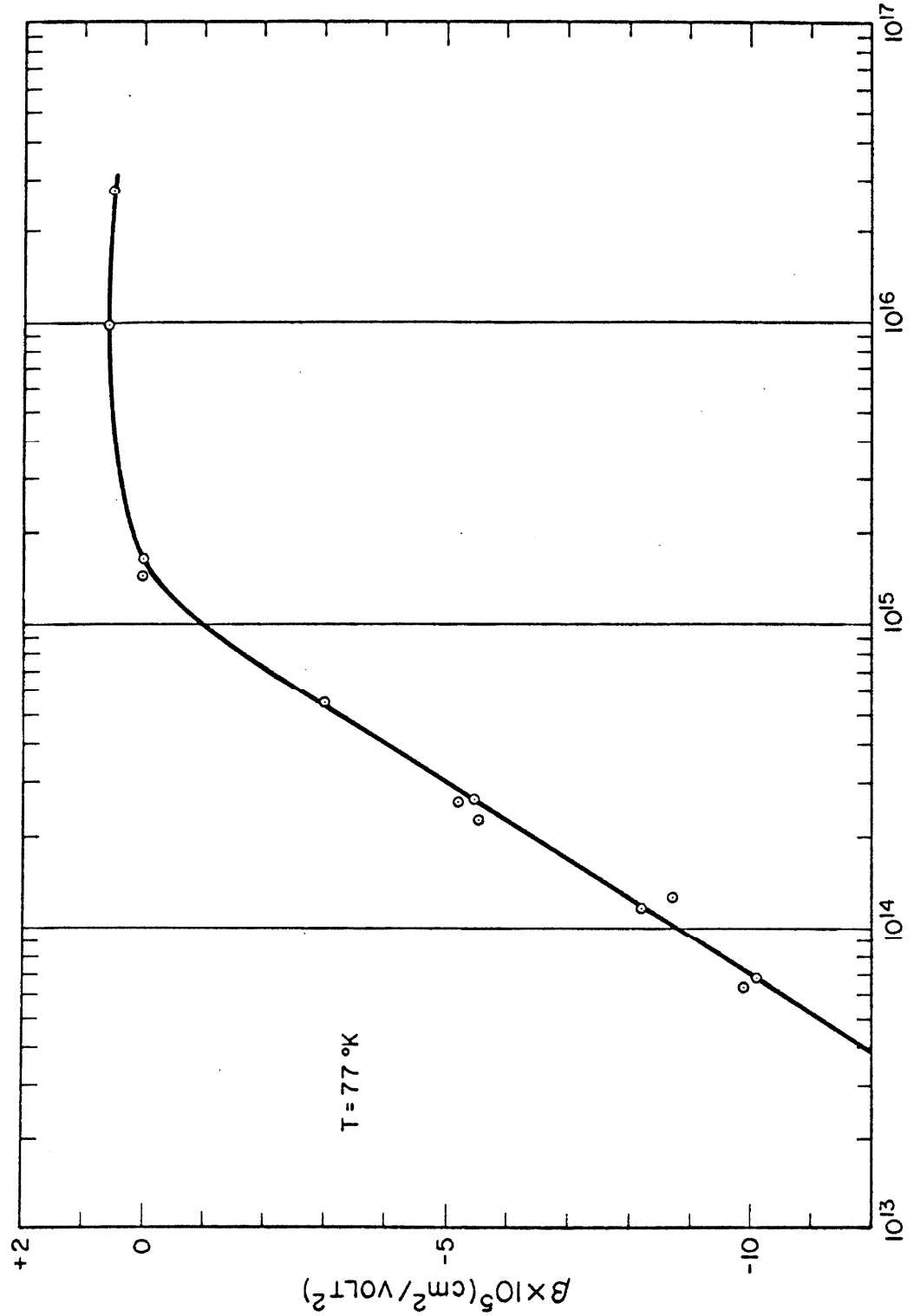
$\beta \times 10^5 (cm^2/volt^2)$
+2
0
-5
-10
T = 77 °K
10^{13}
10^{14}
10^{15}
10^{16}
10^{17}
N_I (cm^{-3})

Figure 3.30

consequently, anisotropy effects must be taken into account. For a treatment of anisotropy the reader is referred to references[3.29,30,31] where it is analyzed both experimentally and theoretically. It is unfortunate that most of the currently available measurements of the field velocity relationship, at least for silicon at 300°K, have been obtained from normalized I-V characteristics by assuming a low field mobility of 1350 cm^2/volt-sec., regardless of the impurity content. This renders some of these data useless since the true relationship has been shifted up or down by a factor dependent on the discrepancy of the low field mobility from the assumed value. A more logical approach would have been to determine the true low field mobility from Hall effect measurements or some other suitable technique. As a last remark, it should be stated that other phenomena - as injection at intermediate and high field strengths - can be responsible for some of the discrepancy observed, however, impurity scattering and anisotropy effects should be considered strong possibilities.

At 77°K, the experimental characteristic of a D-2000 structure is also compared with an analytical model for pure unipolar sclc which assumes a field-velocity relationship of the type (1,26). However, in this instance, the comparison is not as accurate as at 300°K because a clearly defined square range is not present. A low field mobility of approximately 2.3×10^4 cm/volt-sec is obtained from the

analysis. The field-velocity relationship is found to be represented by the relation

$$v_d = 1.4 \times 10^7 \tanh E/7.0 \times 10^2 \quad . \qquad (3.28)$$

The accuracy of this expression is to some extent questionable except at high field strengths where a clearly defined limiting velocity range is observed in the V-I characteristics. A better determination is possible if monochromatic light is used to photoexcite the trapped carriers and reduce the threshold voltage. Our present result, however, at least reflects the general tendency of the field-velocity relationship as the temperature is decreased.

In figure (3.31), the relation 3.28 is compared with Jorgenson's determination of the drift velocity at 77°K, with an n-type 25 Ω-cm sample[3.32]. Much of the discrepancy can be explained in terms of impurity scattering. D. Long et al.[3.25] have obtained the temperature dependence of the electron mobility in a set of n-type silicon samples of varying impurity content and compensation between 30° and 100°K. For a 25 Ω-cm sample, the low field mobility at 77°K should be of the order of 10^4 cm^2/volt-sec. But this merely sets a lower limit to μ_o because the resistivity is not a good measure of the total concentration of impurities when compensation is present. The value of 2.10^4 used by Jorgenson is in disagreement with the

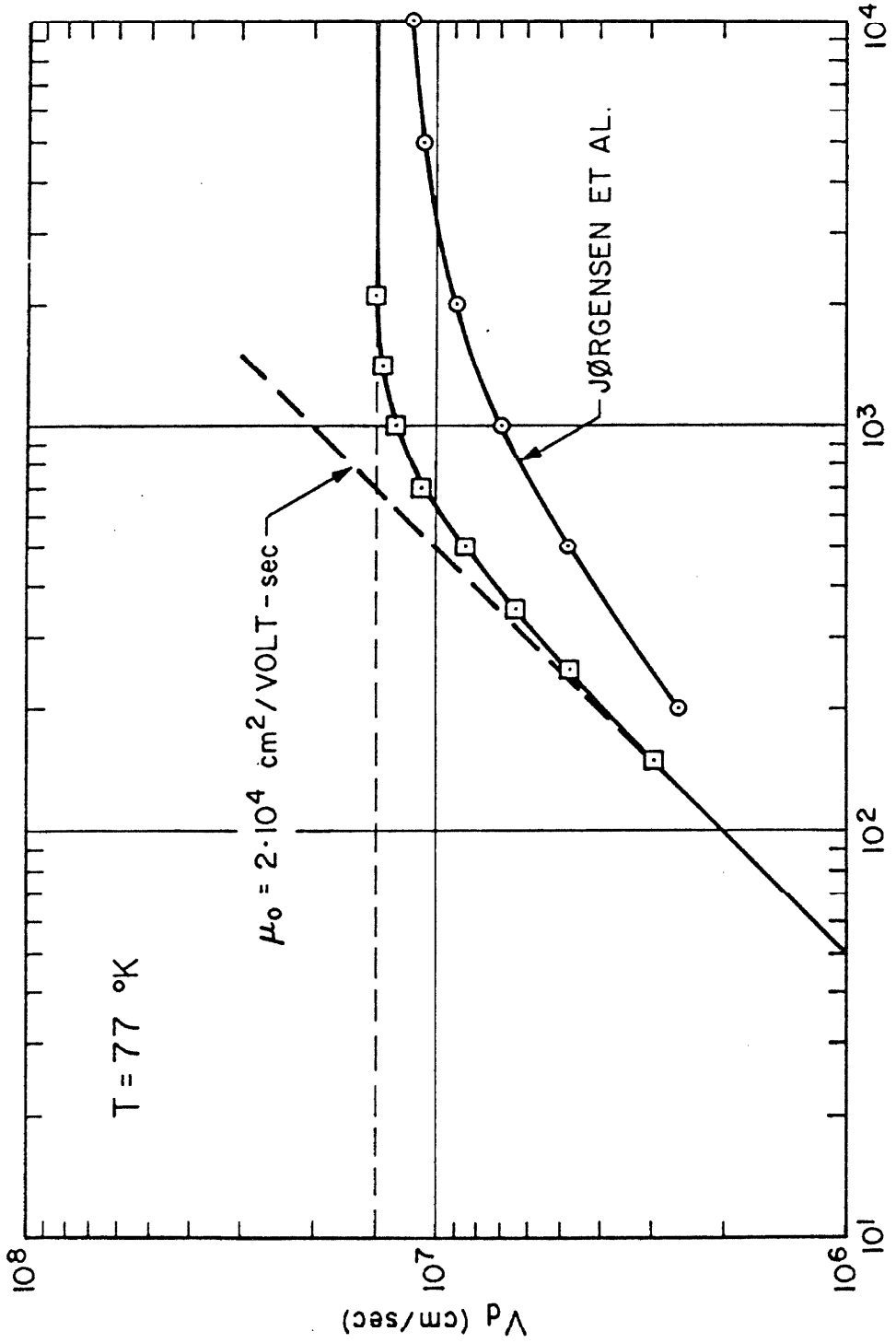
JØRGENSEN ET AL.
$\mu_o = 2 \cdot 10^4$ cm^2/VOLT-sec
T = 77 °K
V_d (cm/sec)
E (VOLT/cm)
10^8
10^7
10^6
10^1
10^2
10^3
10^4

Figure 3.31

previous estimate. For a sample with an impurity concentration of the order of 10^{13} cm^{-3}, as present in the R- and D-2000 structures, the low field mobility should be about 2.10^4, in agreement with our finding. Hence, it seems reasonable that Jorgenson's low field mobility was reduced by impurity scattering. Lattice scattering then starts dominating the mobility at higher field strengths which would explain the absence of a limiting velocity range in his measurement. Also, it should be noticed in figure (2) of his work, that anisotropy effects seem to be still present for the sample with the closest orientation to the (111) direction, which would tend to increase the transition region at intermediate field strengths. Our samples are almost free of impurity scattering and a well defined limiting velocity range is observed.

Below 77°K, the V-I characteristics contain no information about the mobility at low and intermediate field strengths since the behavior is linear above threshold. Photoexciting the trapped carriers an extension of the linear range and the probable appearance of the transition and square regimes in the V-I characteristics could be accomplished. Nevertheless, it is possible to infer from the previous analysis that the field-velocity relationship will most probably exhibit the temperature dependence illustrated in figure (3.32). This result is qualitative except at high field strengths where information has been obtained about the limiting velocity from the V-I characteristics.

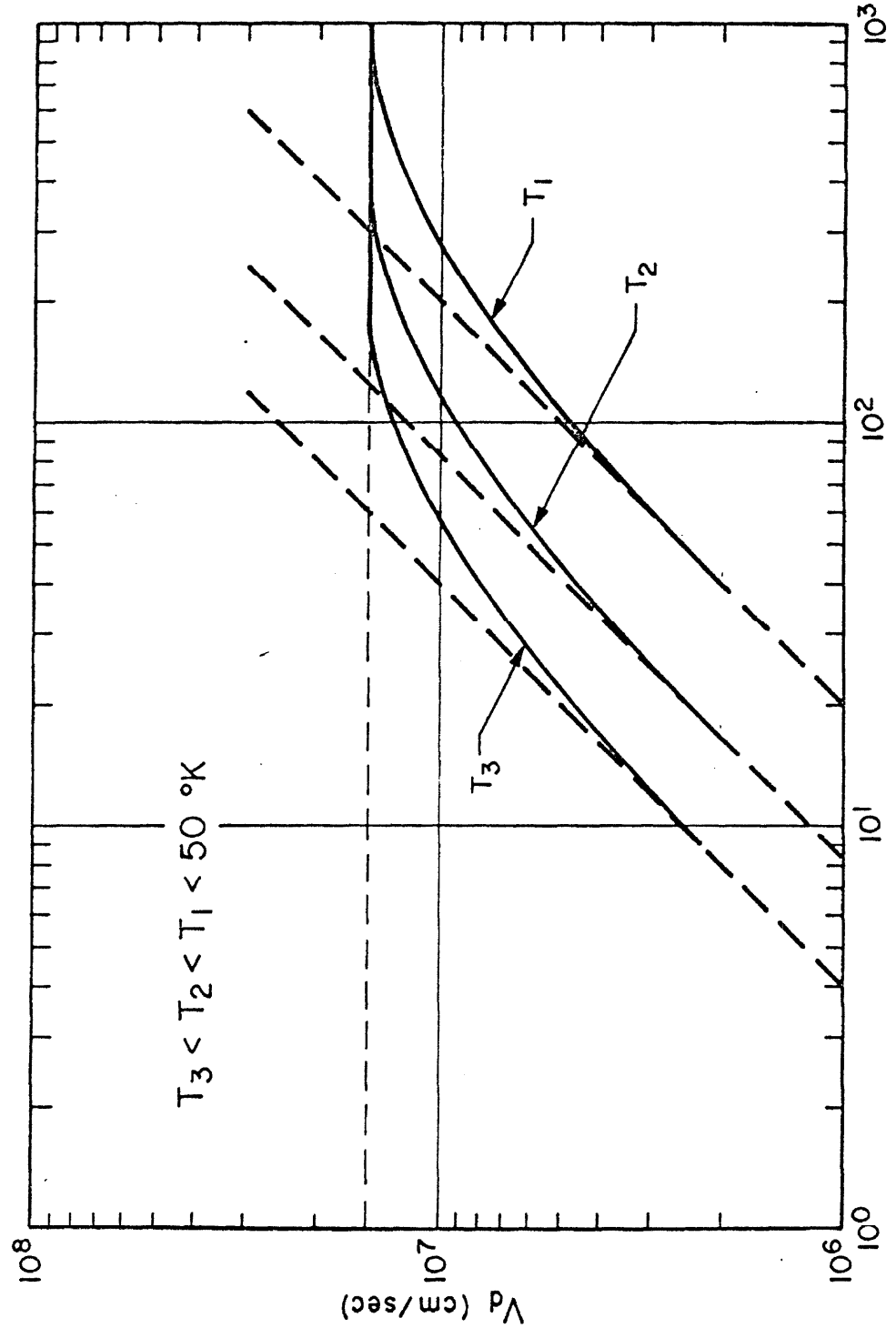
$T_3 < T_2 < T_1 < 50$ °K
T_1
T_2
T_3
V_d (cm/sec)
E (VOLT/cm)
10^8
10^7
10^6
10^0
10^1
10^2
10^3

Figure 3.32

The behavior at low and intermediate field strengths will be strongly affected by impurity scattering which has considerable strength at very low temperature.

The previous analysis of the field-velocity relationship is qualitative rather than quantitative and provides only guidelines for most extensive studies. At 300°K, however, the fit found between the V-I characteristics and that obtained analytically from a model which assumes a field-velocity relationship of the type (1.26) is striking. A comparison with other determinations also yields fairly good agreement.

3.3 Heating effects. The following is an estimate of the error caused by heat generated in the structures during the application of the signal. The range of ambient temperatures covered extends from 4.2°K to 300°K. Data are available in the literature[3.33,34] for the heat capacitance and the thermal conductivity of silicon as functions of lattice temperature. Figures (3.33) and (3.34) illustrate their dependence over that temperature range. According to these data, heating is significant primarily at low temperatures, and particularly in the vicinity of 4.2°K where both the heat capacitance and the thermal conductivity achieve very low values. Figure (3.35) illustrates the temperature dependence of the product C_v/κ for silicon, which is approximately proportional to the thermal time constant of the structure if one of the boundaries is an ideal sink. The proportionality factor is determined by the geometrical configuration and

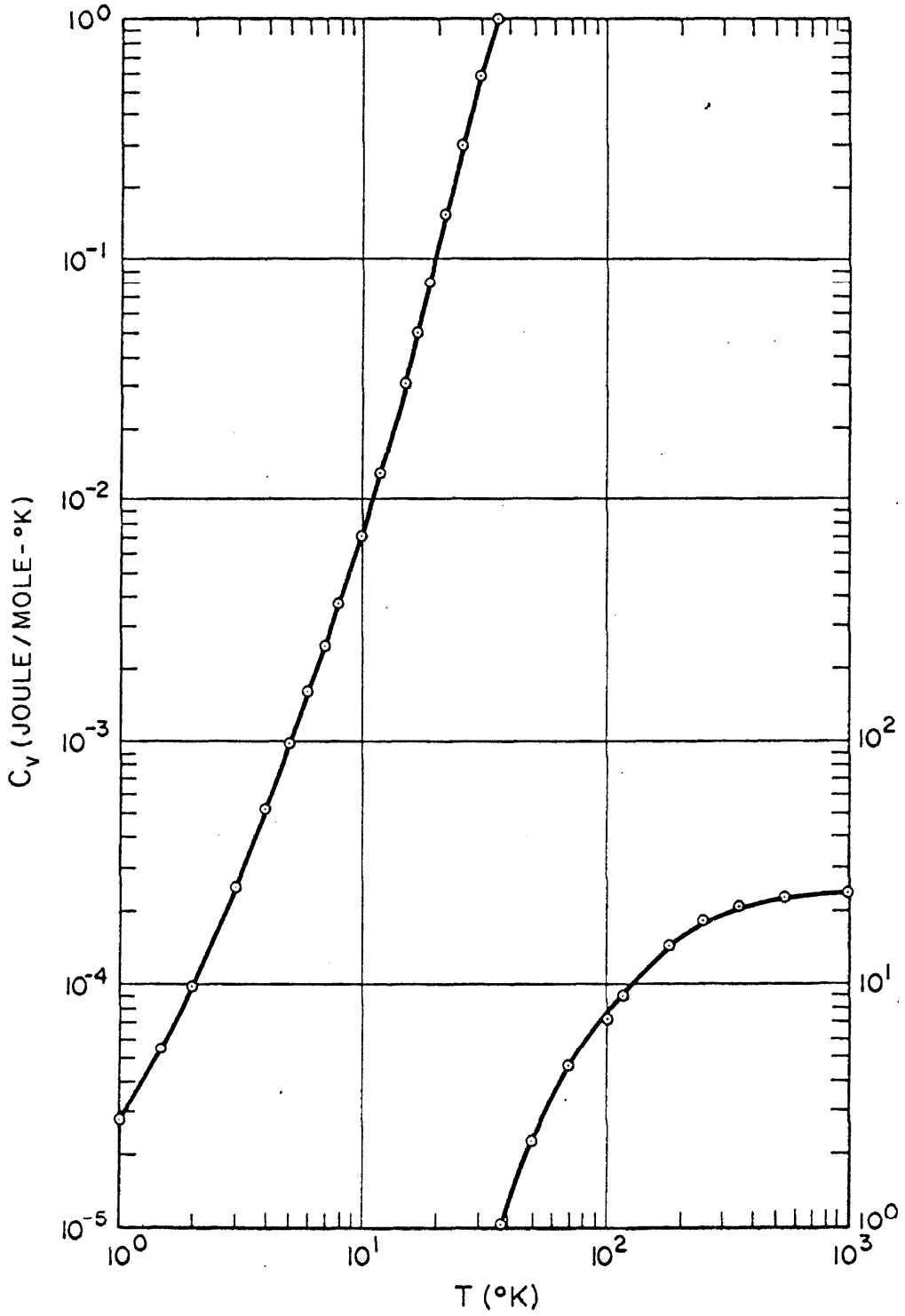
10^0
10^{-1}
10^{-2}
10^{-3}
10^{-4}
10^{-5}
C_v (JOULE / MOLE - °K)
10^2
10^1
10^0
10^0
10^1
10^2
10^3
T (°K)

Figure 3.33

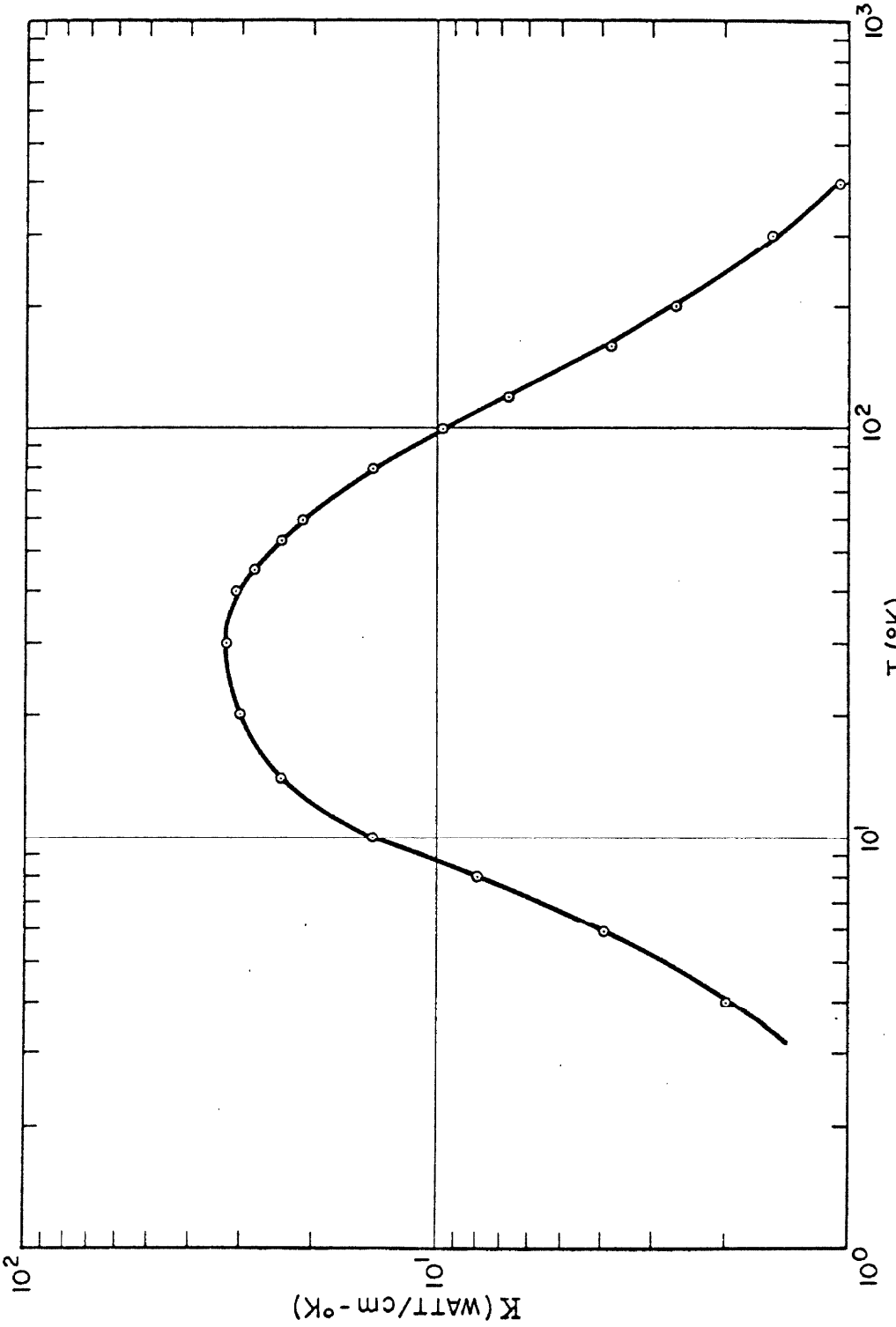

Figure 3.34

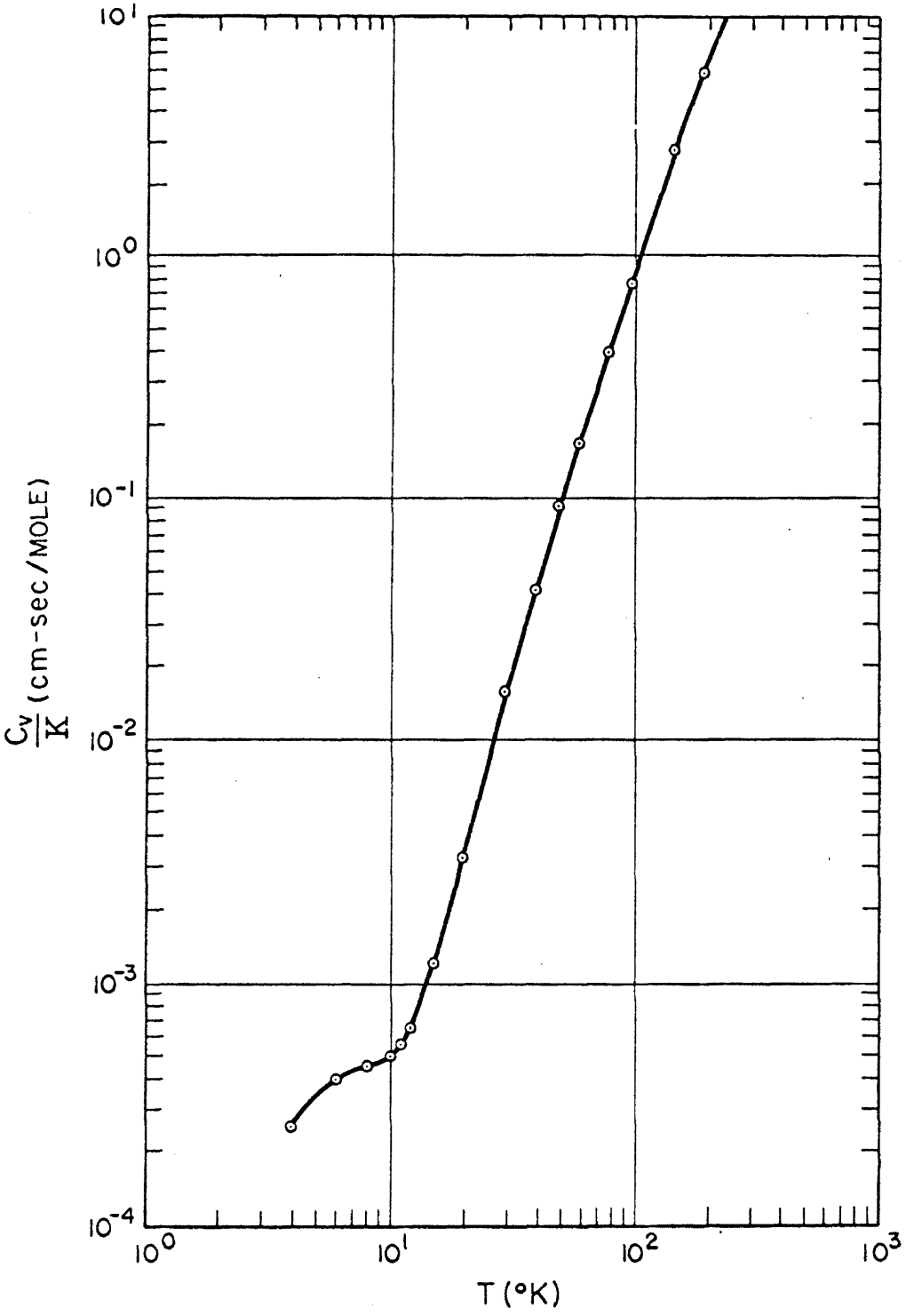

Figure 3.35

the boundary conditions for the structure. If the thermal contact of the sample to its holder is poor, a small amount of energy - of the order of microjoules - can raise the lattice temperature considerably.

The V-I characteristics of the structures are measured with a ramp shaped pulse whose duration can be varied from 2 microseconds to dc. Figure (3.36) illustrates the time dependence of the voltage and current pulses. Since, to a first approximation, both increase linearly with time, they can be represented by the following expressions

$$V(t) = V_m \, t/T \tag{3.29}$$

and

$$i(t) = \begin{cases} I_m \, (t - t_o)/(T - t_o), & (t > t_o) \\ 0 \qquad\qquad\quad , & (t < t_o) \end{cases} , \tag{3.30}$$

where T is the time width of the voltage ramp, t_o the time at which $v(t) = V_{th}$, V_m the maximum applied voltage and I_m the maximum current flowing through the structures. The total energy dissipated in the structures for a single ramp is

$$E = \int_o^T v(t) \, i(t) \, dt \quad , \tag{3.31}$$

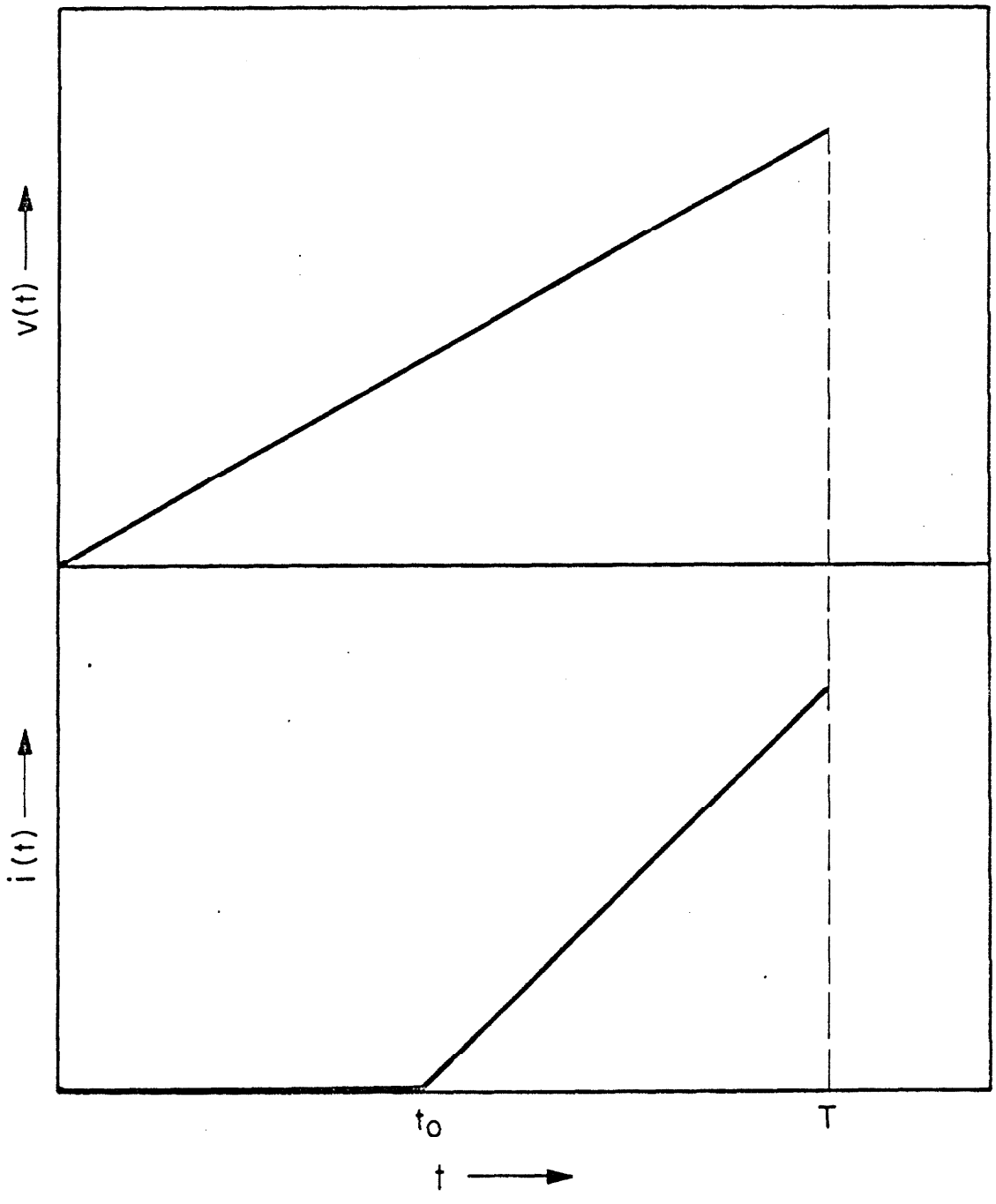

Figure 3.36

$$E = \frac{V_m I_m T}{3 (1 - \gamma)} [1 - 3/2 \gamma + 1/2 \gamma^3] \quad , \qquad (3.32)$$

where $\gamma = t_o/T$.

This result is also applicable when the repetition rate is such that the time interval between two ramps is long compared with the thermal time constant. A value of $\gamma = 1/2$ represents a reasonable average, since at twice the threshold voltage V_{th} the V-I characteristic is usually linear. Also, let V_m and I_m equal to 100 volts and 50 ma , respectively. Substituting into (3.32), one finds that for this set of values the energy in joules is approximately given by the time duration T in seconds, i.e., E (joules) ≈ T(sec). Thus, with the present experimental setup, the minimum generation of energy possible is 2 microjoules.

To estimate the temperature increase ΔT in the sample with respect to the temperature T_o of the sample holder, it is assumed that the duration of the signal and the inverse of the duty cycle are, respectively, short and long as compared to the thermal time constant τ_{th} . The increase in temperature is then given by $\Delta T = E/C_V$. This expression is only valid at high temperatures, where C_V reaches the Dulong and Petit classical limit. At low temperatures, in particular close to $4.2^{\circ}K$, C_V depends on the temperature according to the empirical expression[3.35]

$$C_V = AT + BT^3 \quad . \qquad (3.33)$$

The linear and cubic terms are the electronic and lattice contributions to the heat capacitance, respectively. This representation is valid up to approximately 50°K. ΔT is now found by integrating (3.33) with respect to T from T_o to $T_o + \Delta T$. The resulting expression is

$$E = B/4 \left[(T_o + \Delta T)^4 - T_o^4\right] \quad , \tag{3.34}$$

where the linear contribution to the heat capacitance has been dropped since it is negligible for temperatures above 4.2°K. This transcendental equation can be solved by an iteration technique.

To detect the increase in temperature experimentally, two voltage ramps are applied in rapid succession. The first one heats up the structure and the second one samples the increase in temperature. The separation of the two ramps in time is short compared to τ_{th}. This yields an upper limit for ΔT since the second ramp causes heating of its own and increases the temperature of the structure even further. This procedure is particularly effective at quite low temperatures where the first ramp causes a large ΔT, thereby increasing the heat capacitance and strongly reducing the heating effect of the second ramp. The difference in the limiting drift velocity of the two ramps and the temperature dependence of the limiting velocity - assumed to be correct to a first approximation

for this purpose - then yield ΔT. Another independent indication of the amount of heating taking place at low temperatures is given by the change in threshold voltage observed in the second pulse. The variation of V_{th} with temperature is then utilized as a calibration curve to determine ΔT. Since it is difficult to determine V_{th} accurately from the display of the V-I characteristics on the scope, this method is primarily useful at very low temperatures where threshold is varying strongly with temperature. A lower or upper limit to the temperature of the sample for ambient temperatures in the vicinity of 4.2°K is readily obtained by noting if the threshold voltage has changed on the scope. According to figure (3.7), this limit is T_c', approximately 15°K. Also, a comparison of the experimental V-I characteristics with the analytical model, will reveal if appreciable heating is taking place.

The two series of structures - D and R - have to be treated independently because of their different geometrical configuration. As will be shown, the D-structures exhibit poor thermal dissipation, while the R-structures behave almost ideally. The previous analysis applies mainly to the D-structures. The thermal time constant has been measured for a typical D-structure at 4.2°K, and found to be orders of magnitude bigger than what is expected theoretically from bulk properties (see figure (3.35)). This means that the limiting thermal resistance is that of the contact to the sample holder and

not that of the bulk of the crystal. Figure (3.37) illustrates the temperature dependence of the thermal time constant measured for a D-structure under conditions of excessive heating at 4.2°K. A very approximate analysis indicates an effective thermal conductivity of about 10^{-3} watts/°K for the thermal contact between the sample and its holder. This value is about an order of magnitude smaller than that of the crystal. This justifies the assumption made in the analysis that heat dissipation during the ramp is negligible for the D-structures. In figure (3.38), the variation with temperature obtained experimentally for ΔT is shown for a 10 and 50 microseconds ramp. Figures (3.39), (3.40) and (3.41) are photographs of the V-I characteristics taken with a double pulse of variable width at 4.2°, 77°, and 300°K. They exhibit quite clearly the change of the limiting velocity and threshold due to excessive heating. Notice that at 4.2°K, even with a sizable ramp duration (100 microseconds), the change of the limiting velocity is small. This is due to its weak temperature dependence. The determination of the V-I characteristics and the limiting velocity were made under the best possible circumstances.

Since the R-structures are produced in large numbers on one big chip, an individual structure is surrounded by an ideal heat sink. The thermal time constant should therefore be proportional to C_v/κ.

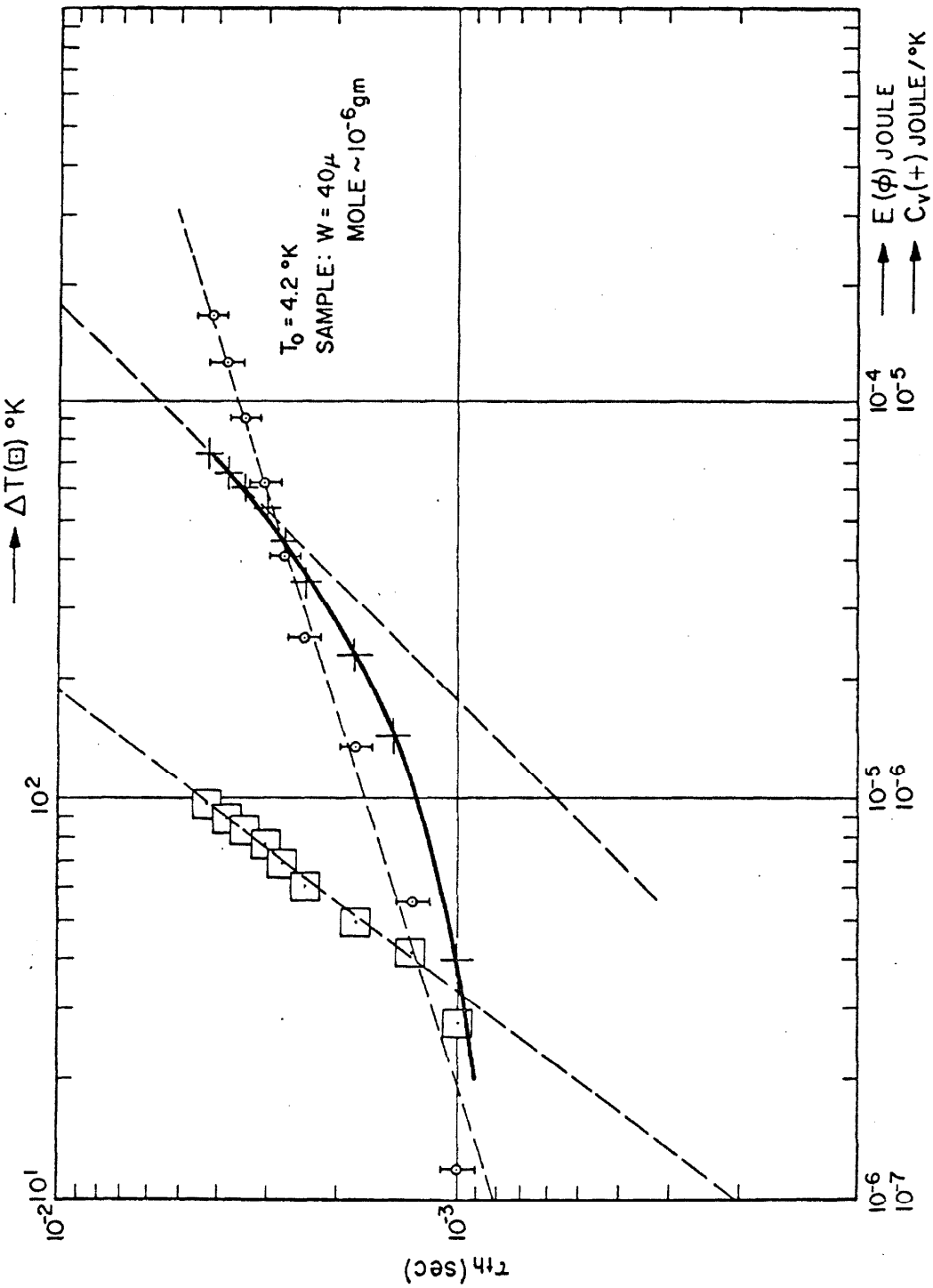
ΔT(⊡) °K
T_o = 4.2 °K
SAMPLE: W = 40μ
MOLE ~ 10^{-6}gm
E (φ) JOULE
C_v(+) JOULE/°K
10^{-4}
10^{-5}
10^{-5}
10^{-6}
10^{-6}
10^{-7}
10^{2}
10^{1}
10^{-2}
10^{-3}
τ_{th} (sec)

Figure 3.37

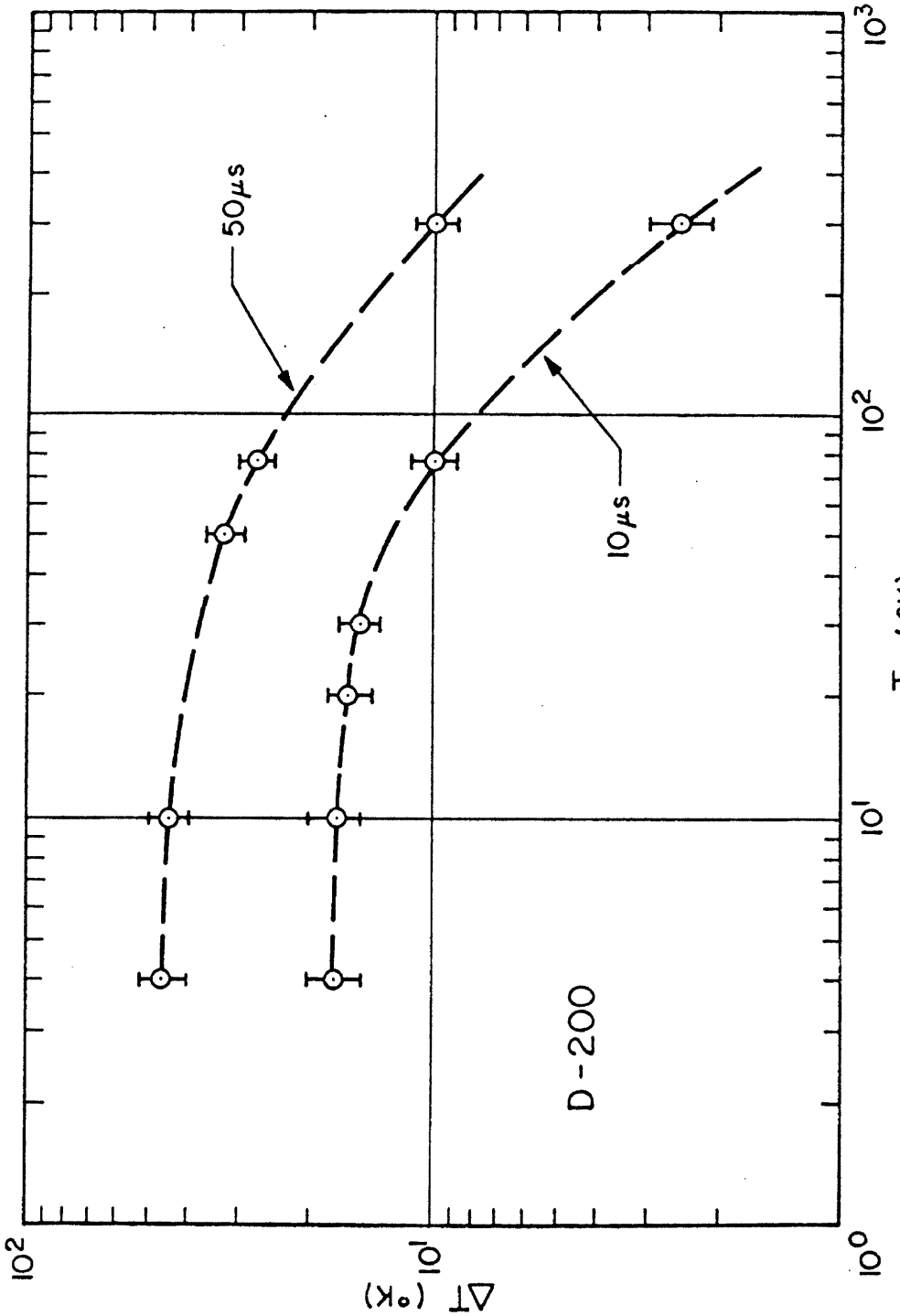

Figure 3.38

D - 200
T = 4.2 °K
DOUBLE PULSE

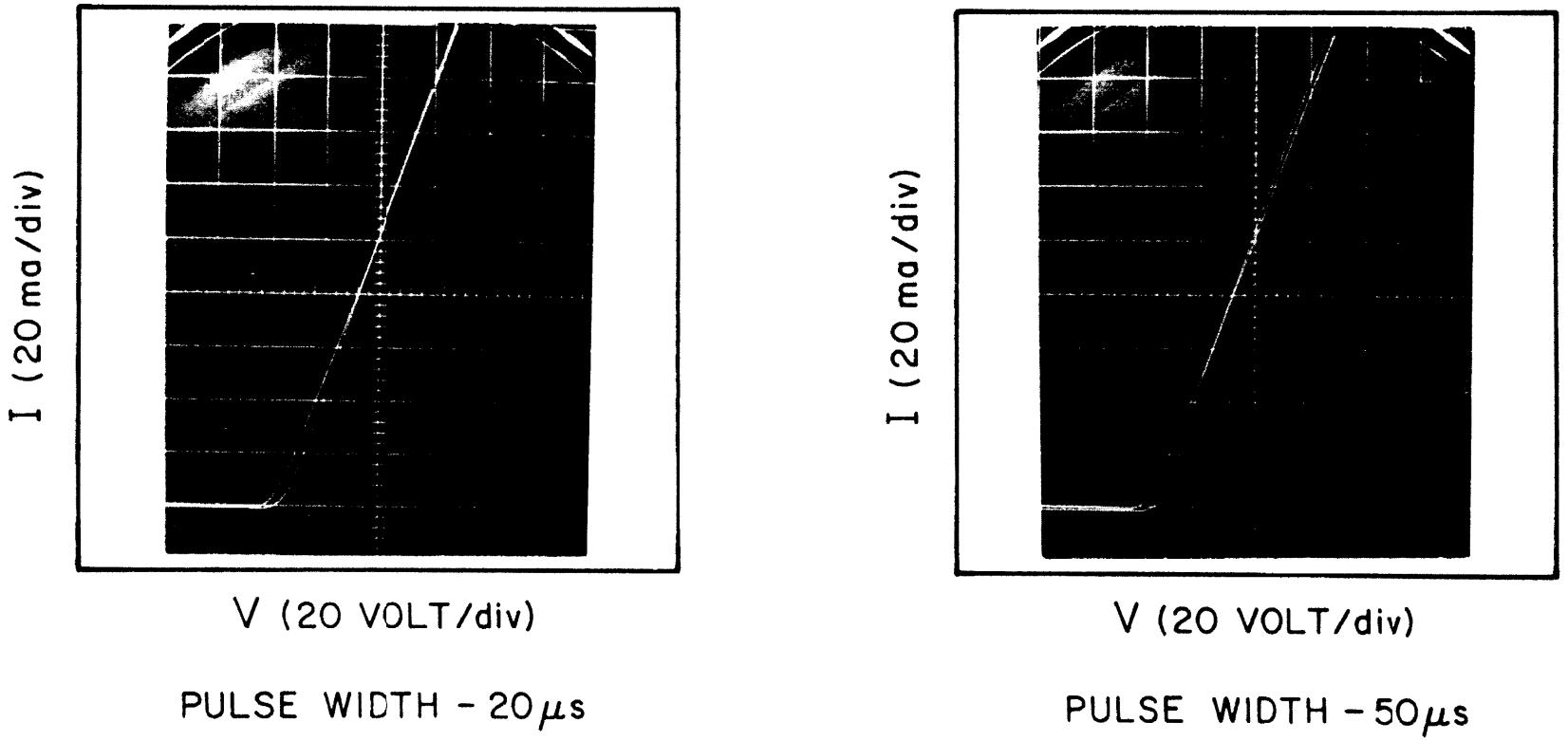

Figure 3.39

D - 200
T = 77 °K

DOUBLE PULSE

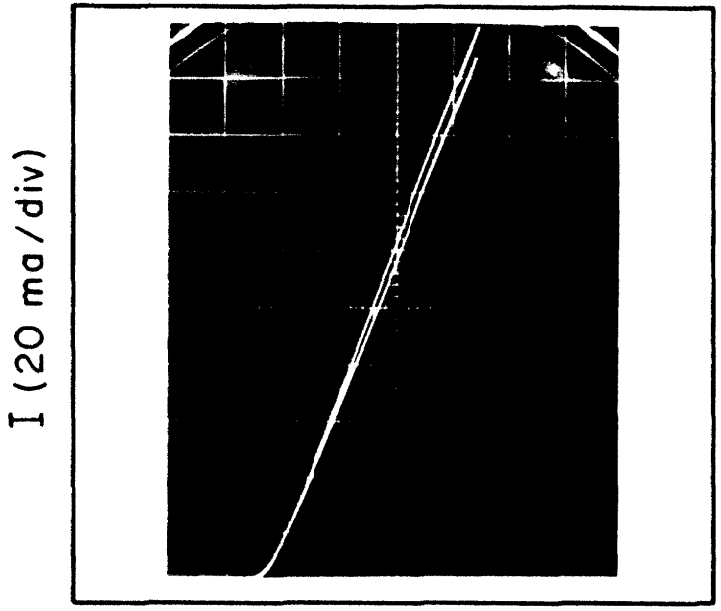

PULSE WIDTH - 50μs

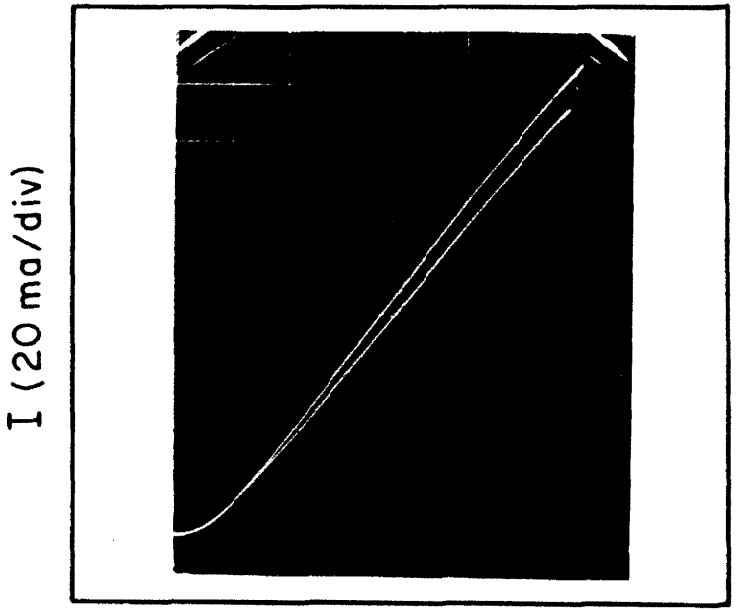

PULSE WIDTH - 100μs

Figure 3.40

D - 200

T = 300 °K

DOUBLE PULSE

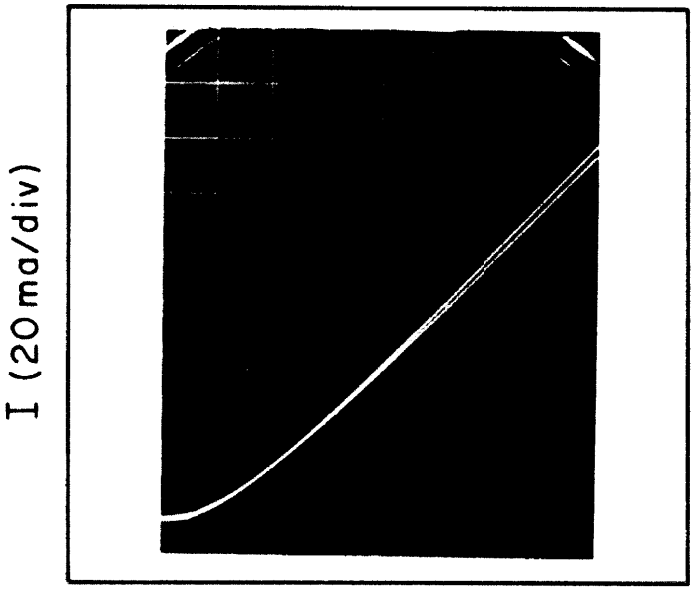

PULSE WIDTH - 50μs

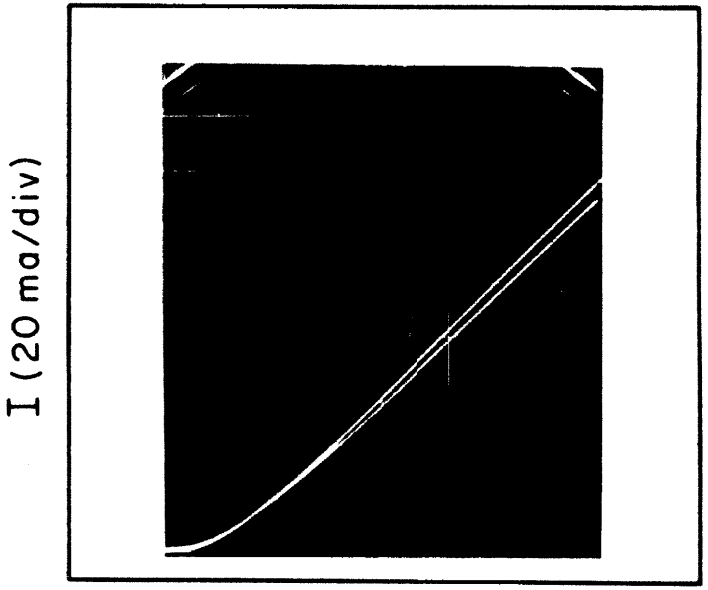

PULSE WIDTH - 100μs

Figure 3.41

Considering the size of the active region, the thermal time constant is at all temperatures smaller than the smallest time width for the ramps. Heat is therefore removed from the active region more rapidly than it is generated so that the temperature does not increase noticeably. The double pulse technique confirms this and yields no indication of heating whatsoever at any temperature for reasonable pulse widths. Figure (3.42) is a photograph of the V-I characteristics for an R-structure taken with a double pulse of 100 microseconds total duration at 4.2°K. The traces for the two ramps are indistinguishable from one another.

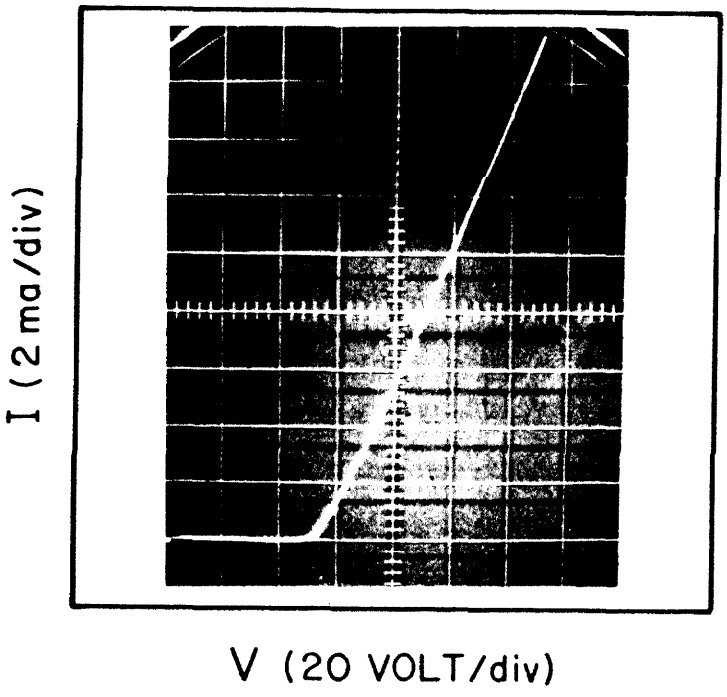

R = 2000
T = 4.2 °K
DOUBLE PULSE
PULSE WIDTH - 50μs

Figure 3.42

Chapter IV

THEORETICAL ANALYSIS AND EXPERIMENTAL RESULTS FOR THE LIMITING DRIFT VELOCITY

4.1 Introduction. The first experiments which show that in germanium and silicon, at high field strengths, the drift velocity is no longer proportional to the electric field were performed by Ryder[3.20] and subsequently expanded by several authors[3.21,22,23]. Figure (3.29) illustrates the field-velocity relationships as obtained by these authors in n-type silicon. The general trend is for the drift velocity to first increase linearly with applied electric field (constant mobility), and to eventually reach a limiting value at high enough field strengths (constant drift velocity). Shockley[4.1] put forward an explanation of these results by considering the momentum and energy balance of carriers subject to an electric field and scattering by acoustic and optical phonons. His work was based on the simple parabolic model for the band structure which assumes that: (1) the minimum energy in the conduction band, or maximum energy in the valence band, is possessed by one quantum state of either spin and occurs at the central point of the reduced zone, (2) the bands are non-degenerate, (3) the constant energy surfaces near the edges of the conduction and valence band are spherical in form. The resulting expression for the drift velocity as a function of electric field is[4.2]

$$v_d = \mu_o \sqrt{2} / \{1 + [1 + (3\pi/8)(\mu_o E/u_\ell)^2]^{1/2}\}^{-1/2} E \quad (4.1)$$

where u_ℓ is the longitudinal speed of sound. At low and high field strengths, (4.1) reduces to $v_d = \mu_o E$ and $v_d = (2/3\pi)^{1/4} \cdot (\mu_o u_\ell E)^{1/2}$, respectively. This theoretical determination of the drift velocity compelled Ryder to fit his data in the regime, which now has come to be known as "the warm electron range," to an $E^{1/2}$ - field dependence. At very high field strengths, Shockley includes the effect of optical transitions to explain the experimentally observed limiting velocity regime. He remarks that, for optical phonons to be effective, the carrier energy must be greater than $h\omega_o$, where ω_o is the characteristic frequency of the optical phonons, but that when they do come into action, they are more effective than acoustic phonons. An interaction with an optical mode absorbs most of the carrier energy; thus, the existence of a limiting velocity range when this type of scattering is predominant.

A comparison between theory and experiment reveals that carriers are able to dissipate their excess energy more effectively than expected on the basis of (4.1). A deviation from thermal equilibrium is observed experimentally for electric fields about three orders of magnitude bigger than what theory predicts. Hence, an added energy loss mechanism must be introduced in the theoretical analysis to account for the discrepancy at low fields. As noted by Shockley, this could be obtained by considering the correct band structure.

Since the original work of Shockley and Ryder, the state of the art has progressed in the sense of attaining a better physical or qualitative understanding of the observed phenomena. The simple parabolic model offered decided mathematical advantages and was capable of coping with most basic optical and electrical properties observed until recently. However, the discovery of longitudinal and transverse anisotropy effects of hot electrons, made it compelling to deal with a transport theory for a many-valley semiconductor. Cyclotron resonance experiments, as suggested by Shockley and carried out by Dresselhaus et al.,[4.3] established that the one-band, many-valley model is appropriate to describe the conduction band of silicon and germanium. It is now well known that the bottom edge of the conduction band for these two elements is composed of equivalent energy minima located at symmetrical positions in the Brillouin zone. The surfaces of constant energy at each valley are prolate spheroids represented by equations of the type

$$\varepsilon = \hbar^2/2 \left(\frac{2 k_t^2}{m_t} + \frac{k_\ell^2}{m_\ell} \right) , \qquad (4.2)$$

where the k's and m's are the wave numbers and effective masses perpendicular and parallel to the spheroid axes, respectively.

In a many-valley semiconductor, lattice vibrations of optical or acoustic nature can cause two types of electronic transitions, intravalley and intervalley, or transitions between two states

within or in different valleys, respectively. Intravalley scattering by an acoustic mode is an elastic process since it involves phonons with sizable momentum and low energy. Optical phonons, on the other hand, are very energetic and carry relatively little momentum, consequently this type of scattering is inelastic. Intravalley scattering involves phonons (either acoustic or optical) of definite momentum prescribed by the relative location of the energy minima in the Brillouin zone. In general, optical phonon scattering will be of importance for lattice temperatures or electric fields high enough that a sizable number of electrons have energies comparable to $\hbar\omega_0$. It should be mentioned, however, that the greater size of these phonons more than compensates, in some instances, for the smaller probability of emission as compared to acoustic phonons.

It is evident from the previous discussion that before an analysis of the carrier mobility can be carried out, knowledge must be obtained about: (1) the spectrum of lattice vibrations to determine the energies of the phonons taking part in the scattering processes, (2) the number and location in k-space of energy minima within the Brillouin zone, (3) the energy distribution of electrons within each valley, and (4) the strength of the different scattering processes as represented by coupling constants.

We are concerned in this chapter, primarily, with the hot electron regime of the field-velocity relationship. Results have

been obtained experimentally which indicate the existence of a limiting velocity regime for electrons in silicon oriented along the [111] crystallographic direction over the temperature range $4.2^{o} \leq T \leq 300^{o}K$. Before these data can be analyzed, however, the behavior of the low field mobility should be understood. Section 4.2 includes the currently available data for silicon, as pertinent to the present investigation, and presents a treatment of the low field mobility as furnished by D. Long[4.4] and Adawi[4.5]. Section 4.3 provides a qualitative description of the type of energy distribution expected for electrons in silicon within a prescribed set of conditions. Section 4.4 presents the available treatments of the limiting velocity, as reported by Reik and Risken, and Jorgenson et al., expanded to cover the case under consideration. Finally, in section 4.5 our experimental results for the hot electron regime of the field-velocity relationship in silicon are illustrated and compared with theory. Throughout this chapter, reference is made to germanium also because of its similarity with silicon in the band structure but its remarkable dissimilarity in behavior at high field strengths and low temperatures.

4.2 The Low Field Mobility. The temperature dependence of the mobility at low field strengths has been determined experimentally for holes and electrons in silicon and germanium. In all instances, the result deviates appreciably from the $T^{-3/2}$ power law predicted from simple acoustic lattice scattering. Long[4.4] has shown that, for electrons in silicon, this deviation can be accounted for by

including intravalley and intervalley scattering by both acoustic and optical phonons. His analysis is presented in part with a threefold purpose: (1) as a means for introducing data about silicon which is relevant to the investigation of the high field mobility, (2) to determine the relative strengths of the dominant scattering mechanisms, and (3) to allow a comparison of the mobility dependence on temperature at both extremes in electric field strengths.

According to Herring and Vogt[4.6], the momentum scattering is described by a relaxation time tensor diagonal in the principal axes of the constant-energy spheroids and given by

$$1/\tau_\alpha = W_{a\alpha}\left(\frac{\varepsilon}{kT_o}\right)^{1/2}\left(\frac{T}{T_o}\right) + \sum_i W_i\left(\frac{T_{ci}}{T_o}\right)^{3/2}\left\{ n_o\left(\frac{\varepsilon}{kT_{ci}} + 1\right)^{1/2} + (n_o + 1)\left[\left(\frac{\varepsilon}{kT_{ci}} - 1\right)^{1/2} \text{ or } 0\right]\right\} \quad , \quad (4.3)$$

$$\text{where} \quad n_o = \left[\exp\left(\frac{T_{ci}}{T}\right) - 1\right]^{-1} \quad ,$$

and α refers to the direction relative to the spheroid axes. The temperatures T, T_{ci}, and T_o are, respectively, the lattice temperature, the characteristic temperature of an ith phonon, and a reference temperature which fixes the absolute magnitude of the coupling constants. ε is the electron energy, and $W_{a\alpha}$ and W_i are

the coupling constants for acoustic and optical phonons, respectively. These authors also found the mobility to be described by

$$\mu_o = \frac{e}{3\langle\varepsilon\rangle}\left[2\frac{\langle\varepsilon\tau_t\rangle}{m_t} + \frac{\langle\varepsilon\tau_\ell\rangle}{m_\ell}\right] \quad , \tag{4.4}$$

where the symbols $\langle\ \rangle$ represent averages over a Maxwellian distribution.

Silicon has a many-valley non-degenerate conduction band. There are six valleys located along the [100] axes in k space at distances of 0.85 ± 0.03 from the center of the first Brillouin zone.[4.4] The surfaces of constant energy at each valley are described by equation (4.2). The transverse and longitudinal effective masses , as determined by C. J. Rauch et al.,[4.7] are $(0.192 \pm 0.001)\ m_o$ and $(0.90 \pm 0.02)\ m_o$, respectively. Intra- and intervalley transitions by optical and acoustic phonons are possible. Intravalley scattering by optical phonons, however, has been shown to be of negligible significance in silicon[4.8]. Besides, this type of scattering can always be ascribed to intervalley scattering by optical phonons since both enter the calculations for the mobility with the same form. Because of the location of the valleys in the conduction band, intervalley scattering always occurs as an Umklapp process. There are two types of intervalley transitions in silicon: (1) f-scattering which involves transfer of an electron to any of four equivalent valleys and (2) g-scattering to the remaining valley. By a geometrical argument, Long found the phonons involved in the

two types of scattering to be well represented by their energy spectrum for the [100] direction. The phonons able to participate in the intervalley scattering processes are then found to lie within two narrow ranges of energy, i.e., from 135°K to 230°K and from 570°K to 730°K which to simplify the theoretical analysis of the mobility, are approximated with characteristic temperatures of 190° and 640°K, respectively.

It is now possible to substitute equation (4.3) into equation (4.4) and to adjust the various coupling constants until a reasonable fit to the experimental temperature dependence of the electron mobility is achieved. Long finds in this manner intervalley scattering by the 630°K optical phonons to be the dominant transition at high temperatures. The ratio of the coupling constant describing the strength of this transition to that for acoustic scattering has a value of $W_o/W_{at} = 2$. The ratio of the coupling constants for acoustic inter and intravalley scattering is $W_1/W_{at} = 0.15$ and the fit is quite insensitive to the value of this ratio since it is possible to vary it by a factor of two before an appreciable worsening is detected. However, the fit is sensitive to a variation of 15% in the former ratio. Thus, to explain the temperature dependence of the low field mobility, it is necessary to include intervalley scattering by acoustic and optical phonons. It is also clear that this type of scattering will gradually become ineffective as the

temperature is lowered since the number of electrons capable of exciting intervalley phonons decreases exponentially with temperature. Consequently, if the effect of impurity scattering is either negligible or accounted for separately, the plot of mobility as a function of temperature approaches assymptotically a $T^{-3/2}$ power law due to intravalley acoustic scattering as the temperature is decreased.

In germanium, a similar analysis has been carried out for the low field mobility by Adawi[4.5]. He concludes that the dominant scattering mechanisms are intravalley transitions by acoustic and optical phonons with a characteristic temperature of 400°K. The ratio of the coupling constants which best fits the experimental data is $W_o/W_{at} = 0.19$. This treatment is, nevertheless, not as accurate as for silicon since the deviation from a $T^{-3/2}$ power law, accounted for by optical phonon scattering, is quite small over the temperature range covered.

In summary, the information made available by the analysis of the low field mobility is outlined. In silicon: (1) coupling to intervalley optical phonons is strong, specially for lattice temperatures which correspond approximately to the optical phonon energy, (2) the temperature dependence of the low field mobility is dominated by intervalley scattering at high temperatures, (3) intravalley scattering is very weak. In germanium: (1) intervalley scattering is insignificant, (2) the temperature dependence of the low field mobility deviates slightly from the $T^{-3/2}$ power law predicted by intravalley

acoustic scattering, (3) optical intravalley scattering is weak but dominates over intervalley scattering.

4.3 The solution of the Boltzmann equation. In the absence of an electric field, the solution to the Boltzmann equation for a non-degenerate semiconductor yields a Maxwellian energy distribution for the carriers

$$f_o = n/N_c \exp^{-(\mathcal{E}/kT)} \quad , \tag{4.5}$$

where n is the density of carriers and N_c the effective density of states in the conduction band. The average thermal energy of the electrons is then 3/2 kT. When an electric field is applied, carriers gain energy at the rate $e\mu_o E^2$, and the thermal energy distribution is perturbed. This energy is dissipated through collisions with the lattice and other carriers. Eventually, a steady state is reached when the rate of energy gained equals the rate of energy lost, i.e.,

$$\left\langle dE/dt \right\rangle_E = e\mu_o E^2 \tag{4.6}$$

where $\langle\ \rangle$ represents an average over the energy distribution of the carriers.

At low field strengths, the solution of the Boltzmann equation consists of the thermal distribution plus a small perturbation

term proportional to the applied field, the relaxation time and the first derivative of f_o, i.e.,

$$f = f_o(\varepsilon,T) + f_1 \quad , \qquad (4.5)$$

where $f_1 << f_o$.

The carriers are still in thermal equilibrium with the lattice and the effect of the electric field is to cause an average velocity proportional to it and along its direction.

Increasing the applied electric field strength, the average energy of the carriers increases above the zero field thermodynamical equilibrium value and the perturbation term f_1 increases accordingly. When f_1 becomes comparable to f_o, the carriers are said to be hot and their energy distribution is no longer well represented by (4.5). However, in some instances, it is possible to represent the situation again with a Maxwellian distribution at a carrier temperature T_e, i.e.,

$$f = f_o'(\varepsilon, T_e) + f_1' \qquad (4.6)$$

where $f_1' << f_o$

This effective temperature is a function of the electric field and approaches the lattice temperature as the field goes to zero. It

the purpose of this section to give a justification for using such a distribution in the case of silicon and germanium at high field strengths.

Reik and Risken[4.9] have solved the Boltzmann equation for electrons in a many-valley semiconductor with scattering by acoustic and optical phonons. These authors obtain a Maxwellian distribution when intervalley scattering is negligible and the average energy of the electrons is greater than the optical phonon energy. The electron temperature within each valley increases approximately with the square of the electric field strength and, in general, is different for each valley since the angle between the electric field and the longitudinal axes of a particular valley is different in each case. In particular, if all the valleys are oriented equivalently with respect to the electric field direction, the electron temperature attains the same value in all equivalent valleys. Other assumptions made in the process of solving the Boltzmann equation are the following: (1) The wave vectors lie within a Δk smaller than 10^7 cm^{-1} from the center of the valleys. The assumption of constant effective masses is valid and scattering to non-equivalent valleys can be disregarded. This places an upper limit for the field strength. (2) The transverse and longitudinal phonons are equipartitioned thermally over the range of lattice temperatures $77^o \leq T \leq 300^oK$. (3) The contribution of acoustic phonons to the

rate of energy loss of the electrons is neglibigle. This also places an upper limit to the value of the field strength. (4)Impurity and electron-electron scattering are neglected.

Germanium lies well within the limits imposed by the previous assumptions over the temperature and electric field ranges $77^{o} \leq T \leq 300^{o}K$ and $10^{3} \leq E \leq 7.10^{3}$ v/cm, respectively. Intervalley scattering is down by a factor of 10^{-3} from the contribution by optical intravalley scattering[4.10]. In silicon, however, the result of a Maxwellian energy distribution will not apply in general. But, if as pointed out by Jorgenson[3.32], the electric field is applied along a direction such that the longitudinal axes of the equivalent valleys are equivalently oriented with respect to it, the electrons attain a Maxwellian distribution regardless of the strength of intervalley scattering. In this instance, intervalley and intravalley scattering by optical phonons lead to expressions of the same type in the Boltzmann equation and can thus be dealt with identically. Such orientations are the [100] and [111]-direction for germanium and silicon, respectively.

4.4 The high field mobility. The general tendency of the drift velocity is to reach a limiting value at high enough field strengths. This value is, in general, dependent on the crystal orientation at a fixed lattice temperature. Reik and Risken[4.11] have derived an expression for the limiting drift velocity through the solution of the Boltzmann equation, i.e.,

$$v_d = \frac{2\hbar u_\ell}{(3\pi)^{1/2}} \frac{W_{at}}{W_o}\left[m_t k T + \frac{\hbar m_t u_\ell^2}{2\omega_o}(2n_o + 1)\left(\frac{W_{at}}{W_o}\right)^2 \right]^{-1/2} \cdot Z \quad (4.9)$$

where Z is the direction dependent part. The analysis can be simplified considerably if the balance-of-energy method is employed to obtain the previous expression.[4.12] Moreover, by using the knowledge of a Maxwellian distribution and a crystal orientation such as to align the valleys equivalently with the electric field, the problem is simplified even further. In this section, the analysis of the drift velocity at high field strengths in that particular case is presented and expanded to encompass silicon over the range of lattice temperature $4.2^o \leq T \leq 300^oK$.

The choice of crystal orientation reduces the problem to a one-valley model. For simplicity, only one type of intervalley transition is considered. Subsequent to the forthcoming analysis of the limiting drift velocity, the true nature of the phonon energy spectrum is included in an approximate manner. The equation for the balance of energy is given by

$$\left\langle \frac{d\varepsilon}{dt} \right\rangle_E = e\mu_o E^2 \quad , \quad (4.10)$$

and the mobility by

$$\mu_{\parallel} = \frac{e}{m^*} \frac{\varepsilon \tau_t}{\varepsilon} \quad , \tag{4.11}$$

where $m^* = \dfrac{3\, k_m}{1 + 2\, k_m}\, m_t$

with $k_m = \dfrac{m}{m_t}$.

Expression (4.11) has been obtained from (4.4) by assuming that the acoustic anisotropy is very weak. There is experimental evidence for both silicon and germanium which indicates this to be the case.[4.13, 14] The momentum relaxation time is obtained from (4.3) under the assumption that $\mathcal{E} >> \hbar\omega_o$. The resulting expression is

$$\frac{1}{\tau_t} = \left(\frac{\varepsilon}{kT_n}\right)^{1/2} \left[W_{at}\left(\frac{T}{T_n}\right) + W_o\,(2n_o + 1)\,\frac{\hbar\omega_o}{kT_n}\right] \tag{4.12}$$

Substituting into (4.11), and averaging over a Maxwellian distribution at T_e, the mobility is given by

$$\mu_o = \frac{e}{m^*}\,\frac{4}{3\sqrt{\pi}}\left(\frac{T_n}{T_e}\right)^{1/2} \left[W_{at}\left(\frac{T}{T_n}\right) + W_o\,(2n_o + 1)\,\frac{\hbar\omega_o}{kT_n}\right]^{-1} . \tag{4.13}$$

The average rate of energy loss is due to carrier interactions with optical and acoustic phonons. However, it can be ascribed

totally to the interactions with optical phonons in the range of field strengths considered here, i.e., $E < 5.10^4$ v/cm. This assumption is discussed further in the following section. The rate of energy loss is then given by(4.15)

$$\left\langle \frac{d\varepsilon}{dt} \right\rangle_{op} = W_o \frac{2}{\sqrt{\pi}} \frac{(\hbar\omega_o)^2}{kT_n} \left(\frac{T_e}{T_n}\right)^{1/2} \quad . \tag{4.14}$$

The balance of energy equation is now easily obtained and solved for T_e by substituting (4.13) and (4.14) into (4.10). This yields

$$kT_e = \frac{2e^2 E^2 (kT_n)^2}{3m^* (\hbar\omega_o)^3 W_o^2} \left[(2n_o + 1) + \frac{W_{at}}{W_o} \left(\frac{kT_n}{\hbar\omega_o}\right)\right]^{-1/2} \quad . \tag{4.15}$$

Introducing (4.15) into (4.13), one finds for the limiting drift velocity(3.22)

$$v_s = \frac{4}{\sqrt{6\pi}} \left(\frac{\hbar\omega_o}{m^*}\right)^{1/2} \left[(2n_o + 1) + \frac{W_{at}}{W_o} \left(\frac{kT_n}{\hbar\omega_o}\right)\right]^{-1/2} \quad . \tag{4.16}$$

This expression, as it stands, is applicable to germanium over the temperature range $77^o \leq T \leq 300^oK$ and for electric field strengths below 10^4 v/cm. In the case of silicon, (4.16) must be modified to include all possible intervalley transitions. Again, rather than complicating the problem by performing a detailed analysis which would include all possible intervalley transitions and their characteristic energies, the approach taken by Long(4.4) in analyzing the low field

mobility is used here. The intervalley phonons are described by just two such phonons with energies $\hbar\omega_o$ and $\hbar\omega_1$, and the strength of the transitions as determined by the coupling constants, by four times W_o and W_1. The factor of four arises from the presence of four equivalent intervalley transitions of type f. g-scattering is accounted for by the choice of phonon energies. The resulting expression for the limiting drift velocity is then

$$v_s = \frac{4}{\sqrt{6\pi}}\left[\frac{\hbar\omega_o}{m^*}\left(1 + \frac{W_1}{W_o}\left(\frac{\omega_1}{\omega_o}\right)^2\right)\right]^{1/2} \left[\left(\frac{W_{at}}{4W_o}\right)\left(\frac{kT}{\hbar\omega_o}\right)\right.$$

$$\left. + (2n_o + 1) + (2n_1 + 1)\frac{W_1}{W_o}\left(\frac{\omega_1}{\omega_o}\right)\right]^{-1/2} . \quad (4.17)$$

This relationship is not expected to provide an accurate fit to our experimental findings for the limiting velocity since, as pointed out before, the true nature of the phonon spectrum has been disregarded. However, it will enable us to determine whether or not it ispossible to describe the temperature dependence of the low and high field mobility by the same set of coupling constants and phonon energies.

4.5 Experimental results and comparison with theory. Experimental determinations of the limiting velocity of electrons have been carried out by several authors in germanium oriented along the [100]-direction. Jorgensen et al.,[3.32] covered the temperature range from 77°K to 200°K. These authors found a good fit between the

observed experimental dependence and that predicted by expression (4.16) with an optical phonon energy of k · 430°K and a coupling constants ratio for optical and acoustic intravalley scattering of 0.17; in good agreement with that found by Adawi[4.5] from low field mobility measurements. Its magnitude is, nevertheless, off by about 25%. They also found that the limiting velocity range extends beyond the upper limit in field strength (about 7.10^3 v/cm) imposed by the assumptions within which the theoretical model is valid. In a subsequent paper[4.16], a semiquantitative explanation of these phenomena was put forward by considering the contribution of acoustic phonons to the rate of energy loss of the electrons, and by introducing scattering to non-equivalent valleys. Gunn et al.[4.17] covered the range below 77°K and found that the field velocity relationship exhibits a negative differential mobility and the existence of current instabilities at high field strengths. The phenomena are explained in terms of scattering of electrons to non-equivalent valleys. Germanium has six such valleys in the [111]-direction and one at k = 0, at 0.20 ev from the energy minima at the edges of the conduction band. This type of scattering, regardless of its strength, can only be significant at high field strengths when the electrons gain sufficient energy to make the transition possible. For high lattice temperatures, the field strength required for this to occur might be very large since collisions with the lattice are very frequent and electrons gain

little energy from the applied field. Lowering the lattice temperature, however, the mobility increases and the electrons are able to gain sufficient energy between collisions to make the transition possible at lower applied fields strengths. It has been found experimentally by applying pressure to germanium[4.18] that if the equivalent and non-equivalent valleys are brought to coincide in energy, the coupling for transitions to non-equivalent valleys is very strong. Thus, once electrons achieve energies comparable to 0.2 ev, they will be scattered into the non-equivalent valleys and their behavior is prescribed by the transport properties of these valleys. This gives rise to a negative differential mobility if as in the present case, the mobilities in the two valleys are drastically different. The treatment is then similar to that for Ga As.

Silicon differs from germanium in at least two counts, coupling to intervalley scattering is very strong and the non-equivalent valleys (six in the [100]-direction and one at k = 0) are located at higher energies from the energy minima at the edges of the conduction band. Conwell[4.19] has compared the ratios of energy loss to acoustic and optical phonons in germanium. The contribution of optical phonons is dominant up to a certain value for the average electron energy where the acoustic contribution takes over. The location of this intercept depends on the relative strengths of the scattering rates and the lattice temperature. In silicon, since coupling to intervalley phonons is very strong, the electron energy at which the intravalley acoustic

contribution dominates should occur at very high field strengths, close to or above breakdown fields, at all lattice temperatures. Thus, the assumption which ascribes the rate of energy loss to optical phonons, introduced in the process of solving the Boltzmann equation and in deriving expressions (4.16) and (4.17), should be valid over the electric field strengths covered (approximately $E < 5.10^4$ v/cm). Also, since the difference in energy between equivalent and non-equivalent valleys is large (about 0.5 ev), non-equivalent scattering is not expected to be of significance in that range of electric fields regardless of its strength. A negative differential mobility range is thus not expected in silicon.

Our experimental results for the limiting drift velocity of electrons in silicon extend over the range of lattice temperatures from 4.2°K to 300°K. The limiting drift velocity has been obtained from the V-I characteristics of pure unipolar sclc. To observe this current, structures of the type n^+ n n^+ and n^+ p n^+ were manufactured by masking and diffusion techniques. The linearity of the characteristics above the threshold voltage V_{th} proves that the drift velocity reaches a limiting value. In that case, a simple model of pure unipolar sclc predicts that the current density J is given by

$$J = 2 \epsilon\epsilon_o v_s (V - V_{th})/W^2 \quad .$$

The dielectric constant is independent of lattice temperature in high purity materials. Thus, the change in the slope of J as a

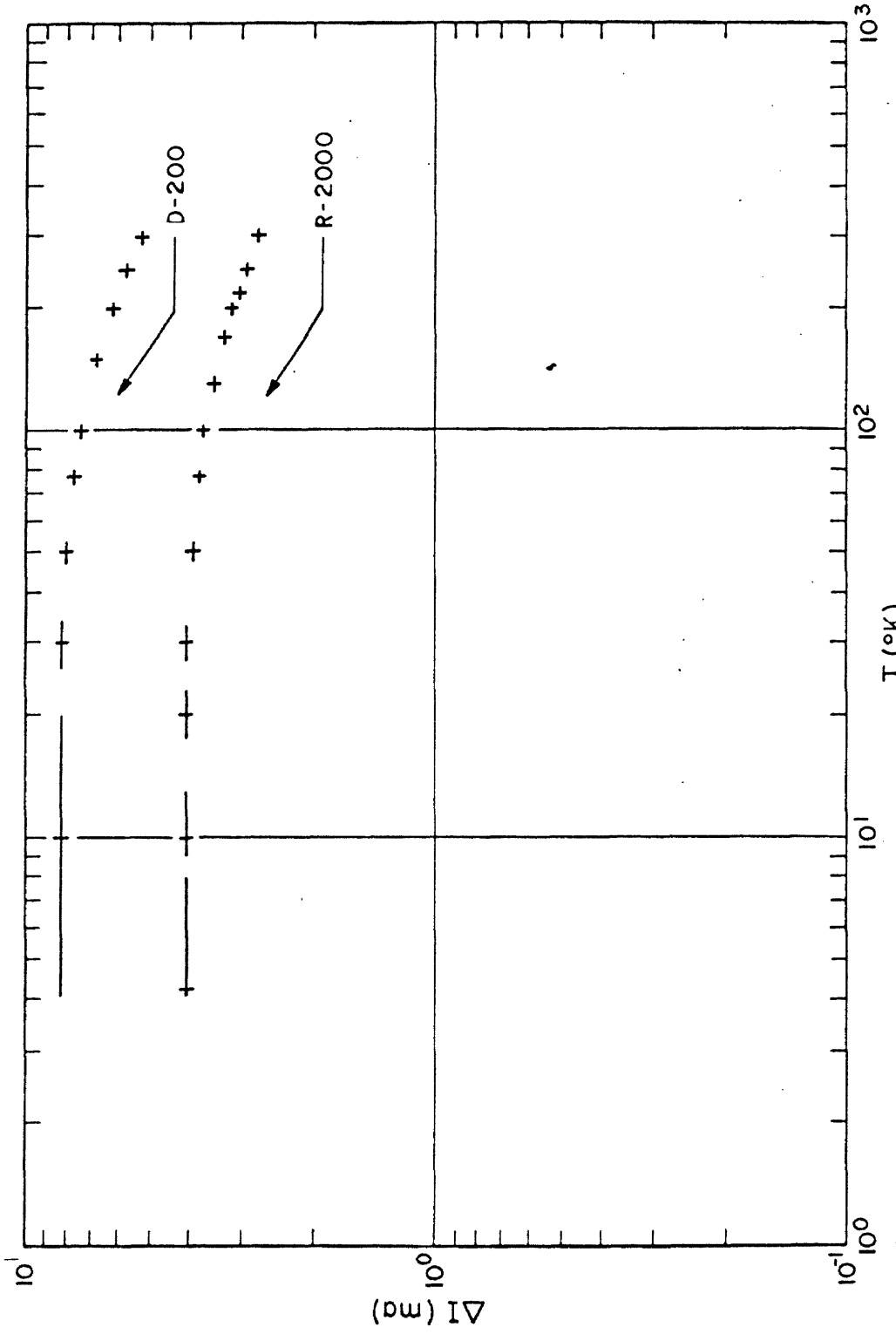

Figure 4.1

function of lattice temperature yields the temperature dependence of the limiting drift velocity. Figure (4.1) has been obtained from the V-I characteristics of pure unipolar sclc by measuring the increase in a ΔI for a fixed ΔV as a function of lattice temperature. The results for two structures (R-2000 and D-200) are given in that figure. The different magnitude of ΔI in the two plots at a fixed lattice temperature is a consequence of the different geometries of the two structures. The slightly larger temperature dependence of ΔI observed in the D-200 structures at high temperatures is a consequence of the poor thermal properties of these structures as compared with the R-2000. Figure (4.2) has been obtained by rescaling the ordinate of the plot for the R-2000 structure in figure (4.1) to yield the known values of $1.0 \cdot 10^7$ cm/sec at 300^{o}K. This procedure is adopted to circumvent the uncertainty in the effective area of the geometrically non-symmetrical devices. Figure (4.2) also illustrates expression (4.17) for two sets of parametric values.

Equation (4.17) has been plotted for the average phonon energies and coupling constant ratios obtained by Long[4.4] from the temperature dependence of the low field mobility (upper curve of figure (4.2)). A discrepancy between theory and experiment is observed in the magnitude of the limiting drift velocity and its temperature dependence. It is thus concluded that the limiting drift velocity cannot be fully explained in terms of the coupling constants and phonon energies which describe the low field mobility. In order to provide a good fit to

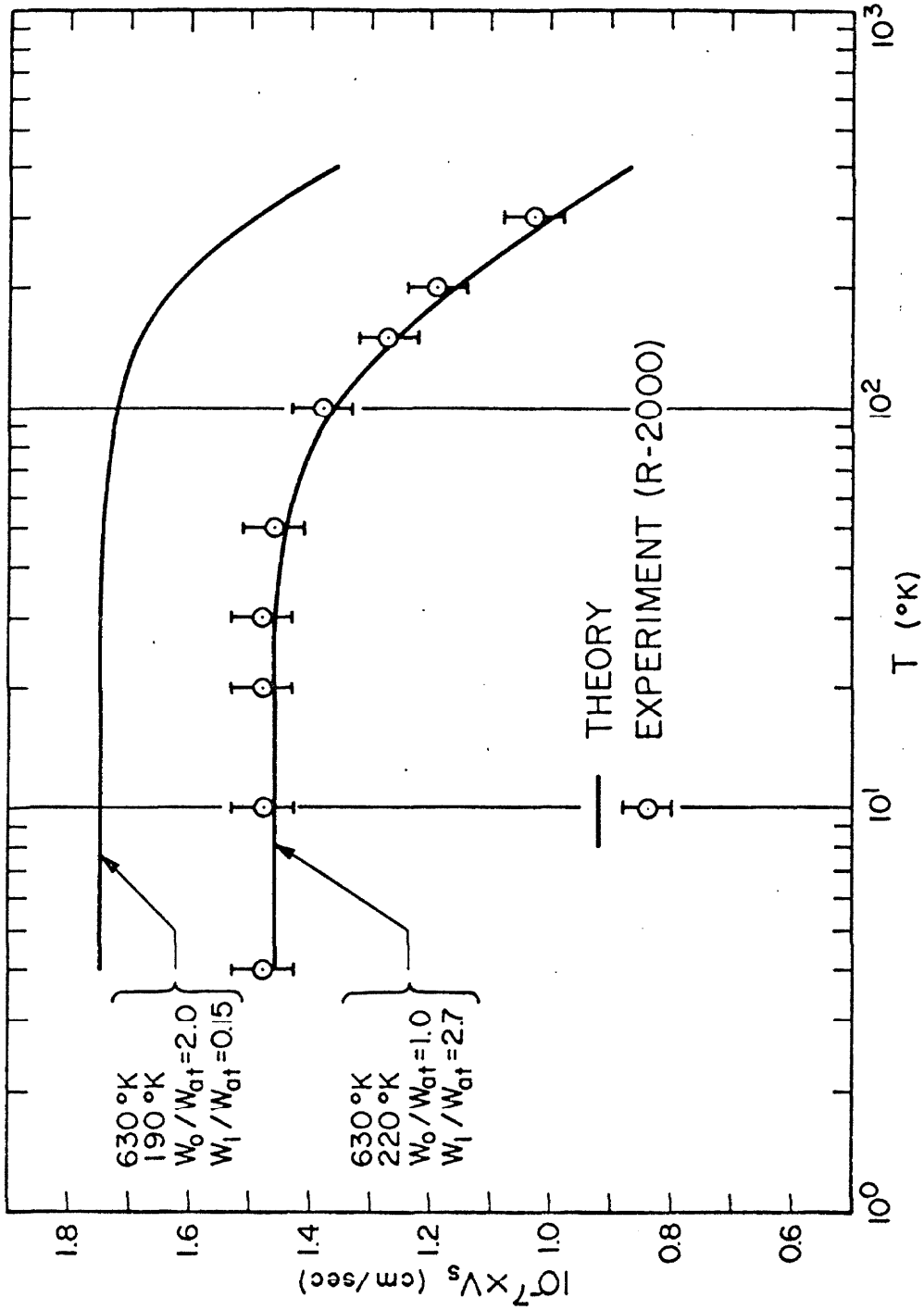
$10^7 \times V_s$ (cm/sec)
1.8
1.6
1.4
1.2
1.0
0.8
0.6
10^0
10^1
10^2
10^3
T (°K)
THEORY
EXPERIMENT (R-2000)
630°K
190°K
W_o/W_{at}=2.0
W_1/W_{at}=0.15
630°K
220°K
W_o/W_{at}=1.0
W_1/W_{at}=2.7

Figure 4.2

our experimental data it is necessary to attach more importance to the intervalley transitions with transverse acoustic phonons by increasing their strength as determined by the coupling constants ratio W_1/W_{at} . This is in accordance with what has been determined by Dumke(4.20). He found the intervalley phonons to be represented with effective temperatures of 530°K and 270°K which contribute 22% and 56%, respectively, of the total scattering, the remaining being intravalley scattering by acoustic phonons. An attempt is made to provide a better fit to the experimental temperature dependence (also illustrated in figure (4.2)) by using phonons with effective temperatures of 630°K and 220°K and coupling constant ratios of $W_o/W_{at} = 1$ and $W_1/W_{at} = 2.7$, respectively. These values are not necessarily accurate since the best possible fit has not been attempted. This would require a more elaborate analysis. However, the previous values do indicate the importance of the acoustic intervalley phonons in determining the temperature dependence of the limiting velocity.

At very low lattice temperatures, equipartition of energy for the intravalley acoustic phonons is no longer valid and the zero point lattice condition should be present. Equipartition gives rise to an $\varepsilon^{1/2}$ and -T- dependence for the acoustic relaxation time, while in the latter case it is independent of lattice temperature and proportional to the energy of the electrons. In a situation

where the zero point lattice condition dominates, the mobility would be field dependent at high field strengths. In particular, for a Maxwell-Boltzmann energy distribution[4.21], one obtains $\mu \sim E^{-0.8}$. However, for the case at hand, the zero point lattice condition is not expected to be significant since the coupling to acoustic and optical intervalley phonons is very strong, at least in the range of electric field strengths considered. Thus, expression (4.17) is valid over the entire temperature range covered experimentally. Acoustic intravalley scattering plays a very unimportant role in determining either the magnitude or the temperature dependence of the limiting drift velocity.

As a last remark, it is emphasized that the analysis in this chapter is incomplete. Nevertheless, it is probably the best description possible within the context of an experimental work and with the currently available theories. The values obtained for the phonon energies and the coupling constants may not really describe the energy losses and the strength of the transitions actually present. They may account for approximations made in the derivations of the limiting drift velocity and for the heating of the structures, if any, but they do describe the observed magnitude and temperature dependence.

CONCLUSIONS

The flow of pure unipolar sclc in silicon has been analyzed to deduce the field dependence of the electron mobility over a wide range of electric field strengths and lattice temperatures. The existence of a limiting drift velocity is established and its magnitude measured over the temperature range $4.2^{o} \leq T \leq 300^{o}K$. The experimental results obtained offer a consistent picture and the theoretical models adopted are simple but adequate.

Our findings demonstrate the usefulness of pure unipolar sclc as a tool to study the electrical transport properties of materials. It has been said, repeatedly, that this type of measurement is unsuited for a detailed evaluation of individual factors, and that other techniques are better adopted to study hot electron effects. The discrepancies in the results published so far for the field-velocity relationship seem to indicate otherwise. The technique of sclc can admittedly not satisfy those interested in the fine structure of solids. But, the ease with which information about a multitude of phenomena is obtained by this technique, over a wide range of lattice temperatures and electric field strengths, certainly establishes its usefulness even if, perhaps, a small price in accuracy is paid. Also, the results are obtained in a form relevant to practical applications.

In addition to the information on the drift velocity of electrons, a fairly complete treatment of unipolar sclc is presented. The various structures manufactured in the course of this investigation made it possible to study also the influence on sclc of: (1) trapping, (2) geometry, (3) ionized impurities, and (4) thermal carriers. In particular, the effect of giant and normal trapping is studied in detail. The variation of the threshold voltage, over the temperature range $4.2^{o} \leq T \leq 77^{o}K$, is correlated to the temperature dependence of the trapping cross-section for the compensated donor atoms. The variation of the threshold voltage for temperatures above $50^{o}K$, in the case of D-200 and D-2000 structures, is linked to the temperature dependence of the Debye length. In the case of R-2000 structures, over the same temperature range, an analysis of the V-I characteristics below threshold reveals the presence of traps. These traps are believed to be caused by a gold contaminant introduced during the diffusion step. A method is also described which provides a simple technique to obtain the degree of compensation of the material.

The field-velocity relationship for electrons in silicon is compared with other determinations currently available at $77^{o}K$ and $300^{o}K$. An effort is made to explain the various discrepancies by invoking electron injection at the negatively biased contact, impurity scattering, and anisotropy effects. The treatment is qualitative because of the lack of information on essential parameters. The temperature dependence of the limiting drift velocity is compared with

an analytical expression originally derived by Reik and Risken, and extended in this work to apply for silicon oriented in the [111] direction, at very low temperatures and at high field strengths. A reasonable fit to both its magnitude and temperature dependence is obtained if coupling constants and phonon energies are used different from those employed to describe the low field mobility. Owing to the approximations and assumptions made in deriving the analytical expression, the physical significance of these parameters is uncertain.

REFERENCES

(Chapter I)

1.1 N. F. Mott and R. W. Gurney, "Electronic Processes in Ionic Crystals" (Oxford University Press, Oxford, 1940), Second Edition, 172 (1957).

1.2 A. Rose, "Space-Charge-Limited Currents in Solids," Phys. Rev., 97, 1538 (1955).

1.3 W. Schockley and R. C. Prim, "Space-Charge-Limited Emission in Semiconductors," Phys. Rev., 90, 753 (1953).

1.4 G. C. Dacey, "Space-Charge-Limited Hole Current in Germanium," Phys. Rev., 90, 759 (1953).

1.5 M. A. Lampert, "Volume-Controlled Current Injection in Insulators," RCA Technical Report PTS-1445, 49 (1964).

1.6 C. E. Patton, "The Effect of Field Dependent Carrier Velocity on Single Injection SCLC in Planar Diodes," Internal Report, Caltech (1964).

1.7 W. C. Dunlap, Jr. and R. L. Watters, "Direct Measurement of the Dielectric Constants of Silicon and Germanium," Phys. Rev., 92, 1396 (1953).

1.8 M. Cardona, "Dielectric Constant Measurements in Germanium and Silicon at Radio Frequencies as a Function of Temperature and Pressure," Proc. Internat. Conf. on Solid-State Phys. in Electronics and Telecommunications (Brussels), 206 (1958).

1.9 J. B. Gunn, et al., "Bulk Negative Differential Conductivity and Traveling Domains in n-Type Germanium," Appl. Phys. Letters, 11, 253 (1967).

(Chapter II)

2.1 S. Denda and M. A. Nicolet, "Preparation of n π n Structures for the Study of Space-Charge-Limited Current in Silicon," JPL Space Programs Summary, 4, 57 (1966).

(Chapter III)

3.1 R. D. Middlebrook, "Conditions at a Reverse-Biased Junction in the Presence of Collected Current," Internal Report, Caltech (1963).

3.2 R. Stratton and E. L. Jones, "The Effect of Carrier Heating on the Diffusion Currents in Space Charge Limited Current Flow," J. Appl. Phys., 38, 4596 (1967).

3.3 S. Koenig, "Rate Processes and Low-Temperature Electrical Conduction in n-Type Germanium," Phys. Rev., 110, 986 (1958).

3.4 S. H. Koenig, "Hot and Warm Electrons," J. Phys. Chem. Solids, 8, 227 (1959).

3.5 G. Ascarelli and S. C. Brown, "Recombination of Electrons and Donors in n-Type Germanium," Phys. Rev., 120, 1615 (1960).

3.6 M. Lax, "Cascade Capture of Electrons in Solids," Phys. Rev., 119, 1502 (1960).

3.7 G. Ascarelli and S. Rodriguez, "Recombination of Electrons and Donors in n-Type Germanium," Phys. Rev., 124, 1321 (1961).

3.8 R. A. Brown, Ph. D. Dissertation, Purdue University (1964).

3.9 R. S. Levitt and A. Honig, "Low Temperature Electron Trapping Lifetimes and Extrinsic Photoconductivity in n-Type Silicon Doped with Shallow Impurities," J. Phys. Chem. Solids, 22, 269 (1961).

3.10 W. Shockley, "Electrons and Holes in Silicon," (D. Van Nostrand Co., Inc.), 472 (1950).

3.11 R. A. Brown, "Effect of Impurity Conduction on Electron Recombination in Germanium and Silicon at Low Temperatures," Phys. Rev., 148, 974 (1966).

3.12 M. Loenenstein and A. Honig, "Photoexcited Electron Capture by Ionized and Neutral Shallow Impurities in Silicon at Liquid-Helium Temperatures," Phys. Rev., 144, 781 (1966).

3.13 B. L. Gregory and A. G. Jordan, "Experimental Investigations of Single Injection in Compensated Silicon at Low Temperatures," Phys. Rev., 134, A1378 (1964).

3.14 A. Rose and R. W. Smith, "Space-Charge-Limited Currents in Insulators," Phys. Rev., 92, 857 (1953).

3.15 M. A. Lampert, "Simplified Theory of Space-Charge-Limited Currents in an Insulator with Traps," Phys. Rev., 103, 1648 (1956).

3.16 C. B. Collins, et al., "Properties of Gold-Doped Silicon," Phys. Rev., 105, 1168 (1957).

3.17 J. M. Brown and A. G. Jordan, "Injection and Transport of Added Carriers in Silicon at Liquid-Helium Temperatures," J. Appl. Phys., 37, 337 (1966).

3.18 V. Rodriguez and M. A. Nicolet, "Influence of Geometry on Space-Charge-Limited Current in Solids and in Vacuum," J. Appl. Math. and Phys. (Zamp), 18, 273 (1967).

3.19 C. B. Norris and J. F. Gibbons, "Measurement of High-Field Carrier Drift Velocities in Silicon by a Time-of-Flight Technique," IEEE Trans. on Electron Devices, ED-14, 38 (1967).

3.20 E. J. Ryder, "Mobility of Holes and Electrons in High Electric Field," Phys. Rev., 90, 766 (1953).

3.21 A. C. Prior, "The Field-Dependence of Carrier Mobility in Silicon and Germanium," J. Phys. Chem. Solids, 12, 175 (1959).

3.22 E. A. Davies and D. S. Gosling, "Non-Ohmic Behaviour in Silicon," J. Phys. Chem. Solids, 23, 413 (1962).

3.23 B. L. Boichenko and V. M. Vasetskii, "Temperature Dependence of the Conductivity of Silicon in Strong Electric Fields," Soviet Physics Solid State, 7, 1361 (1966).

3.24. H. Brooks, "Advances in Electronics and Electron Physics," (Academic Press, Inc., New York), 7, 85 (1955).

3.25 D. Long and J. Myers, "Ionized-Impurity Scattering Mobility of Electrons in Silicon," Phys. Rev., 115, 1107 (1959).

3.26 E. Paige, "The Electrical Conductivity of Germanium," Progress in Semiconductors, 8, 179 (1964).

3.27 J. B. Gunn, "Effect of Electron and Impurity Density on the Field-Dependence of Mobility in Germanium," J. Phys. Chem. Solids, 8, 239 (1959).

3.28 K. S. Mendelson and R. Bray, unpublished data (1957).

3.29 M. I. Nathan, "Anisotropy of the Conductivity of n-Type Germanium at High Electric Fields," Phys. Rev., 130, 2201 (1963).

3.30 M. Shibuya, "Hot Electron Problem in Semiconductors with Spheroidal Energy Surfaces," Phys. Rev., 99, 1189 (1955).

3.31 K. J. Schmidt-Tiedemann, "Symmetry Properties of Warm Electron Effects in Cubic Semiconductors," Phys. Rev., 123, 1999 (1961).

3.32 M. H. Jorgensen, et al., "Hot-Electron Effects in Silicon and Germanium," Proc. 7th Intern. Conf. (Paris), 457 (1964).

3.33 N. Pearlman and P. H. Keesom, "The Atomic Heat of Silicon Below 100°K," Phys. Rev., 88, 398 (1952).

3.34 P. D. Maycock, "Thermal Conductivity of Silicon Germanium, III-V Compounds and III-V Alloys," Solid-State Electronics, 10, 161 (1967).

(Chapter IV)

4.1 W. Shockley, "Hot Electrons in Germanium and Ohm's Law," Bell System Tech. J., 30, 990 (1951).

4.2 E. M. Conwell, "High Field Transport in Semiconductors," Academic Press (New York and London), 165 (1967).

4.3 G.Dresselhaus, et al., "Observation of Cyclotron Resonance in Germanium Crystals," Phys. Rev., 92, 827 (1953).

4.4 D. Long, "Scattering of Conduction Electrons by Lattice Vibrations in Silicon," Phys. Rev., 120, 2024 (1960).

4.5 I. Adawi, "Variational Treatment of Warm Electrons in Nonpolar Crystals," Phys. Rev., 120, 118 (1960).

4.6 C. Herring and E. Vogt, "Transport and Deformation-Potential Theory for Many-Valley Semiconductors with Anisotropic Scattering," Phys. Rev., 101, 944 (1956).

4.7 C. J. Rauch, et al., "Millimeter Cyclotron Resonance in Silicon," 4, 64 (1960).

4.8 W. A. Harrison, "Scattering of Electrons by Lattice Vibrations in Nonpolar Crystals," Phys. Rev., 104, 1281 (1956).

4.9 H. C. Reik and H. Risken, "Distribution Functions for Hot Electrons in Many-Valley Semiconductors," Phys. Rev., 124, 777 (1961).

4.10 G. Weinreich, et al., "Acoustoelectric Effect in n-Type Germanium," Phys. Rev., 114, 33 (1959).

4.11 H. G. Reik and H. Risken, "Drift Velocity and Anisotropy of Hot Electrons in n Germanium," Phys. Rev., 126, 1737 (1962).

4.12 E. M. Conwell, "High Field Transport in Semiconductors," Solid State Physics, Supplement 9, 187 (1967).

4.13 D. Long and J. Myers, "Scattering Anisotropices in n-Type Silicon," Phys. Rev., 120, 30 (1960).

4.14 C. Herring, et al., "Analysis of Phonon-Drag Thermomagnetic Effects in n-Type Germanium," B.S.T.J., 38, 657 (1959).

4.15 E. Conwell, "Lattice Mobility of Hot Carriers," J. Phys. Chem. Solids." 8, 234 (1959).

4.16 N. I. Meyer and M. H. Jorgenson, "Influence of Non-equivalent Inter-valley Scattering on Hot-Electron Effects in Germanium," J. Phys. Chem. Solids, 26, 823 (1965).

4.17 J. B. Gunn, et al., "Bulk Negative Differential Conductivity and Traveling Domains in n-Type Germanium," Appl. Phys. Letters, 11, 253 (1967).

4.18 M. I. Nathan, et al., "Interhand Scattering in n-Type Germanium," Phys. Rev., 124, 391 (1961).

4.19 E. M. Conwell, "Relative Energy Loss to Optical and Acoustic Moles of Electrons in Avalanche Breakdown in Ge." Phys. Rev., 135, A1138 (1964).

4.20 W. P. Dumke, "Two-Phonon Indirect Transitions and Lattice Scattering in Silicon," Phys. Rev., 118, 938 (1960).

4.21 B. V. Paranjape, "Field Dependence of Mobility in Semiconductors," Proc. Phys. Soc. (London), B70, 628 (1957).

FIGURE CAPTIONS

(Chapter I)

1.1 Energy band diagram of an n-type crystal provided with two electron injecting contacts at thermal equilibrium.

1.1b Energy band diagram of a p-type crystal provided with two electron injecting contacts at thermal equilibrium and for an applied voltage V.

1.2 Theoretical V-I characteristic of pure unipolar sclc in an n^+ n n^+ structure assuming thermal carriers (constant mobility) and normalized to J_{pt} and V_{pt} related by $J_{pt} = 9/8\ \varepsilon\varepsilon_o \mu\ V_{pt}^2/W^3$.

1.3 Theoretical V-I characteristic of pure unipolar sclc in an n^+ p n^+ structure assuming thermal carriers (constant mobility) and normalized to J_{pt} and V_{pt} related by $J_{pt} = 9/8\ \varepsilon\varepsilon_o \mu\ V_{pt}^2/W^3$.

1.4 Empirical field-velocity relationships for electrons in silicon.

1.5 Theoretical V-I characteristic of pure unipolar sclc in an n^+ p n^+ structure assuming hot carriers (constant drift velocity) and normalized to J_{pt} and V_{pt} related by $J_{pt} = 2\ \varepsilon\varepsilon_o\ v_s\ V_{pt}/W^2$.

1.6 Theoretical V-I characteristic of pure unipolar sclc for an ideal insulator assuming $v(E) = v_s \tanh E/E_o$.

3.2 V-I characteristics of a D-200 structure at 77°K with and without illumination present.

3.3 Temperature dependence of the punch-through voltage (V_{pt}) for a D-2000 structure 70 μ thick.

3.4 Schematic representation of a floating base transistor at thermal equilibrium. The condition $N_d >> N_a$ is present so that the transition region lies entirely in the p-region.

3.5 Temperature dependence of the capture cross-section of photo-excited carriers in phosphorus doped silicon for two samples with different impurity contents.

3.6 Electron trapping lifetime dependence on compensating acceptor concentration in phosphorus doped silicon at 1.3°K.

3.7 Temperature dependence of the threshold voltage in the range $4.2^{o} \leq T \leq 77^{o}K$ for the R-2000, D-2000 and D-200 structures.

3.8 V-I characteristics of an R-2000 structure at 4.2°K with and without illumination present. Measurements taken with 20 μs pulses and dc.

3.9 V-I characteristics of a D-200 structure at 4.2°K with and without illumination present. Measurements taken with 10 μs pulses and dc.

3.19 V-I characteristic of a D-2000 structure at 77°K in the dark. Measurements taken with 20 μs pulses.

3.20 V-I characteristic of a D-200 structure at 300°K in the dark. Measurements taken with 20 μs pulses and dc.

3.21 V-I characteristic of a D-200 structure at 77°K in the dark. Measurements taken with 20 μs pulses and dc.

3.22 V-I characteristics of a D-2000 structure at 4.2°K with and without illumination present. Measurements taken with 2 μs pulses and dc.

3.23 V-I characteristic of pure unipolar sclc obtained by Brown and Jordan[3.17] with an n^+ n n^+ structure with 4.2°K. The solid line represents the model of pure unipolar sclc with hot electrons ($v(E) = v_s$). The dashed lines are the slopes to the experimental characteristic: (1) as found by those authors, and (2) as given by the previous model.

3.24 Thickness dependence of the current density as obtained by Brown and Jordan[3.17] with n^+ n n^+ structures at 4.2°K.

3.25 Cross-section of an R-2000 structure and schematic representation of the electric field and equipotential lines for the case when the top junction is forward biased.

3.26 Cross-section of an R-2000 structure and schematic representation of the electric field and equipotential lines for the case when the bottom junction is forward biased.

3.27 V-I characteristic of an R-2000 structure at 77°K in the dark with the bottom junction forward biased. Measurements taken with 20 μs pulses and dc.

3.28 Comparison of the field-velocity relationship for electrons in silicon at 300°K as obtained by a time-of-flight technique[3.19] and from pure unipolar sclc (present work).

3.29 Comparison of the field-velocity relationship for electrons in silicon at 300°K as obtained by several authors[3.19-23] (includes present determination).

3.30 Impurity dependence of β as obtained by Gunn[3.27] in n-type germanium at 77°K.

3.31 Comparison of the field-velocity relationship for electrons in silicon at 77°K as obtained by Jorgensen[3.32] and Rodriguez (present work).

3.32 Temperature dependence of the field-velocity relationship below 50°K for electrons in silicon.

3.33 Temperature dependence of the heat capacitance (C_v) of silicon.

3.34 Temperature dependence of the thermal conductivity (κ) of silicon.

3.35 Temperature dependence of the product C_V/κ which is proportional to the thermal time constant τ_{th}.

3.36 Schematic representation of the current and voltage pulses for a typical structure as functions of time.

3.37 Thermal time constant of a D-200 structure as a function of the increase in temperature ΔT, the energy E, and the heat capacitance C_V.

3.38 Temperature dependence of ΔT in a D-200 structure for 10 μs and 50 μs pulses.

3.39 V-I characteristics of a D-200 structure at 4.2°K taken with a double pulse. Single pulse widths: 20 μs and 50 μs.

3.40 V-I characteristics of a D-200 structure at 77°K taken with a double pulse. Single pulse widths: 50 μs and 100 μs.

3.41 V-I characteristics of a D-200 structure at 300°K taken with a double pulse. Single pulse widths: 50 μs and 10 μs.

3.42 V-I characteristic of an R-2000 structure at 4.2°K taken with a double pulse. Single pulse width: 50 μs.

Chapter IV

4.1 Temperature dependence of the limiting drift velocity in terms of a Δ I for a Δ V of 20 volts. Δ I related to ΔV by $\Delta I = 2 \varepsilon\varepsilon_o v_s A \Delta V/W^2$.

4.2 Comparison with theory of the observed temperature dependence for the limiting drift velocity in an R-2000 structure.